# Considerations for the implementation of the radio interferometric positioning system on a single wireless node

Dissertation submitted in fulfilment of the requirements for the degree
*Master of Engineering* in Computer Engineering at the Potchefstroom campus of the
North-West University

## D.J. van der Merwe

**20276826**

Supervisor:    M.J. Grobler

November 2011

# Declaration

I, David Johannes van der Merwe declare that the dissertation entitled "Considerations for the implementation of the radio interferometric positioning system on a single wireless node" is my own original work and has not already been submitted to any other university or institution for examination.

_____

D.J. van der Merwe

Student number: 20276826

Signed on the 18th day of November 2011 at Potchefstroom.

# Acknowledgements

# Abstract

The ability to localise objects and persons is a useful ability, that is currently used in everyday life in the form of Global Positioning System (GPS) navigation. Localisation is also useful in data networks. The ability to localise nodes in a network paves the way for applications such as location based services, beamforming and geographic routing.

The Radio Interferometric Positioning System (RIPS), is a method originally designed for localisation in wireless sensor networks. RIPS is a promising method due to the fact that it is capable of localisation with high accuracy over long ranges. This is something which other existing methods are not capable of.

RIPS makes localisation measurements in a different manner from conventional methods. Instead of making pairwise measurements between a transmitter and receiver, RIPS uses sets of four nodes in each of its measurements. Furthermore, RIPS requires multiple measurements to obtain the correct RIPS measurement value. This value is referred to as a q-range. Multiple q-ranges are required in order to localise a node. This creates overhead in terms of co-operation between the nodes participating in a RIPS measurement.

The focus of this research is to provide a possible solution to this problem of overhead. In this dissertation an investigation is launched into the considerations and benefits of implementing RIPS on a single node. This is done by creating a conceptual design for a single wireless node capable of implementing RIPS through the use of multiple antennas. In order to test this conceptual device, a simulation model is created.

This simulation model is then validated, verified and used in experiments designed to test the effects of certain design considerations and variables on the conceptual device's localisation accuracy. The analysis of the results from these experiments shows that the conceptual device's use of multiple antennas makes RIPS sensitive to errors.

Increasing the distances separating the conceptual device's antennas is found to decrease this sensitivity to errors. This is shown to be caused by the distances separating the antennas imposing limits on the range of q-ranges values that are possible, with smaller distances resulting in smaller ranges of possible q-range values. It is also found that the use of higher frequencies in RIPS measurements results in greater accuracy. This is with the assumption that these frequencies can be accurately transmitted.

# Contents

# List of Figures

# List of Tables

# List of Algorithms

# List of Acronyms

**AOA** Angle of Arrival

**BLR** Beaconless Routing

**DP** Direct Path

**GPS** Global Positioning System

**LOS** Line of Sight

**MANET** Mobile Ad-Hoc Network

**MFR** Most Forward Progress

**MIMO** Multiple-Input Multiple-Output

**MPC** Multi Path Component

**NOI** Node of Interest

**POA** Phase of Arrival

**RIPS** Radio Interferometric Positioning System

**RSS** Radio Signal Strength

**SNR** Signal to Noise Ratio

**TAC** Test All Combinations

**TDOA** Time Difference of Arrival

**TOA** Time of Arrival

**TOF** Time of Flight

# List of Symbols & Subscripts

## List of Symbols

| | |
|---|---|
| $c$ | Speed of light in free space |
| $\lambda$ | Wavelength |
| $f$ | Frequency |
| $\varphi$ | Phase |
| $d$ | Distance |
| $d_{ABCD}$ | Q-range |
| $a$ | Amplitude |
| $t$ | Instant of time |
| $s(t)$ | Signal at instant of time $t$ |
| $I(t)$ | Interference signal at instant of time $t$ |
| $k$ | Number of completed wavelengths |
| $n$ | Number of carrier frequency wavelengths added to ambiguous q-range |

## List of Subscripts

| | |
|---|---|
| $c$ | Carrier frequency |
| $e$ | Envelope frequency |
| $A$ | Node/Antenna A |
| $B$ | Node/Antenna B |
| $C$ | Node/Antenna C |

| | |
|---|---|
| *D* | Node/Antenna D |
| *XY* | Denotes a value as being relative to any node/antenna X and Y |
| *ABCD* | Denotes any value as being dependent on nodes/antennas A,B,C and D |
| *min* | Minimum possible value |
| *max* | Maximum possible value |

# Chapter 1

# Introduction

*This chapter starts by providing a background for the research presented in this dissertation. This background is divided into two sections, a general background and a background of the Radio Interferometric Positioning System (RIPS). From this background a motivation for the research is derived. Next, the problem statement is given and research goals are identified. Different issues that need to be addressed are also given. A methodology for achieving these goals is given and finally, the structure of the remainder of the dissertation is laid out.*

## 1.1 Background

### 1.1.1 General Background

The ability to localise objects and persons is a useful ability, that is currently used in everyday life in the form of Global Positioning System (GPS) navigation. There are also many applications that require localisation in data communication networks. Examples of such applications include location based services, geographic routing and beamforming. Localisation also has applications in wireless sensor networks. In cases

where sensor networks require location information to accompany sensor measurements, it is useful to have the sensor nodes dynamically determine sensor node positions. This eliminates the need to manually assign each sensor with a physical position. Nodes in such sensor networks are often configured to function as wireless ad-hoc networks.

Wireless ad-hoc networks, just as the name implies, are defined by nodes communicating directly with each other in an ad-hoc fashion. Such networks provide advantages in terms of how robust they are. Since multiple paths are provided for communication, wireless ad-hoc networks are able to respond to changes network topology and keep nodes communicating. Commonly encountered wireless access points are usually used in infrastructure mode and are used as a last means of distribution. Although these are not ad-hoc networks, the possibility for this infrastructure to be used in ad-hoc networks exists according to [2]. This is because of the density of wireless access points in urban environments.

Although ad-hoc networks provide possible advantages in terms of robustness, routing is still a major challenge in wireless ad-hoc networks in general. This problem can possibly be solved through the use of nodes that are capable of performing localisation. Nodes in a wireless ad-hoc network are usually only aware of the network's logical topology. Although this is sufficient when it is only required to route data from a source node to a destination node using conventional routing protocols, knowledge of a network's physical layout opens the door to the use of geographic routing.

Geographic routing has many advantages. Maintenance of routing tables and route construction during forwarding is not required. This is due to the fact that routing tables are not used in geographic routing. The role of routing tables is replaced by two lists, with one containing the positions of a node's physical neighbours and the other containing the positions of possible destinations. When a source wants to send data to a destination it compares the positions of its physical neighbours with that of its intended destination. It then chooses the neighbour with the most favourable position

metric as the next hop. This process continues until the data reaches its destination. [1]

Thus geographic routing is not computationally demanding and does not have large overheads. This makes it highly scalable and therefore applicable in wireless ad-hoc networks [3]. The use of the physical topology rather than just the logical topology also provides additional metrics to use in the determination of the next hop [1]. However, in order to use such a method, nodes need to know each other's physical positions [4].

Many techniques exist to localise nodes in a network [4–6]. These techniques use different kinds of mediums to make measurements, such as radio waves, ultrasonic sound and infrared [4]. However, these existing techniques are limited in that they are either accurate or possess the ability to function over long ranges, but not both simultaneously [7].

### 1.1.2 Background of RIPS

The Radio Interferometric Positioning System (RIPS), is a localisation method that makes use of interferometry. It was first presented in [7]. RIPS was originally developed for use in wireless sensor networks and results provided from tests done using RIPS are promising in terms of accuracy, with resolutions in the order of centimetres and with ranges of up to 160 m [8]. It differs from conventional localisation techniques, in that whilst conventional localisation techniques determine the pairwise distance between a receiver and a transmitter, RIPS measurements return a linear combination of the distances between a group of four nodes denoted as $d_{ABCD}$. The combination of distances $d_{ABCD}$, is called a q-range and is defined in (1.1).

$$d_{ABCD} = -d_{AC} + d_{AD} + d_{BC} - d_{BD} \qquad (1.1)$$

Where $d_{XY}$ is the notation for the distance between any two nodes, $X$ and $Y$. In a RIPS measurement, two nodes act as transmitters and the other two as receivers. Such a measurement is illustrated in Figure 1.1 with nodes A and B transmitting and nodes C and D receiving.
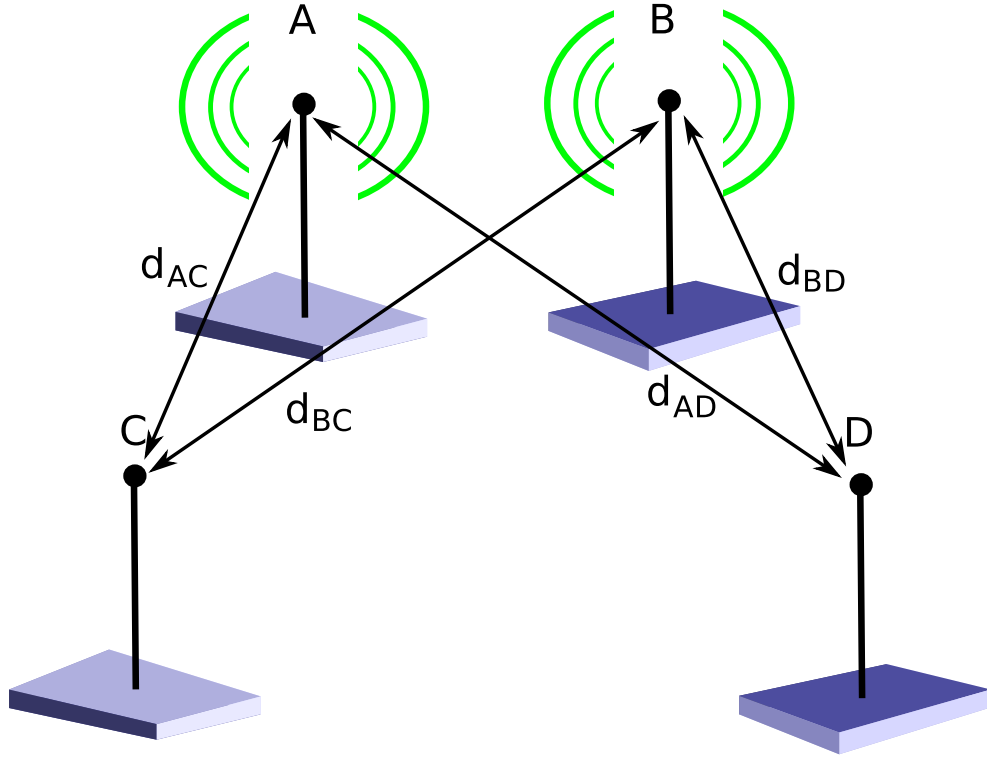
Figure 1.1: Illustration of a RIPS q-range measurement, with nodes A and B acting as transmitters while C and D act as receivers

The signals transmitted by the transmitter nodes create an interference signal. This interference signal contains a component with a frequency of $f_e$ which is referred to as the envelope or beat frequency. The envelope frequency is defined in (1.2).

$$f_e = f_A - f_B \tag{1.2}$$

Where $f_A$ is the frequency of the signal transmitted by node A and $f_B$ is the frequency of the signal transmitted by node B. The component of the interference signal at the envelope frequency also has a special property in terms of its phase. Its phase at the receiver nodes, $\varphi_C$ when measured at node C, is equal to the relative phase difference between the two signals transmitted by nodes A and B. This relationship is given in (1.3) for a measurement made at receiver node C.

$$\varphi_C = \varphi_{AC} - \varphi_{BC} \tag{1.3}$$

Where $\varphi_{AC}$ and $\varphi_{BC}$ are the phase values of the signals from nodes A and B measured at node C. In a RIPS measurement each of the receivers, C and D measure the phase of the envelope signal and determine the relative phase offset between these phases defined as $\varphi_{ABCD}$ in (1.4).

$$\varphi_{ABCD} = \varphi_C - \varphi_D \tag{1.4}$$

Where $\varphi_D$ is the phase of the interference signal measured at node D. The relative phase, $\varphi_{ABCD}$ is then used to calculate the q-range. The q-range as defined in (1.1) is a linear combination of the distances between each of the four receivers and transmitters. Since the phases measured are dependent on the same linear combination of distances they can be used to calculate the q-range.

However, there is a complication, in that the phase measurements only contain information about the distances travelled by the signals in the current signal period. The distances travelled by the previously completed wavelengths of the signals cannot be determined by a single set of phase measurements from the receiver nodes. Therefore the q-range value cannot be determined from a single RIPS measurement.

This problem is called q-range ambiguity and can only be solved by making multiple RIPS measurements using different transmitter frequencies and using the bounds set by these measurements to determine the correct q-range value. Thus the calculation of a single q-range value requires multiple RIPS measurements.

Furthermore, in order to determine the individual distances that make up the q-range values, multiple q-ranges must be determined using different combinations of receivers and transmitters in such a way that the resulting q-ranges are linearly independent. This must be done in order to have enough linearly independent equations to solve the distance variables that make up each q-range. Once these distances have been solved they can be used to determine the positions of individual nodes in the network.

As previously stated, results from tests done using RIPS show that it is capable of high degrees of accuracy [8]. However, RIPS requires multiple q-ranges to determine

node positions and multiple measurements to determine individual q-ranges. Each of these measurements requires co-operation between four nodes in terms sharing measurement results and synchronisation for phase measurements. The nodes used to produce these q-ranges must also be chosen correctly so that they are linearly independent and thus solvable. All of this co-operation between nodes, increases the measurement overhead. [9].

A solution that requires only one node to localise other nodes in the network would bypass many bottlenecks caused by conventional cooperative localisation [10]. This is especially true in the case of RIPS. If RIPS could be implemented using a single node, this overhead could be reduced. However, RIPS relies on measurements taken from different points. This problem can be overcome if a node is used that has multiple antennas. These antennas could then provide different points for measurements to be made from, with each antenna acting as an individual node would when RIPS is implemented in the conventional sense. This concept is illustrated in figure 1.2.
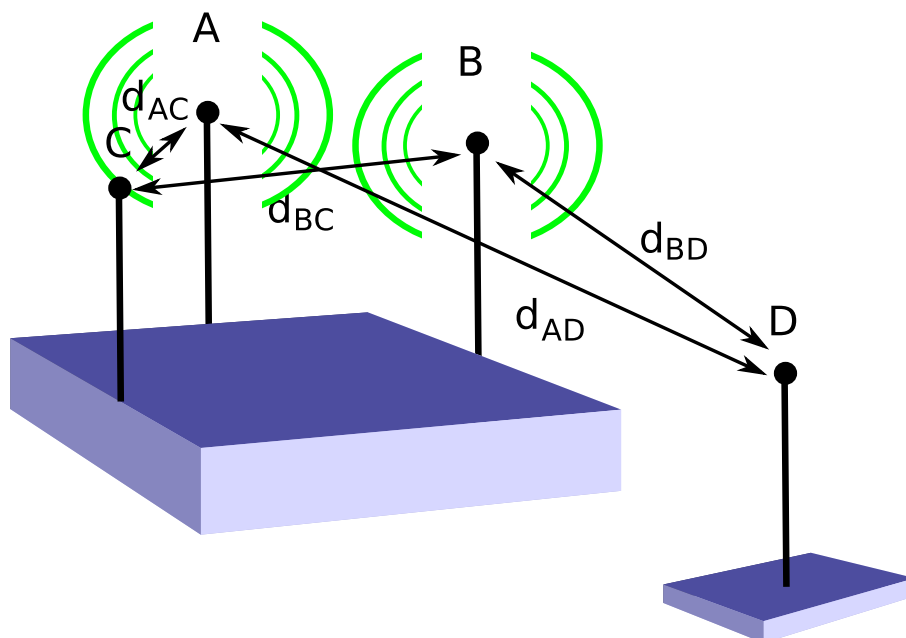


Figure 1.2: An illustration of RIPS being implemented on a single device with multiple antennas

It should be noted that although such a device would have multiple outputs and multiple inputs, it need not necessarily be a Multiple-Input Multiple-Output (MIMO) device in the conventional sense. This is because abilities commonly associated with MIMO devices, such as spacial multiplexing and spacial diversity [11], would not be a requirement for such a multiple antenna device using RIPS. The only requirement for the proposed multiple antenna device would be that it needs to be able to implement RIPS by having its antennas act as individual nodes would in RIPS. The requirements resulting from this are investigated further in this dissertation.

## 1.2   Motivation for Research

In section 1.1.1, it is explained that localisation is a useful ability, especially in wireless ad-hoc networks as it is an enabler for geographic routing. It is then argued that RIPS is a promising means of localisation due to its accuracy and long range. It is also shown that RIPS has large overheads in terms of co-operation between nodes. This is due to the number of measurements required to localise nodes and the fact that each individual measurement requires the participation of four nodes. The implementation of RIPS on a single node with multiple antennas is then identified as a possible solution to this problem.

The antennas on such a device would have fixed positions and therefore the distances between them would be constant and known. This would mean that more of the distance values that make up the q-ranges would already be known, even before measurements are made. Therefore less q-ranges would be required to solve the remaining unknown distances between the antennas on the single multiple antenna node and the node it is attempting to localise, hence forth referred to as the Node of Interest (NOI).

This idea can be clarified by referring to figure 1.2. In the case presented in figure 1.2, the three antennas on the device are acting as nodes A, B and C would, in the case presented in figure 1.1. The NOI is shown as node D in figure 1.2. In this case the

q-range $d_{ABCD}$ as defined in (1.1) consists of two known distances, $d_{AC}$ and $d_{BC}$, and two unknown distances, $d_{AD}$ and $d_{BD}$. Thus half of the values making up the q-range are already known.

With such a device the co-ordination required between nodes to produce linearly independent q-ranges could also be less, since a single device would be fulfilling the role of multiple nodes. There would be no need to use wireless communication to negotiate which of the antennas would act as transmitters or receivers for the current measurement to produce linearly independent q-ranges.

Such an approach could also have benefits in terms of individual q-range measurements. Less synchronisation would be required since the "nodes" are now on the same device. With synchronisation only being required between the multiple antenna device and the NOI. The antennas on the multiple antenna device would have direct access to the same reference time.

Therefore the implementation of RIPS on a single device using multiple antennas could be a solution to the overheads in RIPS in terms of co-ordination and synchronisation between nodes, as well as the number of q-ranges required to localise the NOI.

## 1.3   Problem Statement, Research Goal and Scope of Work

There are many uses for localisation in wireless ad-hoc networks. RIPS is a method that can provide this capability and can possibly be improved by being implemented on a single node. The research problem and goal can thus be stated as the following:

**Research Problem:** Investigation into the considerations and benefits of implementing RIPS on a single wireless node.

**Research Goal:** To develop a conceptual design for a node capable of implementing

RIPS to localise other nodes with minimum co-operation and to test this system by means of simulation.

**Scope of Work:** The scope of this research is limited to experimentation by use of a simulation model. Practical experiments using physical hardware are not conducted. The simulation model will be used to investigate the effects of RIPS measurements made from points which are separated by a distance of a metre or less on the localisation accuracy of RIPS. This will provide insight into whether the implementation of RIPS on a single multiple antenna node is viable or not.

## 1.4   Issues to be Addressed

To achieve the goal set for the research the following issues need to be addressed:

- A high level conceptual design of a node that is capable of localisation using RIPS with minimum co-operation from other nodes;

- A simulation model of the conceptual design;

- Determination of conceptual design viability through simulation.

## 1.5   Research Methodology

The research methodology followed is illustrated in figure 1.3. This methodology is broken down into steps that are discussed in the following sections.
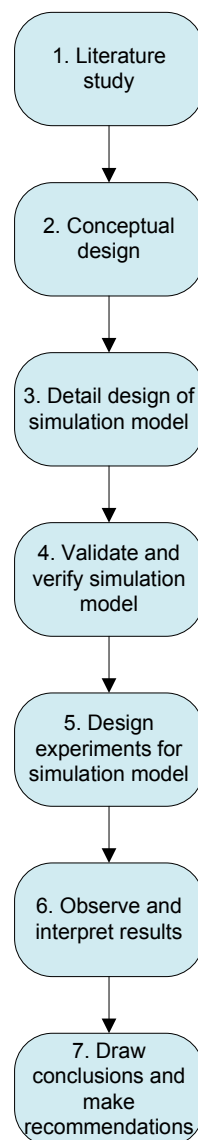
Figure 1.3: An illustration of the research methodology followed

### 1.5.1  Literature Study

A literature study is done regarding radio localisation in general as well the various uses for localisation. This provides greater insight into the field of localisation in general. This literature study continues with an in depth study of RIPS. The entire process that RIPS follows from the initial measurements to the processing of these measurements into NOI positions is discussed in detail.

### 1.5.2   Conceptual Design

Knowledge gained from the literature study is then used to create a high level conceptual design for a single node that is capable of implementing RIPS, as stated in section 1.4.

### 1.5.3   Detail Design of Simulation Model

From the conceptual design a detail design for a simulation model is created based on the conceptual design. This detail design encompasses a high lever design of the simulation model that breaks the simulation model into functional sections. These sections are then described in further detail, through the use of pseudo code.

### 1.5.4   Validation and Verification of Simulation Model

The simulation model is implemented in MATLAB. This is then validated and verified using methods specifically designed for the validation and verification of simulation models, as given in [12].

### 1.5.5   Design Experiments for Simulation Model

Experiments are designed to evaluate the conceptual device. These experiments are designed to test the impact of specific variables and design choices on the localisation accuracy of the conceptual device.

### 1.5.6   Observations and Interpretations

Observations are then made from the results of the experiments. This is done with the aim of identifying patterns in the results in terms of the system's accuracy. Once iden-

tified these patterns are interpreted by explaining them in terms of the fundamental theory of RIPS, which the system is based on.

### 1.5.7   Conclusions and Recommendations

The interpretations made are then used to draw conclusions about the proposed system's viability and recommendations are made for possible further research.

## 1.6   Dissertation Structure

The remainder of this dissertation is structured in the following way: In chapter 2 the literature study regarding localisation and its general applications is given. The literature study is continued in chapter 3 through a detailed study of RIPS. In chapter 4 an alternative solution for q-range ambiguity is presented.

In chapter 5 a conceptual design for a multiple antenna device using RIPS is developed using the knowledge gained from the literature study. The detail design of the simulation model of the conceptual device is given in chapter 6. This simulation model is then verified and validated in chapter 7. Once the simulation model has been verified and validated, the experimental methodology is developed in chapter 8. The results from these experiments are then presented in chapter 9 along with observations made from them. In chapter 10 interpretations are made that explain the observations made from the results for the experiments done. Finally, these interpretations are used to make conclusions and recommendations for future work in chapter 11.

# Chapter 2

# Literature Study

---

*In this chapter a literature study is done regarding localisation and applications that require the positioning information supplied by localisation. In the section on localisation two aspects of localisation are studied, the different methods of making localisation measurements and the different methods of how these measurements are processed into useful positions. Three different fields that make use of location information are studied: beamforming, location based services and geographic routing. Finally, a brief overview of possible hardware considerations for the conceptual device is given.*

---

## 2.1   Localisation

### 2.1.1   Definitions

To avoid any confusion a few, possibly ambiguous terms that are common in the literature regarding localisation must first be defined.

**Definition 1** *Localisation is the determination of the position of an object. This position*

---

*can either be relative or absolute. Only position is determined, movement is not.*

**Definition 2** *Accuracy is a metric defining how close a determined position is to the true position.*

**Definition 3** *Node of Interest(NOI) is a node of which the position is to be determined by localisation.*

**Definition 4** *Relative Position is a position that is relative to another node.*

**Definition 5** *Absolute Position is a position that is not dependent on the position of another node.*

This section of the literature study first studies localisation in general. Localisation can be viewed as a two step process. Firstly, physical measurements are made, the results of these measurements contain information about the position of the NOI, but not the NOI's position itself. In order to extract this information a location information processing method must be used. Therefore this section of the literature study is further divided into two sections. In section 2.1.2 different types of localisation measurements are studied. Different location processing methods are then studied in section 2.1.3.

## 2.1.2   Localisation Measurements

Different basic methods exist for gathering information about the position of a NOI. These can be divided into two groups: Those that determine the direction between a pair of nodes and those that determine the direction from one node relative to another.

**Angle of Arrival**

Angle of Arrival (AOA) measurements, determine the direction from which a received signal originated relative to a receiver. Two AOA measurements or an AOA along with a Time of Arrival (TOA) measurement are enough to determine the two dimensional position of a signal's origin [13].

The majority of AOA measurements make use of antenna arrays. Antennas on such an array are spaced a fraction of a wavelength apart and placed in specially designed geometric arrangements. An incoming signal reaches antennas on the array at different times. Therefore the antennas will measure slightly different time and phase delayed versions of the same signal. This concept is illustrated in figure 2.1. In figure 2.1 there is an array of three antennas measuring a signal. Since the signal's direction of propagation is at an angle with respect to the array, each of the antennas measure different stages of the signal, as is indicated by the dotted lines emanating from the antennas in figure 2.1. These time and phase delays in the different versions of the signal measured by each of the antennas contain information about the signal's AOA. Therefore the AOA can be determined from them using specially designed AOA algorithms. [14]
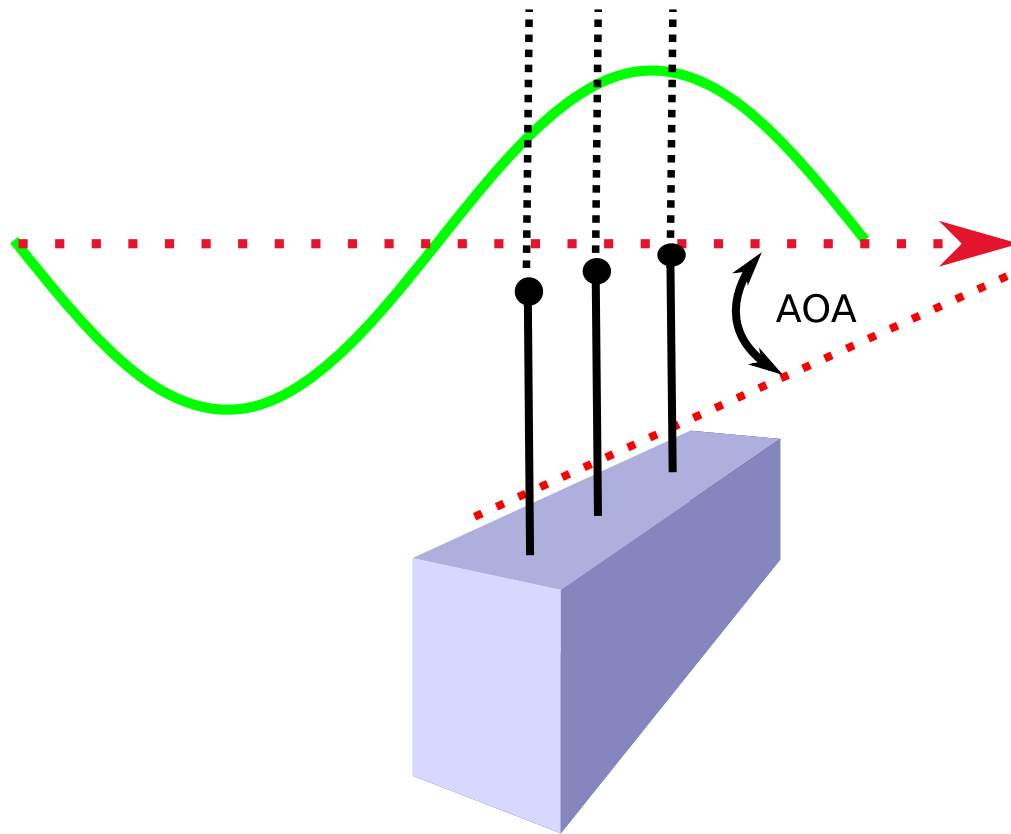
Figure 2.1: A graphic depiction of the basic concept behind AOA

AOA measurements are unreliable indoors as well as in urban environments [13]. This is because AOA is very sensitive to the effects of multipath. Multipath conditions are caused by signals reflecting from obstacles and creates signal components that arrive at the receiver with an increased propagation delay and at a different angle [15]. This difference in angle causes problems for AOA measurements.

**Time of Arrival**

If the propagation speed of the medium is known and the transmitter and receiver have Line of Sight (LOS), the propagation delay of the signal can be used to determine the distance between a transmitter and receiver. For radio signals this speed is assumed to be $c$, which is the speed of light in a vacuum. To make such a measurement there has to be synchronisation between the receiver and the transmitter. This is required to

determine the signal's time of flight by subtracting the the time of transmission from the time of arrival.
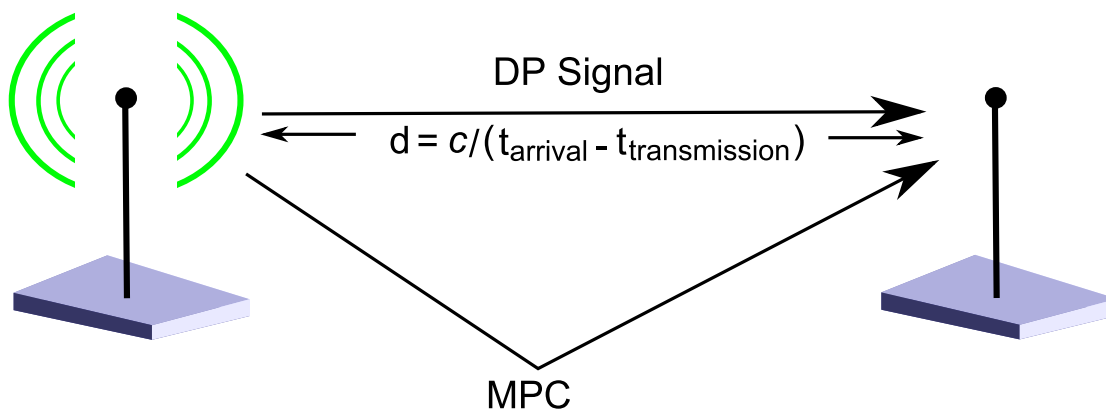


Figure 2.2: A graphic depiction of the basic concept behind TOA

The concept behind TOA is illustrated in figure 2.2. In figure 2.2 there is a transmitter and a receiver that have LOS and possess internal clocks that are synchronised and therefore provide them with the same reference time. The transmitter transmits a radio signal and the receiver measures the Direct Path (DP) signal that travelled along the LOS. If the times of the signal's transmission and arrival are known, the difference between them along with the assumed propagation speed can be used to calculate the straight line distance between the receiver and transmitter. This method has advantages over AOA and Radio Signal Strength (RSS) methods in that its variance does not increase with distance [14]. However, it is sensitive to the effects of multipath and any changes in a signal's propagation speed.

There are three main effects that this measurement method is sensitive to, these are multipath interference, obstacles and blockage. The effect of multipath is also illustrated in figure 2.2. In figure 2.2 a Multi Path Component (MPC) is shown alongside the DP signal. The MPC travels along a longer path than the DP, therefore its propagation delay will be longer and the distance calculated with TOA will be greater than the true DP distance. As long as the DP signal is stronger that the strongest MPC to such

an extent that the receiver can identify it, the TOA method will still function correctly. If this is not the case, TOA breaks down.

The second effect is caused by obstacles along the DP. When the signal passes through an obstacle its propagation speed is slower than $c$. This causes the propagation delay to increase and therefore an overestimation in the distance between receiver and transmitter. Finally, there is the effect of blockage. Blockage occurs when the DP signal is completely blocked by an obstacle, leaving only MPCs arriving at the receiver. The effects of such a case are much greater than those of the two previously mentioned cases. [13]

**Time Difference of Arrival**

Time Difference of Arrival (TDOA) is based on the same principles as TOA, with the assumptions once again made that the received signal is a DP signal and that its propagation speed is equal to $c$. The difference is that TDOA aims to measure the difference in the arrival time of a signal sent from a single transmitter at two spatially separated receivers. This essentially boils down to measuring the difference in distance between the transmitter and the two receivers. [14]

TDOA measurements can be achieved in two different ways. The first way is to have the two receivers measure the TDOA directly. This approach is illustrated in figure 2.3. In figure 2.3 the two receivers each measure the incoming signal's TOA. They then compare these times to work out the TDOA and can then calculate the difference in distance from this. For the receivers to be able to compare each of their TOA, they need to synchronised, working from the same time reference. This is illustrated in figure 2.3, through the clock that the receivers both use as a reference for time. [14]
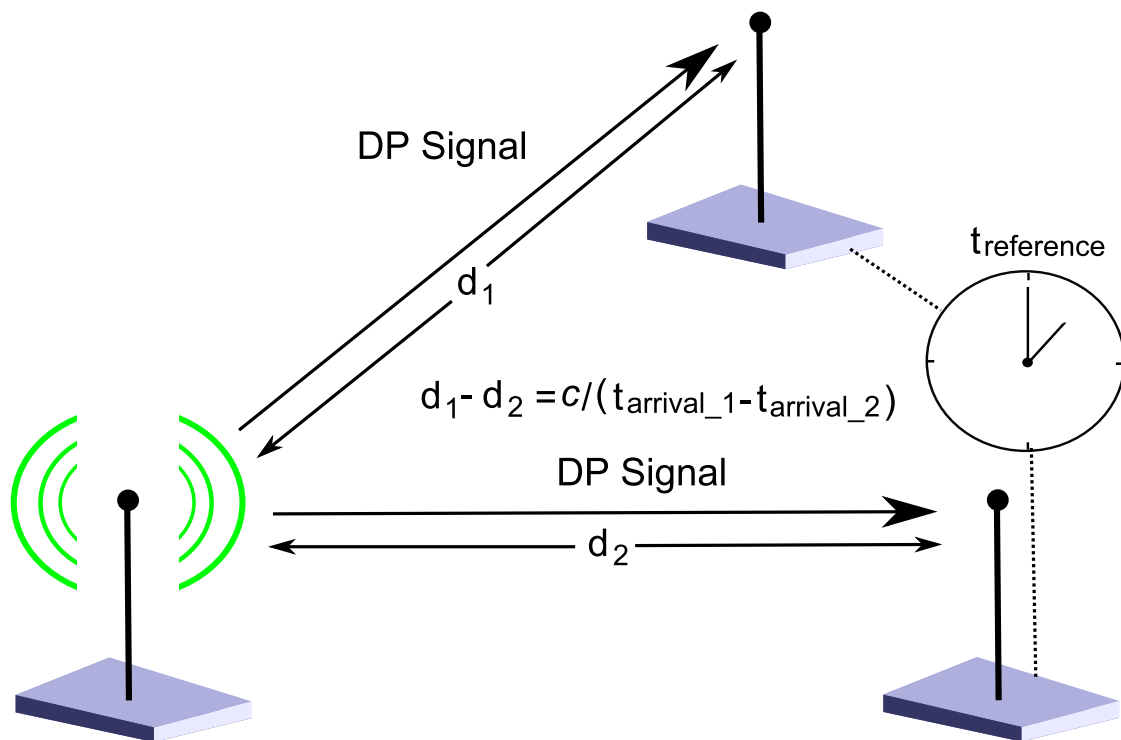
Figure 2.3: A graphic depiction of the basic idea behind TDOA

The second approach is to simply use two separate TOA measurements using the same transmitter. The drawback to such an approach is that it requires double the synchronisation to take place. This is due to the fact that each of the receivers would need to be synchronised with the transmitter in such a case. [14]

**Phase of Arrival**

Phase of Arrival (POA) measurements are also related to TOA, in the assumption that the received signal reaches the receiver by travelling along a direct path [16]. POA measurements also aim to determine the distance between the receiver and transmitter. The difference between the two is that while TOA determines this distance by measuring a signal's Time of Flight (TOF), POA achieves this by measuring a signal's phase.

An illustration of a POA measurement is given in figure 2.4. In figure 2.4 the receiver measures the phase of the signal sent by the transmitter. If the signal's wavelength, $\lambda$, is known this phase measurement can be converted into the distance travelled by the signal from its last completed wavelength using (2.1).

$$d_\varphi = \frac{\varphi_{measured}}{2\pi} \tag{2.1}$$

Where $d_\varphi$ is the distance travelled by the signal in its last wavelength before reaching the receiver and $\varphi_{measured}$ is the phase value measured by the receiver. If the distance separating the receiver and the transmitter is less than than $\lambda$, the converted phase measurement will be equal to this distance. However as can be seen in the scenario illustrated in figure 2.4, if this distance is greater than $\lambda$ the signal completes a $k$ number of wavelengths before it reaches the receiver. If the value of $k$ is known it can be used along with the phase measurement to calculate the complete distance between the receiver and transmitter.
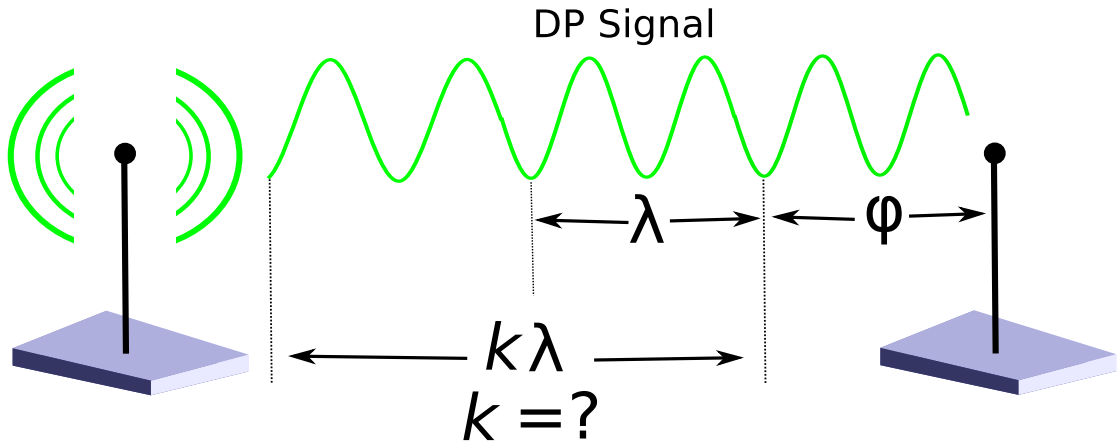


Figure 2.4: A graphic depiction of the basic idea behind POA

However, there is no way of determining the value of $k$ from a single POA measurement. This is one of the main shortcomings of using the POA to determine distances. POA is also known to be unreliable in indoor environments [13].

**Received Signal Strength**

The power density of an electro magnetic wave is inversely proportional to the distance that it has travelled [13], this effect is called signal attenuation. A RSS measurement measures the power density of a signal, therefore such a measurement can be used by a receiver to calculate the distance travelled by a signal from receiver to transmitter. However, signal attenuation is dependent on the signal's propagation environment. Therefore a receiver using a RSS measurement to determine this distance must make use of a propagation model. A propagation model predicts the signal attenuation that will occur based on the environment. Propagation models exist for environments such as indoors, outdoors, built up and rural. The RSS method is vulnerable to large and small scale fading [14] and its accuracy is dependent on the chosen propagation model. Although the RSS method is less accurate than AOA and TOA there are advantages in that RSS measurements can be made using simple hardware and without the use of complex timing protocols [16].

### 2.1.3   Location Information Processing Methods

In section 2.1.2 methods for gathering location information were discussed. Information gathered from such measurements do not yield the position of a NOI, only relative distances and directions. In order to determine the actual position of the NOI, this information must be processed using a location information processing method. Information processing methods require multiple measurements usually from multiple locations, in order to determine a NOI's position.

Location information processing methods can be divided into two groups, multilateration and multi-angulation. Multilateration makes use of distance values and is thus associated with TOA, TDOA, RSS and POA. Multi-angulation uses directions to determine positions and therefore makes use of AOA measurements. It is also possible to use a combination of angulation and lateration to determine the NOI's position.

**Rho Theta**

Rho theta, is the exception in the location information processing methods studied in this section. Although it requires two measurements, these measurements must be made from the same point. All other methods covered require different points of measurement to be used. The concept behind rho theta is illustrated in figure 2.5. Rho theta requires different types of measurements. Firstly, it requires a metric defining the direction of the NOI relative to the point of measurement. This is provided by an AOA measurement. Secondly it requires the distance between the point of measurement and the NOI. This distance can be obtained through the use of many different localisation measurement methods, such as TOF, RSS or POA. [16]
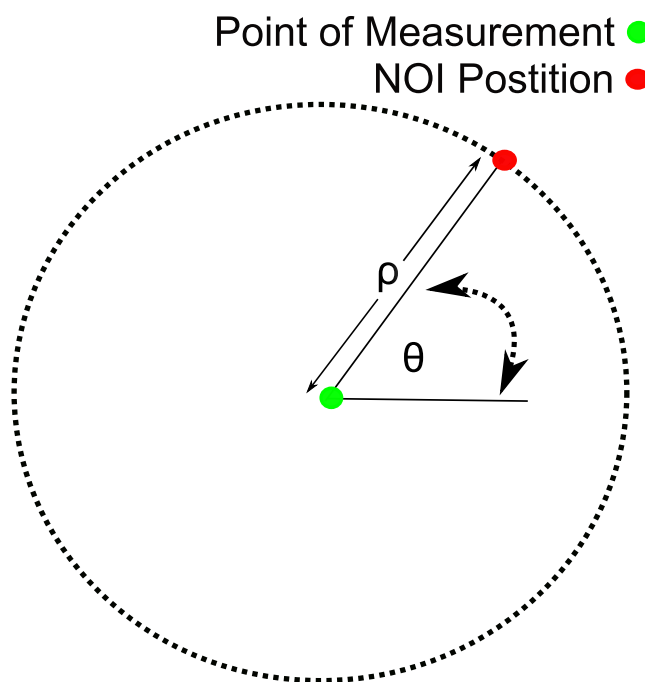


Figure 2.5: An illustration of the rho theta location information processing method

This distance defines a locus containing all the possible positions of the NOI, as can be seen in figure 2.5 in the form of a circle. This circle has the point of measurement at its centre and a radius equal to the distance between the NOI and the point of measurement, $\rho$. The angle provided by the AOA measurement also defines a locus for

the NOI position. This locus takes the form of a straight line originating at the point of measurement and passing through the NOI position. This can also be seen in figure 2.5, with the AOA given as $\theta$. The NOI's position can then be found where these two positions intersect.

**Theta Theta**

The theta theta method only makes use of AOA measurements and can therefore be referred to as an angulation method. Two such measurements are required, from two different points of measurement with known positions as is illustrated in figure 2.6. Once again, these two AOA metrics define loci for the NOI's position that take the form of straight lines originating from each point of measurement. The AOA's are shown in figure 2.6 as $\theta_1$ and $\theta_2$. The NOI is then located at the intersection of these two lines. [16]
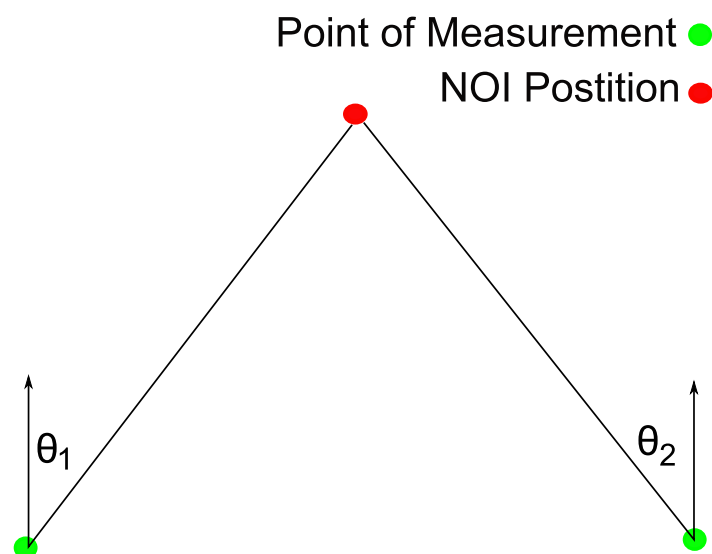


Figure 2.6: An illustration of the theta theta location information processing method

**Rho Rho**

The rho rho method only makes use of measurements that result in the distance between the point of measurement and the NOI being known, such as TOA, RSS and POA. Since rho rho only uses distances, it is referred to as a lateration method. This method is illustrated in figure 2.7. It can be seen from figure 2.7 that rho rho requires three different points of measurement, each with a known position. Each one of the measurements made from these points defines a locus for the NOI's possible positions in the form of a circle. Each of these circles has a radius that is equal to its defining distance. These distances can be seen in figure 2.7 as $\rho_1$, $\rho_2$, and $\rho_3$. The NOI is then located at the intersection of these three circles This method is also commonly referred to as Trilateration. [16]
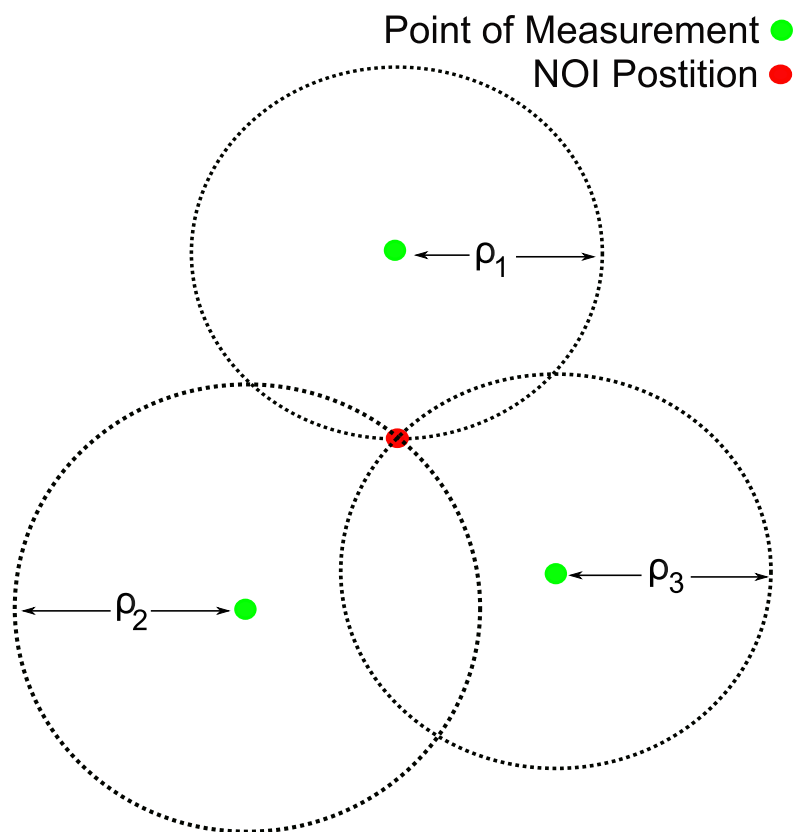


Figure 2.7: An illustration of the rho rho location information processing method

**Hyperbolic Trilateration**

Hyperbolic trilateration is the only method covered in this section that makes use of TDOA measurements. The points of measurement used in the TDOA must have known positions. A hyperbola can be defined as the locus of points where the difference in distances to two specific points has a constant value. Such a difference of distances can be obtained through a TDOA measurement. This value can then be used to define a hyperbola that is a locus of all the possible positions of the NOI. This hyperbola then has the two points of measurement used in the TDOA measurement as its foci. This concept is illustrated in figure 2.8. [16]
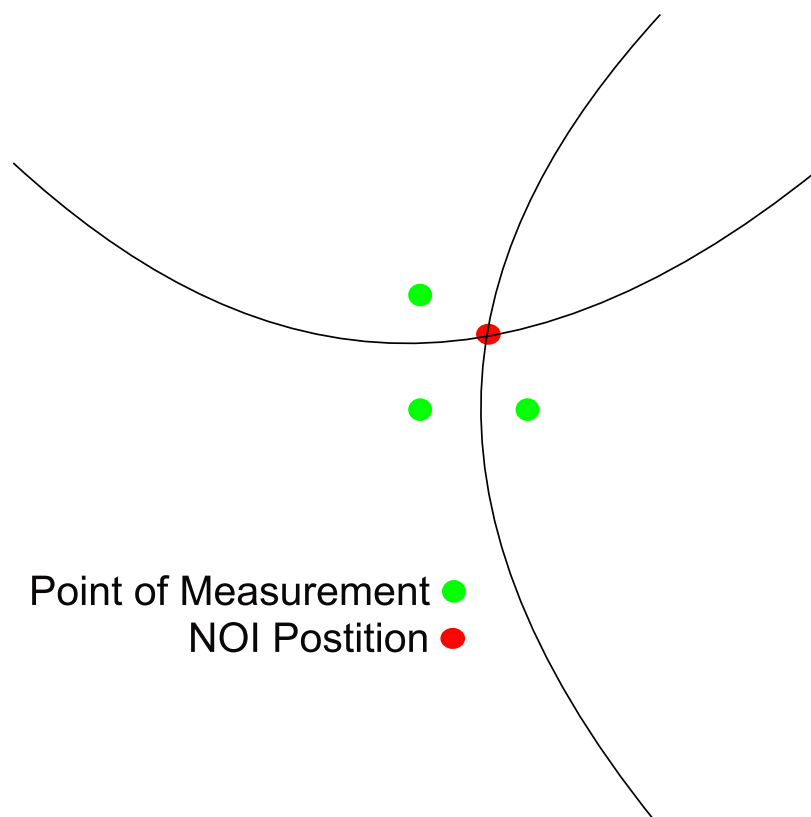


Figure 2.8: An illustration of the hyperbolic trilateration location information processing method

In order to determine the NOI's position two such hyperbolas are required. Another hyperbola can be generated by adding a third point of measurement with a known

position. This third point of measurement is used with one of the other two points to make another TDOA measurement. The second measurement defines a second hyperbola and the NOI is then located at the intersection of the two hyperbolas, as can be seen in figure 2.8. [16]

## 2.2  Applications for Localisation

In this section a study is made of applications that require localisation. Three fields of application are studied, beamforming, location based services and geographic routing. The scope of the study includes the basic working of these applications and what they require in terms of localisation.

### 2.2.1  Beamforming

Beamforming is a term for techniques that maximise or minimise signals received from a specified direction. This is done by manipulation of the phase and amplitude of signals received at multiple antennas and then adding them together. This requires information about the direction of an incoming signal as can be provided by localisation. [17]

Conventional beamforming works by altering the phase of a signal that has been received by the antennas of a multiple antenna device. If the signal is narrowband the versions of a signal that are received by the different antennas only differ in terms of phase. If the signal's direction of arrival is known these shifts in phase can be compensated for, bringing the signals into phase. Once this has been done they can be summed and scaled depending on how many versions of the signal were summed. The use of this method increases the Signal to Noise Ratio (SNR) by a factor equal to the number of antennas used for ambient noise. However when noise is directional this advantage is lost. [17]

Null steering beamforming can be used to cancel out directional noise, effectively ignoring signals coming from a certain direction. One of the most basic forms of null steering beamforming is to use conventional beamforming to isolate directional noise and then subtract this from the receiver output. [17]

Beamforming is referred to as adaptive when the ability exists to dynamically steer signals. Dynamic steering means that the beam is moved to follow a moving object. This can be useful in the case of mobile devices, but adaptive beamforming is computationally intensive. This means that it is usually confined to use by devices that have enough processing power and are therefore not very mobile. [11]

### 2.2.2 Location Based Services

Location based services are services that are provided based on the physical position of an object or user. These services can either be requested by the user (pull), such as a request for the address of the nearest restaurant or sent to the user without a request (push), such as an emergency information when approaching the scene of a traffic accident [18]. From a user's perspective location based services can be divided into three categories:

- Services that provide information to the user, based on where the user is;

- Services that provide information about where other objects or users are;

- Services that regulate access to resources.

Firstly, services can provide information based on where a user is at the moment. Information such as security alerts and public safety announcements can be provided to dynamically warn users when they approach a dangerous area. News and weather forecasts that are most relevant to the user's location can be requested. Users can request walking or driving directions to the locations of services such as banks, shops

etc., that are in proximity to the user's location. The relevance of the information provided by such methods is dependent on how accurate the user's position is, though the type of information also determines the accuracy requirements. For example, news and weather would usually require the general area of the user, such as the city or municipality that the user is currently located in. Driving directions on the other hand would require more accuracy, such as the exact street address of the user's current location. [18]

Secondly, services can provide information about where other objects or users are. In such cases the position of the user is not of primary importance, but the location of the object or person that information is being requested about is. Services such as this are used for tracking fleets of vehicles, monitoring assets and logistics. [18]

Finally, services can control access to resources. The inclusion of location information in access control can lead to more efficient use of shared resources. For example requests by users to resources such as printers can be routed to the nearest available printer. Security can also be enhanced by allowing or denying access based on where they are [19]. For example users can be blocked when trying to access resources from outside a business's premises.

### 2.2.3 Geographic Routing

Geographic routing protocols, are routing protocols that use the positions of nodes in a network to route data from source to destination [1]. Such routing protocols promise to be highly scalable due to computational simplicity, low maintenance overhead and no route discovery overhead [3]. This scalability identifies geographic routing as a possible solution to the routing problems experienced in ad-hoc networks [1].

Geographic routing protocols achieve low maintenance overhead by not making use of routing tables. The role of routing tables in conventional routing protocols is replaced by two lists, one containing the positions of a node's physical neighbours and one con-

taining the positions of destination nodes. The destination list can either be centralised or distributed. When a source wants to send data to a destination, it does not require any prior route discovery. It compares the destination's position with the positions of its neighbours and chooses the one that possesses the most favourable geographic metric as the next hop. Each next hop node does the same until the data reaches its destination. [1]

It can be argued that the process localising nodes in the network should be seen as part of geographic routing's overhead. However localisation has many other uses as has been shown in this chapter. If localisation is a function that already exists in a network, this can simply be further exploited through geographic routing and cannot simply be seen as a routing overhead. [1]

The lists that contain the locations of a node's neighbours do constitute a maintenance overhead. These lists are usually maintained by nodes periodically broadcasting their positions, this is referred to as beaconing. Due to the need for beaconing, geographic routing is not ideal in situations where nodes in a network move around, such as in a Mobile Ad-Hoc Networks (MANETs) [3]. However the need for beaconing can be circumvented through the use of a Beaconless Routing (BLR) protocol. BLR protocols eliminate the need for a neighbour table by simply broadcasting data to all its neighbours. Further excessive broadcasting by each of these neighbours is avoided by having neighbours wait before data is forwarded further by once again broadcasting. The time that a neighbour waits to broadcast is dependent on how close it is to the destination. The closer it is the shorter the waiting time. Ideally there is one neighbour with a position that is the closest to the destination and when it broadcasts first, the other nodes detect this and drop their data. However, the broadcasting that BLR protocols rely on does create an additional overhead. [1, 20]

Geographic routing protocols have two methods of forwarding, geographic forwarding and secondary forwarding strategies. Geographic forwarding methods use geographic metrics to choose the next hop. There are three main methods of geographic

forwarding, Greedy, Most Forward Progress (MFR) and Compass. Greedy forwarding forwards data to the neighbour node that is the closest to the destination. MFR chooses the next hop neighbour that provides the most forward progress.

The concept of most forward progress can most easily be explained by a sports analogy. In team sports played on a field, such as soccer, rugby or American football, a player is said to be winning field when he or she moves forward in the general direction of the opposing teams goal. Most forward progress is the same as winning field in such cases.

Compass selects the next hop that is located in a direction that is closest to the direction of the destination. A case illustrating how each of these three methods function is given in figure 2.9. [1]
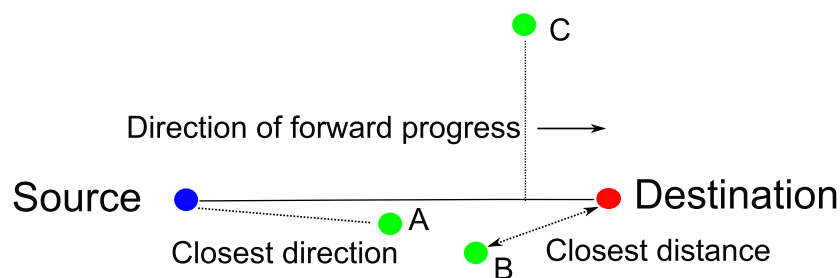


Figure 2.9: An illustration next hop choices using Greedy, MFR and Compass [1]

In figure 2.9 there is a destination node and a source node. The source node has three neighbouring nodes A, B and C. If greedy forwarding is used, the source node would choose neighbour node B as its next hop, due to it being the closest to the destination. If MFR is used, node C would be chosen as the next hop, as it has the greatest progress in the direction of forward progress, as shown in figure 2.9. Finally, if Compass is used the chosen next hop would be node A, as it has a direction from the source that is closest to that of the destination. All of these methods break down when faced with the problem of a local minima. The case of a local minima is illustrated in figure 2.10. [1]
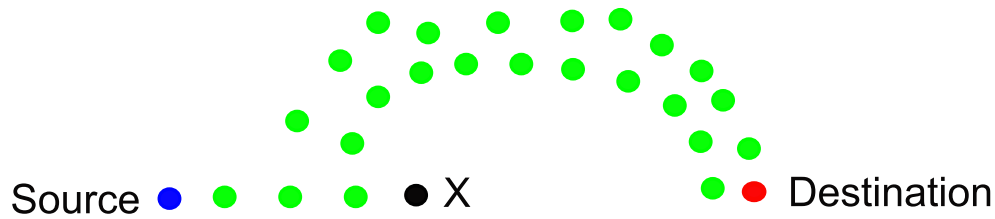
Figure 2.10: An illustration of a local minima in geographic forwarding [1]

The local minima is represented as node X in figure 2.10. If any of the geographic forwarding methods discussed would reach this node they would break down since there are no neighbours that fit their metrics for next choice in range. These geographic forwarding methods reach a point where they cannot continue. In such a case the geographic protocol would switch to its secondary forwarding strategy. [1]

Secondary strategies are used to enable routing to continue when a local minima has been reached. Such strategies include face traversal and depth first search. The area around a local minima is a void where there are no nodes. Face traversal strategies attempt to move around the edge of this void in order to reach the destination. Depth first search handles local minima by going back to the previous hop and then selecting a new next hop node ignoring the local minima that was chosen previously. [1]

## 2.3   Hardware Considerations

As stated in the definition of scope in section 1.3, this research is not concerned with experimentation on physical hardware. However, in this section a brief overview of different aspects to consider when constructing the conceptual device is given in order to provide a greater level of depth to the literature study.

The conceptual device is a single node with multiple antennas which uses RIPS to

localise other nodes. In order to achieve this the device needs to be able to have its antennas transmit and receive independently. Therefore, each antenna would need its own transceiver, with each of these transceivers being controlled by the conceptual device.

Next, the type of antenna to be used by the device would need to be considered. In order to implement RIPS, the antennas would need to have an omnidirectional propagation pattern. However, there are many different antenna types which produce omnidirectional propagation patterns, such as: monopole, ground plane and dipole antennas. Thus a choice of antenna must be made by taking into account the conceptual device's form factor. Most wireless routers make use of quarter wavelength monopole antennas, due to their compact design. Therefore, such an antenna would be the logical choice for the conceptual device.

Finally, the device's antennas need to be placed in such a way that near field coupling does not occur. In other words in order that they are not within each other's near fields. The boundary between an antenna's far and near fields is dependent on the transmissions frequency's wavelength. Therefore antennas can be kept outside each other's near fields by adjusting either the distance separating the antennas or the transmission frequency of the antennas.

## 2.4 Chapter Conclusion

In this chapter a literature study was done regarding localisation and its uses in wireless networks. Methods of performing localisation measurements as well as methods for processing localisation measurements into usable positions were studied. Applications for localisation that were studied included location based services, beamforming and geographic routing. Finally, a brief overview of hardware considerations for the conceptual device was given. The knowledge gained in this chapter forms a basis for chapter 3, where a literature study specific to RIPS is conducted.

# Chapter 3

# RIPS

*In this chapter a discussion of how RIPS functions is presented by means of the fundamental theory that RIPS is based on. Firstly, the basics behind a RIPS measurement are explained. This is followed by an explanation of the problem presented by q-range ambiguity and how this has been solved in previous applications of RIPS. Finally, the methods by which obtained q-ranges are processed into actual NOI positions are discussed.*

## 3.1 RIPS Measurement

The theory presented in this section was first presented in [7]. In order to explain a RIPS measurement a scenario is created were there are four nodes. These nodes are referred to as nodes A, B, C and D. RIPS measurements start with two nodes, in this scenario A and B, transmitting sine waves. A very basic illustration of this is given in figure 3.1.
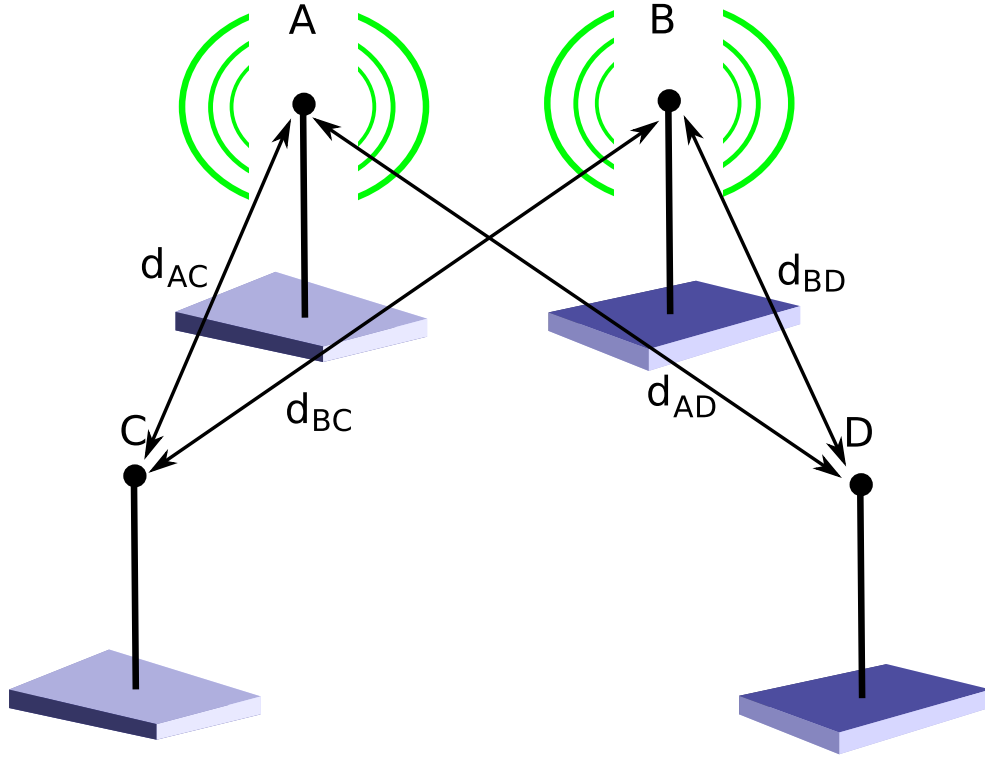
Figure 3.1: Illustration of a RIPS q-range measurement, with nodes A and B acting as transmitters, while nodes C and D act as receivers

Each transmitter uses a slightly different frequency. The difference between these frequencies is important because it creates an envelope frequency, which will be discussed further on. The signals sent by the transmitting nodes can be described by (3.1).

$$s(t) = a cos(2\pi f t) \tag{3.1}$$

Where $s(t)$ is the signal transmitted, $a$ is the amplitude of the signal, $f$ is the transmission frequency and $t$ is the instance of time. The two signals from the two transmitters, A and B, cause an interference signal that is measured by two receiver nodes, in this scenario, nodes C and D. For a set of four nodes A, B, C and D with A and B transmitting and C and D receiving, the interference signal at a receiver C caused by the two signals from A and B is then given by (3.2). The same can easily be done for node D.

$$I_C(t) = a_{AC} cos(2\pi f_A t + \varphi_{AC}) + a_{BC} cos(2\pi f_B t + \varphi_{BC}) \tag{3.2}$$

Where $a_{AC}$ is the amplitude of the signal transmitted by node A at node C and $a_{BC}$ is the amplitude of the signal transmitted by node B at node C. $I_C(t)$ is the interference signal measured at node C and $\varphi_{AC}$ is the phase offset of a signal transmitted by A and received by C. This value can be calculated by using (3.3).

$$\varphi_{AC} = -2\pi f_A \left( \frac{d_{AC}}{c} \right) \tag{3.3}$$

Where $c$ is the speed of light in free space and $d_{AC}$ is the distance between nodes A and C, this notation is used for all distances between nodes. The phase offset for the signal transmitted by B and received by C, $\varphi_{BC}$ is calculated by (3.4).

$$\varphi_{BC} = -2\pi f_B \left( \frac{d_{BC}}{c} \right) \tag{3.4}$$

Where $d_{BC}$ is the distance separating nodes B and C. These phase offsets are what RIPS relies on to function. The envelope frequency $f_e$, created by the two interfering sine wave signals is given by (3.5).

$$f_e = f_A - f_B \tag{3.5}$$

This frequency is important because it is the part of the interference signal that is to be measured. The envelope frequency is much lower than the carrier frequency $f_c$. This can be seen from the definition of the carrier frequency (3.6).

$$f_c = \frac{f_A + f_B}{2} \tag{3.6}$$

Because of this, the envelope frequency can be measured with simple, low cost equipment [7]. The envelope frequency's phase offset is what is measured in RIPS for localisation. This phase offset has a value that is equal to the difference between the phases of the two signals originally transmitted by the transmitter nodes. It is therefore called a relative phase offset. The relative phase offset measured at node C is defined in (3.7).

$$\varphi_C = \varphi_{AC} - \varphi_{BC} \tag{3.7}$$

The relative phase offset measured at node D, $\varphi_D$ can easily be written in the same manner in (3.8).

$$\varphi_D = \varphi_{AD} - \varphi_{BD} \tag{3.8}$$

Where $\varphi_{AD}$ is the phase offset of the signal transmitted by node A and measured at node D. The phase offset $\varphi_{BD}$, is the phase offset of the signal transmitted by node B and measured at node D. With two of these relative phase offsets measured respectively at receiver nodes C and D, the difference between these two values can be calculated. This difference contains information about the distances between the four nodes, that can be used for localising nodes. This can be seen by expanding it in terms of individual phase offsets as shown in (3.9).

$$
\begin{aligned}
\varphi_C - \varphi_D &= (\varphi_{AC} - \varphi_{BC}) - (\varphi_{AD} - \varphi_{BD}) \\
&= (-2\pi f_A(t_A + \frac{d_{AC}}{c}) + 2\pi f_B(t_B + \frac{d_{BC}}{c})) \\
&\quad - (-2\pi f_A(t_A + \frac{d_{AD}}{c}) + 2\pi f_B(t_B + \frac{d_{BD}}{c})) \\
&= \frac{2\pi}{c}(f_A(d_{AD} - d_{AC}) + f_B(d_{BC} - d_{BD})
\end{aligned}
\tag{3.9}
$$

This can be rewritten as (3.10)

$$
\varphi_C - \varphi_D = 2\pi \frac{d_{AD} - d_{BD} + d_{BC} - d_{AC}}{\frac{c}{f_c}} + 2\pi \frac{d_{AD} - d_{AC} - d_{BC} + d_{BD}}{\frac{c}{\delta}}
\tag{3.10}
$$

The variable $\delta$ is defined in (3.11).

$$
\delta = \frac{f_e}{2}
\tag{3.11}
$$

If it is assumed that the two transmitter frequencies have a separation in the order of kilohertz the second term in 3.10 can be ignored [7]. This results in the following simplification (3.12).

$$
\varphi_C - \varphi_D = 2\pi \frac{d_{AD} - d_{BD} + d_{BC} - d_{AC}}{\frac{c}{f_c}}
\tag{3.12}
$$

The q-range, is denoted as $d_{ABCD}$. The notation of the q-range is written in such a manner that the subscript of $d_{ABCD}$ contains all the nodes used to create the q-range. The first two nodes listed in the subscript act as transmitters while the second two act as receivers. The q-range for this case is defined in (3.13).

$$
d_{ABCD} = d_{AD} - d_{BD} - d_{AC} + d_{BC}
\tag{3.13}
$$

Thus (3.12) can be rewritten as (3.14) to calculate the q-range, with $\lambda_C$ being the wave length of the carrier frequency.

$$
d_{ABCD} = \varphi_{ABCD} \frac{\lambda_c}{2\pi}
\tag{3.14}
$$

Where $\varphi_{ABCD}$ is given by (3.15).

$$\varphi_{ABCD} = \varphi_C - \varphi_D \tag{3.15}$$

The q-range is the output of a RIPS measurement. Since it is a linear combination of the distances between the nodes used in the RIPS measurement, it can be used to localise these nodes. But in order to do this, these individual distances must be solved from a q-range. This can be done by making additional measurements using different combinations of nodes in order to generate additional q-ranges. This is done in order to create a set of linearly independent q-ranges, that can be used to solve the individual distance values that the q-ranges are comprised of. The linear independence of these q-ranges is determined by the choice of nodes used to make the RIPS measurements. A guide to choosing nodes for measurements is given in [21]. An iterative algorithm for the collaboration of nodes in RIPS in terms of distributing positions and obtaining the correct q-ranges allowing them to solve their own positions is given in [9].

Then, finally it should be taken into account that the signals could have completed a number of cycles before reaching the receivers, adding a *k* number of wavelengths to the distance. This is a problem in localisation that makes use of phase measurements and was also discussed in section 2.1.2. In RIPS this leads to a problem called q-range ambiguity and is taken into account in (3.16)

$$d_{ABCD} = \varphi_{ABCD}\frac{\lambda_c}{2\pi} + n\lambda_c, n\epsilon Z \tag{3.16}$$

Where *n* is an integer number caused by the *k* number of wavelengths completed by each of the two transmitter frequencies before reaching the receiver nodes C and D. The q-range calculated by (3.16) is the true unambiguous q-range. Q-range ambiguity poses a problem when making q-range measurements, since *n* can have any integer value both positive or negative. This limits the use of RIPS to frequencies that have wavelengths greater than the maximum distance between two nodes. However, a method for solving this problem is given in [8]. This method is discussed in section 3.2, along with another method based on Chinese Remainder Theorem.

## 3.2   Q-range Ambiguity Solution

### 3.2.1   Test All Combinations

This method was first presented in [8]. This solution for q-range ambiguity relies on setting a limit on the range of possible q-range values. To do this there is referred back to (3.16). If (3.16) is rewritten in terms of $n$, (3.17) is obtained.

$$n = \frac{d_{ABCD} - \varphi_{ABCD}\frac{\lambda_c}{2\pi}}{\lambda_c} \qquad (3.17)$$

When looking at (3.17) it can be seen that if the q-range has a limited range of values then $n$ will have a limited set of possible values as well. Due to the practical constraints imposed by node communication range there is a limited range of possible values for a given q-range. By assuming a maximum communication distance of $d_{max}$, the range of possible q-range values can be defined as (3.18).

$$(-2d_{max}; 2d_{max}) \qquad (3.18)$$

This can be explained by referring to (3.19).

$$d_{ABCD} = d_{AD} - d_{BD} - d_{BC} + d_{AC} \qquad (3.19)$$

If distances $d_{BC} \to d_{max}$ and $d_{AD} \to d_{max}$ and distances $d_{AC} \to 0$ and $d_{BD} \to 0$ , it can seen from (3.19) that $d_{ABCD} \to 2d_{max}$. This gives the upper bound. The lower bound is given by having distances $d_{AC} \to d_{max}$ and $d_{BD} \to d_{max}$ and distances $d_{BC} \to 0$ and $d_{AD} \to 0$. This results in (3.19) delivering $d_{ABCD} \to -2d_{max}$.

Now using these limits (3.17) can be rewritten to provide a limit to possible values of $n$ in (3.20).

$$|n| < \frac{2d_{max}}{\lambda_c} + 1 \qquad (3.20)$$

Now a bounded set of possible values has been defined for $n$ in each RIPS measurement. But a way to determine which value of $n$ would result in the correct q-range

is still needed. This is done by making multiple RIPS measurements using different frequencies and calculating all the possible q-range values for each measurement by substituting all the possible values of *n* into (3.16). The correct unambiguous q-range value is present is each measurement's set of possible q-range values. Test All Combinations (TAC) finds the unambiguous q-range value by calculating every single combination of values that is possible by taking one possible q-range value from each measurement's set of possible q-range values. Each one of these combinations is then tested to see if they contain values that are all equal to each other. The combination that contains values that are all equal then delivers the value of the q-range.

This task is made difficult by measurement errors that make it harder to distinguish the repeatedly occurring unambiguous q-range from other values that also occur in all measurements randomly. This problem can be combated by increasing the number of measurements made. Doing so makes it less likely that values randomly occur in each set and are then wrongly identified as the correct q-range. The disadvantage of this method is that it is computationally intensive due to its calculation of each and every combination of possible q-range values.

### 3.2.2   Chinese Remainder Theorem

Another method for solving q-range ambiguity is given in [22]. This method is based on Chinese Remainder Theorem. Chinese Remainder Theorem is a method used for solving sets of simultaneous linear congruences. The definition for the unambiguous q-range given in (3.16), can be rewritten as (3.21).

$$d_{ABCD}(mod\lambda_C) = \varphi_{ABCD}\frac{\lambda_C}{2\pi} \tag{3.21}$$

From this it can be said that $d_{ABCD}$ is linearly congruent to $\varphi_{ABCD}\frac{\lambda_c}{2\pi}$. This linear congruence is formally expressed in (3.22).

$$d_{ABCD} \equiv \varphi_{ABCD}\frac{\lambda_C}{2\pi}(mod\lambda_C) \tag{3.22}$$

If a *m* number of RIPS measurements are made, each using a different frequency, a simultaneous set of linear congruences is produced. This set is defined in (3.23).

$$d_{ABCD} \equiv \varphi_{ABCD1} \frac{\lambda_{C1}}{2\pi} (mod \lambda_{C1})$$

$$\vdots \qquad\qquad (3.23)$$

$$d_{ABCD} \equiv \varphi_{ABCDm} \frac{\lambda_{Cm}}{2\pi} (mod \lambda_{Cm})$$

With the value of the q-range $d_{ABCD}$ being unknown, Chinese Remainder Theorem can be used to solve the case presented in (3.23) for $d_{ABCD}$. Unfortunately a requirement for this is the assumption made in [22], that all phase measurements have the same error values. This constraint is not compatible with the case of RIPS, as there is no way of guaranteeing that this requirement can be met. Therefore, although the method presented in [22], seems well suited to solving the problem of q-range ambiguity, its constraints are not compatible with use in RIPS. Thus, this method is not given further consideration.

## 3.3 Q-range Processing

Once the true q-ranges have been determined unambiguously they must be processed using a location information processing method, as was discussed in section 2.1.3. Three such methods that are applicable to the localisation measurements provided by RIPS will be discussed in the following section. These three methods are hyperbolic trilateration, a numeric solution and finally a genetic algorithm.

### 3.3.1 Hyperbolic Trilateration

Hyperbolic trilateration was also discussed in section 2.1.3, where it was shown to use TDOA measurements. By referring to the definition of the q-range in (3.13), it can be seen that RIPS is also a TDOA measurement method. Therefore hyperbolic trilateration is a suitable method for processing q-ranges.

This section is further divided into two sections. The first section covers a method for hyperbolic trilateration using RIPS. In the second section an effect on the possible values for *n* caused by the use of hyperbolic trilateration in RIPS is identified.

**Method**

The hyperbolic trilateration method shown here was first presented in [23]. Hyperbolic trilateration uses a set of three anchor nodes with known positions to determine the position of another node. With four nodes, two linearly independent RIPS measurements can be made, producing two q-ranges [21]. In hyperbolic trilateration each of these q-ranges defines a hyperbola which have the two transmitters used in the RIPS measurement as foci [24]. These hyperbola contain all the possible positions of the NOI and thus the NOI is located where these two intersect. Hyperbolic trilateration using RIPS is illustrated in figure 3.2.
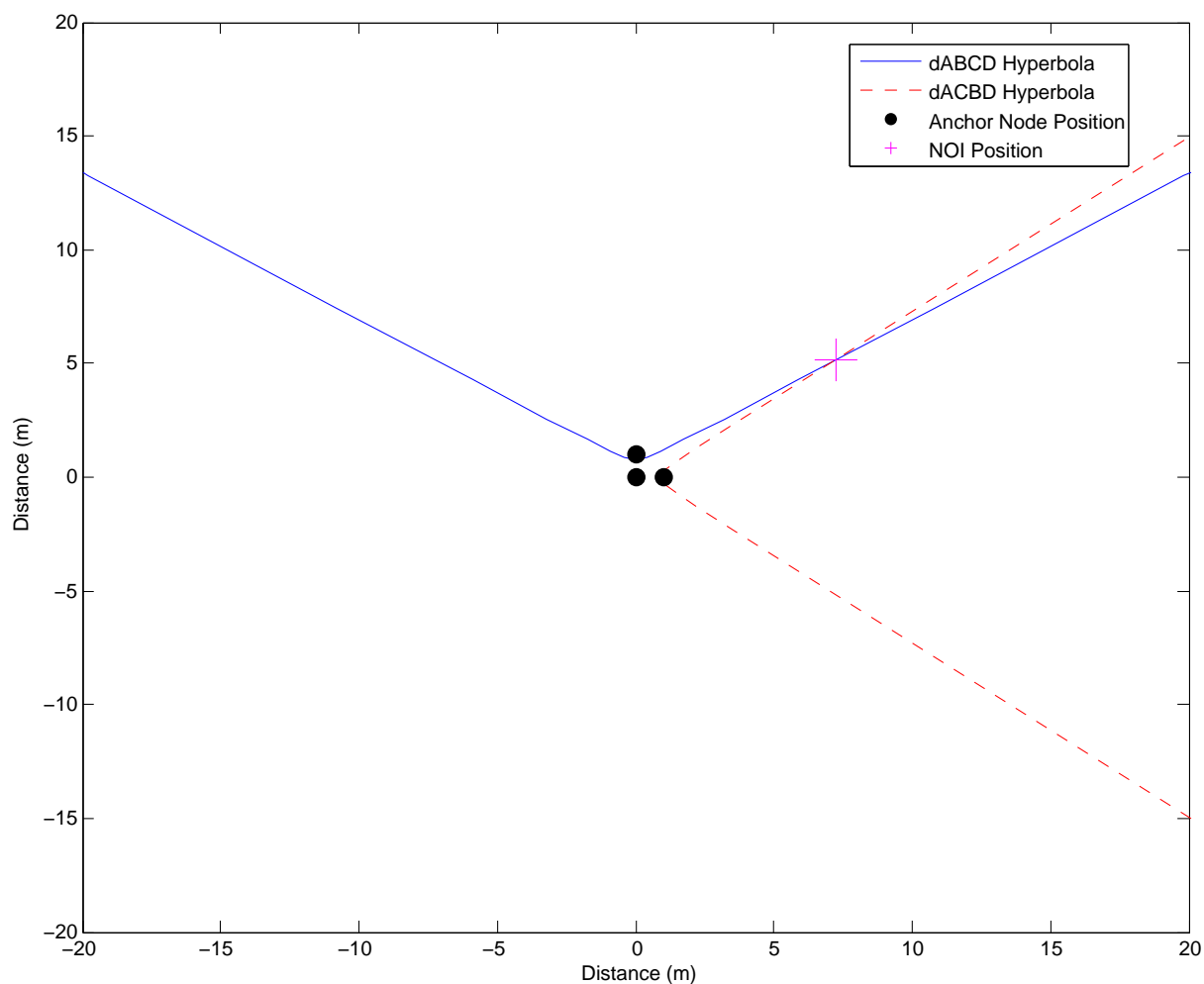
Figure 3.2: An illustration of hyperbolic trilateration using RIPS

In a case where there are four nodes, A, B, C and D, two linearly independent q-ranges are possible. These q-ranges are $d_{ABCD}$ and $d_{ACBD}$. As the notation implies, nodes A and B are used as transmitters and nodes C and D as receivers to generate $d_{ABCD}$. In the case of $d_{ACBD}$, nodes A and C are used as transmitters and nodes B and D as receivers. With these two q-ranges known, (3.24) and (3.25) must first be calculated.

$$m_1 = d_{AC} - d_{BC} + d_{ABCD} \tag{3.24}$$

$$m_2 = d_{AB} - d_{CB} + d_{ACBD} \tag{3.25}$$

When the distances making up each of the q-ranges, $d_{ABCD}$ and $d_{ACBD}$ are substituted into (3.24) and (3.25). It can be seen that (3.24) reduces to the distance difference

$d_{AD} - d_{BD}$ and (3.25) reduces to the distance difference $d_{AD} - d_{CD}$. These differences in distance are used to define the hyperbolas for each q-range. The next step is to use the the positions of nodes B and C in (3.26).

$$S = \begin{bmatrix} x_B & y_B \\ x_C & x_C \end{bmatrix} \tag{3.26}$$

Where $x_B$ and $y_B$ are the x and y co-ordinates of node B on a two dimensional Cartesian grid and $x_C$ and $y_C$ are the co-ordinates of node C on the same grid. The results of (3.24), (3.25) and (3.26) are then used to calculate (3.27), (3.28), (3.29) and (3.30).

$$z = \frac{1}{2} \begin{bmatrix} x_B^2 + y_B^2 - m_1^2 \\ x_C^2 + y_C^2 - m_2^2 \end{bmatrix} \tag{3.27}$$

$$m = \begin{bmatrix} m_1 \\ m_2 \end{bmatrix} \tag{3.28}$$

$$a = S^{-1}z \tag{3.29}$$

$$b = S^{-1}m \tag{3.30}$$

With these calculated, $d_{AD}$ can now be calculated. The number of solutions for $d_{AD}$ is dependent on the value of $b^T b$. Where $b^T$ is the transpose of matrix $b$. If $b^T b < 1$ then there is only one positive real solution to $d_{AD}$ given by (3.31).

$$d_{AD} = \frac{\sqrt{(a^T b)^2 - (b^T b - 1)a^T a} + a^T b}{1 - b^T b} \tag{3.31}$$

If $b^T b > 1$ and $(a^T b)^2 > (b^T b - 1)a^T a$ and $a^T b < 0$ there are two positive real solutions given by (3.32).

$$d_{AD} = \frac{a^T \pm \sqrt{(a^T b)^2 - (b^T b - 1)a^T a}}{b^T b - 1} \tag{3.32}$$

This ambiguity is caused by the two hyperbolas intersecting at two points, as is shown in figure 3.3. This ambiguity is an ambiguity in the position of the NOI produced by hyperbolic trilateration and is not to be confused with q-range ambiguity.
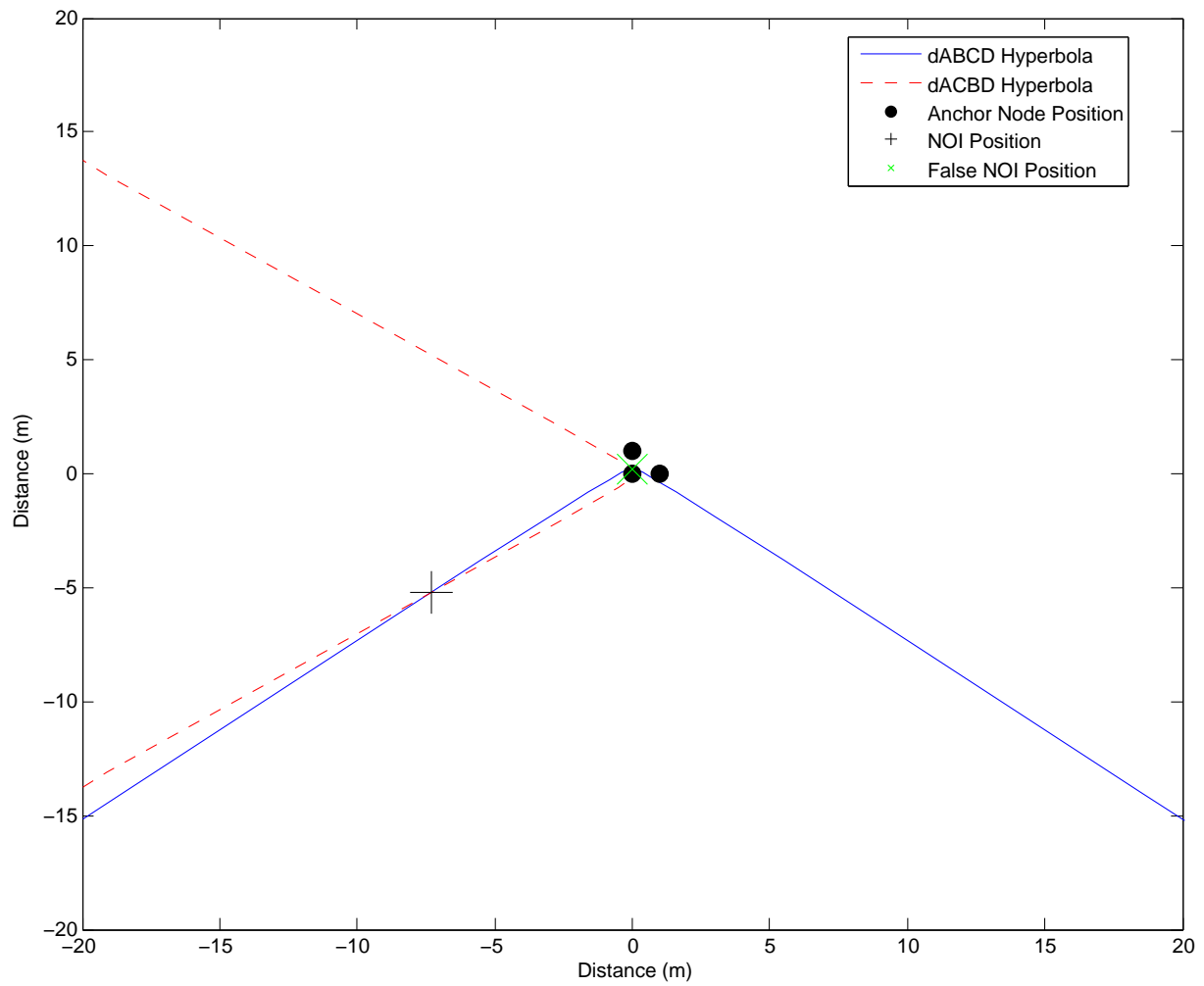
Figure 3.3: An illustration of ambiguity occurring in hyperbolic trilateration using RIPS

A possible solution for this problem is to use measurements from another node to cancel out the incorrect answer. The occurrence of this ambiguity is dependent on the position of the NOI and the arrangement of the three anchor nodes. An illustration of where ambiguous and unambiguous results will be obtained in a case were the anchor nodes are arranged at a ninety degree angle relative to each other is given in figure 3.4. This anchor node arrangement minimises the area in which a NOI placement will result in an ambiguous localisation [25].
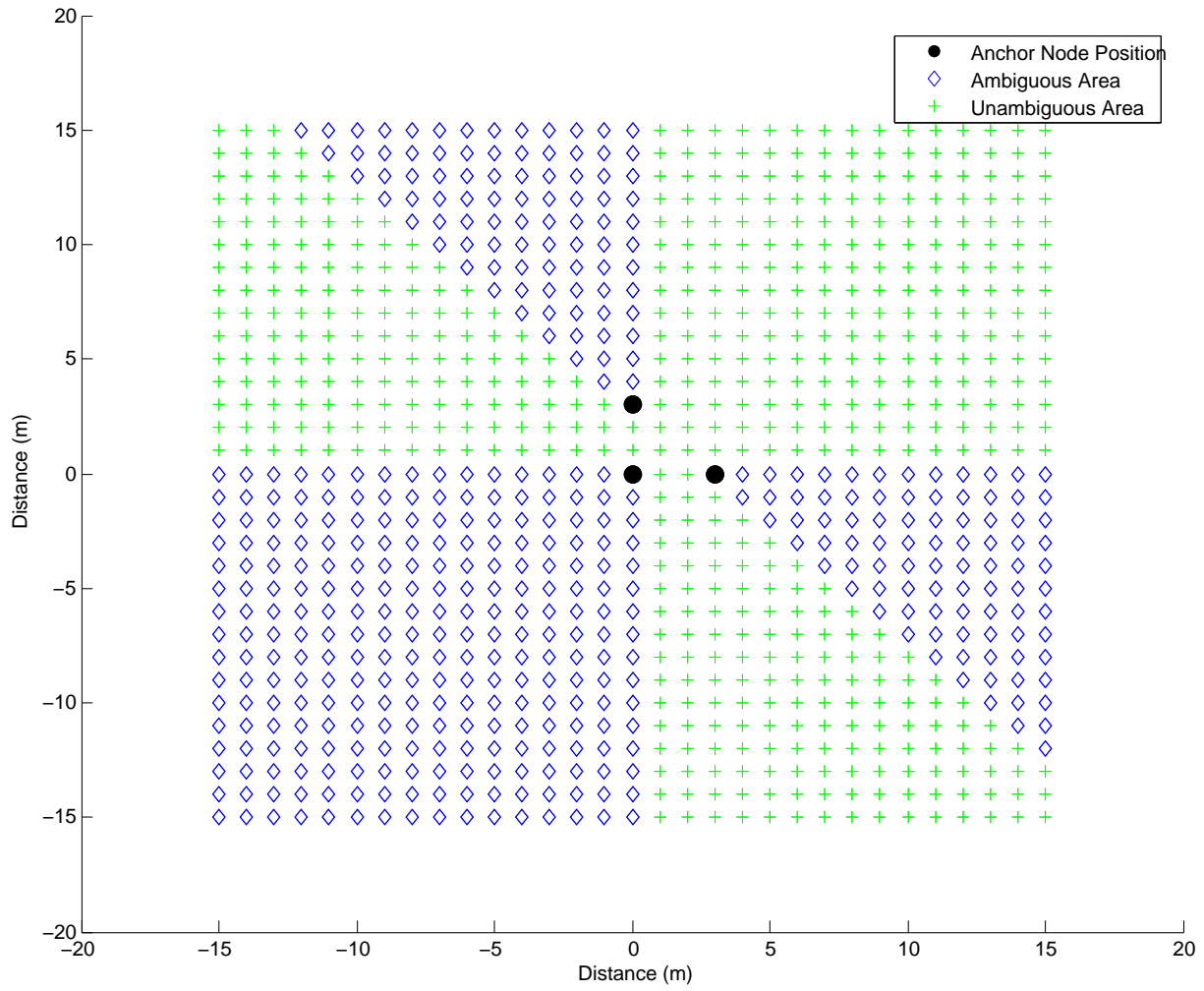
Figure 3.4: An illustration showing where ambiguity occurs in hyperbolic trilateration

With the value of $d_{AD}$ determined, the position of node D can now be determined by using (3.33) and (3.34).

$$x_D = a_1 + b_1 d_{AD} \qquad (3.33)$$

$$y_D = a_2 + b_2 d_{AD} \qquad (3.34)$$

Finally, it should also be noted that it is shown in [25], that when the NOI is located outside the triangle created by connecting the three anchor nodes, the sensitivity of hyperbolic trilateration to errors increases.

**Effect on Limits of $n$**

An interesting characteristic of hyperbolic trilateration is that the use of three station-ary nodes further bounds the range of possible q-range values. In section 3.2.1 a limit on the range of possible q-range values is defined as (3.18). In the case of hyperbolic trilateration with three stationary nodes and one moving NOI, the range of possible q-ranges decreases below the bounds set by (3.18). If the four nodes used in the q-range measurement $d_{ABCD}$ are named A, B, C, and D with the NOI being node D and nodes A and B used as transmitters. The limit of possible q-ranges for $d_{ABCD}$ can be described as (3.35)

$$[-d_{AB} + d_{BC} - d_{AC}; d_{AB} + d_{BC} - d_{AC}] \epsilon R \qquad (3.35)$$

In a case where nodes A, B, and C are stationary the distances that make up the limit (3.35) are all constants and therefore the limits are constant for all possible positions of the NOI D. This limit can be shown by taking a look at the definition of the q-range $d_{ABCD}$ in (3.36).

$$d_{ABCD} = d_{AD} - d_{BD} - d_{AC} + d_{BC} \qquad (3.36)$$

The only terms in the definition of the q-range $d_{ABCD}$ that are subject to change are those that are dependent on the position of the NOI D. Therefore the range of possible q-range values are determined by the difference in the distances between nodes A and D and nodes B and D $d_{AD} - d_{BD}$, or more specifically the minimum and maximum of this difference in distances. The maximum and minimum values of this distance are equal to the distance separating nodes A and B.

## 3.3.2 Numeric Solution

In [26], a numerical method is used to process the q-ranges into positions. This is done by writing out the q-ranges in terms of the distances that they are linear combinations of. This is shown for q-ranges $d_{ABCD}$ and $d_{ACBD}$ respectively in (3.37) and (3.38).

$$d_{ABCD} = d_{AD} - d_{BD} - d_{AC} + d_{BC} \qquad (3.37)$$

$$d_{ACBD} = d_{AD} - d_{CD} - d_{AB} + d_{CB} \tag{3.38}$$

The distances with unknown values, those between nodes with known positions and unknown positions are expanded further in terms of known and unknown positions as is shown in (3.39) (3.40).

$$d_{ABCD} = \sqrt{(x_A - x_D)^2 + (y_A - y_D)^2} - \sqrt{(x_B - x_D)^2 + (y_B - y_D)^2} - d_{AC} + d_{BC}$$
$$\tag{3.39}$$
$$d_{ACBD} = \sqrt{(x_A - x_D)^2 + (y_A - y_D)^2} - \sqrt{(x_C - x_D)^2 + (y_C - y_D)^2} - d_{AB} + d_{BC}$$
$$\tag{3.40}$$

Once this has been done a set of $m$ equations with $m$ unknowns is produced. The only problem is that the unknowns are stated implicitly. That is why a numeric method must be used to calculate the values of these unknowns. The main drawback of this method is that correct localisation is dependent on choosing a correct starting point for the numeric solution, otherwise an incorrect value from a local minima will be returned.

### 3.3.3   Genetic Algorithm

Genetic algorithms mimic the workings of evolution and genetics. Populations of solutions are considered, with only the solutions that are the closest to being correct, continuing on to produce new solutions. New solutions can be created from existing ones either through mutation or crossover where solutions exchange traits to create new solutions. This process continues until the algorithm converges to the correct solution. [27]

The use of such a method provides the possibility of avoiding the pitfalls of using a numeric solution when it comes to choosing a starting point. This is because a genetic algorithm can be seen as using multiple starting points, through its use of an initial population of different solutions. In [7], a genetic algorithm was used to determine the positions of nodes given a $M$ number of q-ranges. The basic problem is to determine

what combination of node positions would result in the given set q-ranges obtained from measurements. This is done in [7], by making use of (3.41) and the following steps:

$$error(s) = \frac{1}{n}\sqrt{\sum_{ABCD\epsilon M}(d_{ABCD} - d_{ABCD}(s))^2} \qquad (3.41)$$

1. Firstly, a set of random "guessed" solutions is generated;

2. A smaller subset of solutions is randomly selected from the original set of solutions;

3. Each solution is then evaluated using the error function (3.41);

4. The subset is then sorted according to error;

5. The bottom 20% is then deleted and new solutions are generated randomly from the top 20% by using these solutions as parents and applying genetic operators on them;

6. Go back to step (2).

In this case a solution is a set of node positions and $d_{ABCD}(s)$ is the resulting q-range from the solution $s$. A measured q-range is denoted as $d_{ABCD}$.

New solutions are generated from the top 20% of a set by using the following genetic operators:

1. A new solution has a 50% chance of being inherited from each parent;

2. Mutations (all of which have an equal chance of occurring).

   (a) The position of one node from the solution is moved by a Gaussian random number with a variance of $\varepsilon$;

   (b) One node is moved to new randomly determined position;

(c) All nodes in a solution are moved by the same Gaussian random number with a variance of $\varepsilon$.

The value of the variance $\varepsilon$ is determined by the value of the current error given by (3.41). In this way the size of the jumps used by the genetic operators will be controlled by how far off a solution was.

There are two disadvantages to the use of the genetic algorithm. Firstly, it is computationally intensive and therefore takes longer to process q-ranges into a NOI position. Secondly it requires a large population of solutions to function. Each solution is provided by a q-range measurement, therefore many q-range measurements are required. [25]

## 3.4 Chapter Conclusion

In this chapter an in depth study of RIPS has been presented. The basics behind a RIPS measurement have been covered, from the initial measurement to the calculation of the q-range. The problem of q-range ambiguity was discussed and different methods for solving this problem were studied. Finally, different methods of processing q-ranges into a NOI position were discussed. In chapter 4 a special case of q-range ambiguity is identified and a solution for q-range ambiguity that exploits this special case is presented.

# Chapter 4

# Development of an Alternative Solution to Q-range Ambiguity

*In this chapter an alternative to the TAC q-range ambiguity solution discussed in section 3.2.1, is developed. This work is done as part of this dissertation and has been published in [28], by van der Merwe et al. This alternative solution to q-range ambiguity is developed by firstly investigating q-range ambiguity in RIPS through an empirical approach. A model is created in MATLAB that uses the fundamental formulas that RIPS is based upon. This model is then used in an experiment designed to test where q-range ambiguity occurs on a two dimensional plane. Results from this experiment are used to search for patterns in where ambiguity occurs. Once identified, these patterns are used as a guide to identify causes for the observed patterns in the mathematics that RIPS is based on. Finally, a special case of q-range ambiguity is identified and a possible method of exploiting this special case is presented.*

## 4.1   Basic Model of RIPS Q-range Ambiguity

The first step of the empirical approach used in this chapter is to create a model that shows where q-range ambiguity occurs on a two dimensional plane. This is done by creating a simple model of a single RIPS measurement in MATLAB using the equations that were given in section 3.1. The model functions by using the positions of four nodes and their transmission frequencies as inputs. These nodes are referred to as nodes A, B, C and D. Firstly, the positions of the nodes are used to calculate the four distances separating the nodes that make up the q-range as defined in (4.1).

$$d_{ABCD} = d_{AD} - d_{BD} - d_{AC} + d_{BC} \tag{4.1}$$

These distances are then used to determine the absolute phase offset of each signal at each receiver, $\varphi_{AC}$, $\varphi_{AD}$, $\varphi_{BC}$ and $\varphi_{BD}$. This is done by using (4.2).

$$\varphi_{AC} = -2\pi \frac{Rem_{AC}}{\lambda_A} \tag{4.2}$$

Where $Rem_{AC}$ is the remainder of $\dfrac{d_{AC}}{\lambda_A}$. This equation is used instead of (4.3) since it takes into account that the phase measured at the receiver will only be from the wavelength that the received signal is currently in at the receiver. The use of (4.3) does not result in ambiguous q-ranges whereas (4.2) does.

$$\varphi_{AC} = -2\pi f_A (\frac{d_{AC}}{c}) \tag{4.3}$$

These phases are then substituted into (4.4) to calculate $\varphi_C$ and $\varphi_D$.

$$\varphi_C = \varphi_{AC} - \varphi_{BC} \tag{4.4}$$

These two values are then substituted into (4.5) to calculate $\varphi_{ABCD}$, the relative phase between the two interference signals at the receivers.

$$\varphi_{ABCD} = \varphi_C - \varphi_D \tag{4.5}$$

This value is then used in (4.6) to calculate the ambiguous q-range for the current positions of nodes A, B, C and D.

$$d_{ABCD} = \varphi_{ABCD} \frac{\lambda_c}{2\pi} \tag{4.6}$$

The true q-range is also calculated using the definition of the q-range as given in 4.1. The final step then involves comparing the true q-range value calculated using 4.1 with the ambiguous q-range obtained from (4.6). This is done under the assumption that the ambiguous and unambiguous q-range values will differ when ambiguity occurs. In other words when $n$ in (4.7) does not equal zero.

$$d_{ABCD} = \varphi_{ABCD}\frac{\lambda_c}{2\pi} + n\lambda_c, n\epsilon Z \tag{4.7}$$

When q-range ambiguity does not occur, otherwise stated when $n$ in (4.7) does equal zero, it is assumed that the ambiguous and unambiguous q-ranges will have equal values. Since the value of $n$ is the only cause of q-range ambiguity, these assumptions are valid.

## 4.2   Experimentation and Results

This simple model of RIPS is used to investigate q-range ambiguity by moving the position of node D over a 20 m×20 m grid of positions at intervals of 0.25 m and calculating both the ambiguous and unambiguous q-ranges for each position. Only the position of node D is varied in order to keep the case studied as simple as possible by limiting the number of variables that have an effect on the q-range values. The ambiguous and unambiguous q-ranges are then compared for each of the positions of node D to determine where ambiguity occurs. It is expected that ambiguity would occur for all positions of node D that resulted in a distance between node D and any other node that is greater than $\lambda_C$. This is because phase measurements have no knowledge of the number of wavelengths that a signal has completed prior to the one being measured, as was explained in section 2.1.2. However, the results shown in figure 4.1 indicate that this is not the case.
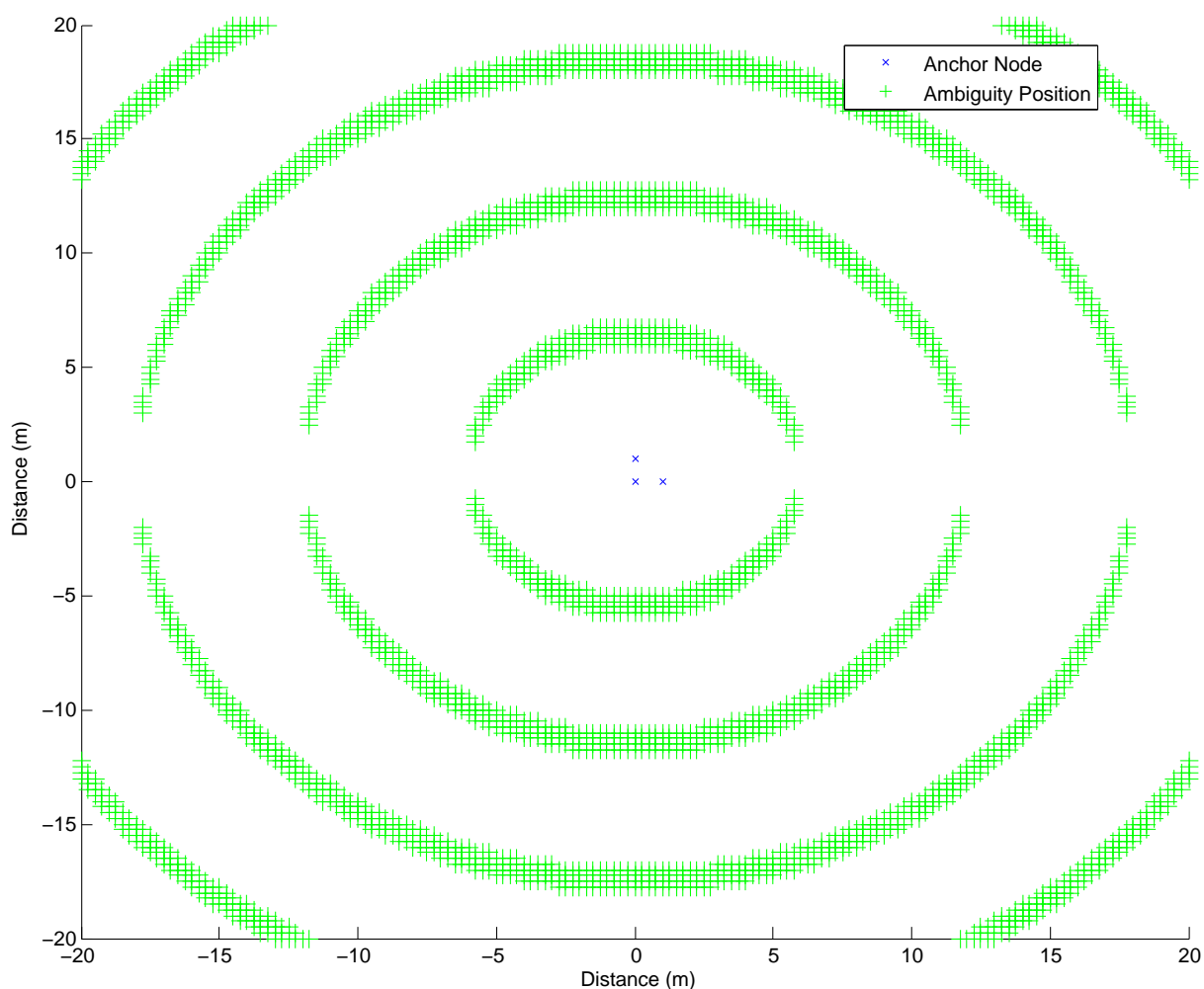
Figure 4.1: A two dimensional map showing where ambiguity occurs

For the scenario presented in figure 4.1 a carrier frequency of 50 MHz is used with a frequency separation of 1 kHz between the transmitter nodes, the distance between the stationary anchor nodes is 1 m and a resolution of 25 cm is used for the different positions of node D.

The results from the experiment illustrated in figure 4.1 show that ambiguity only occurs in intervals. These intervals centre around the the transmitter nodes and then radiate outward. The distance separating these intervals appears to correlate with the carrier wavelength $\lambda_C$. The areas between these intervals seem to produce correct q-ranges. Since the other nodes are all kept stationary with distances less than $\lambda_C$

separating them, only the position of node D contributes to ambiguity.

## 4.3 Mathematical Explanation

Q-range ambiguity occurs when $n$ in (4.7) is not equal to zero. Therefore the variables that $n$ is dependent on in the scenario of the experiment must be isolated. As it has been stated in section 4.2, node D is the only node that has an effect on q-range ambiguity in the scenario of the experiment. Thus a stage in the mathematics of RIPS must be found where the variables relating to node D are separate from the rest. The equation for the phase offset measured at node D fulfils this requirement. There are two forms of this equation, (4.3) and (4.2). Using (4.3) will always result in an unambiguous q-range, since all of the completed wavelengths are taken into account by using the full distance from receiver to transmitter.

Therefore the measured phase offset given by (4.2), will differ from (4.3) when the distances between the nodes in question, are greater than the wavelength of the transmission frequency:

$$\varphi_{unambiguous} = -2\pi \left( k\lambda + \frac{Rem}{\lambda} \right) \tag{4.8}$$

$$\varphi_{measured} = -2\pi \left( \frac{Rem}{\lambda} \right) \tag{4.9}$$

Where *Rem* is the current phase of the signal converted to a distance measured in metres. The variable $k$ is equal to the number of periods that the signal has completed before reaching the receiver and should not be confused with $n$ as given in (4.7). The number of completed periods is not taken into account in (4.9), because there is no way of gaining this information from a single phase measurement. A phase measurement only measures the current phase of the signal. This concept is illustrated in figure 4.2.
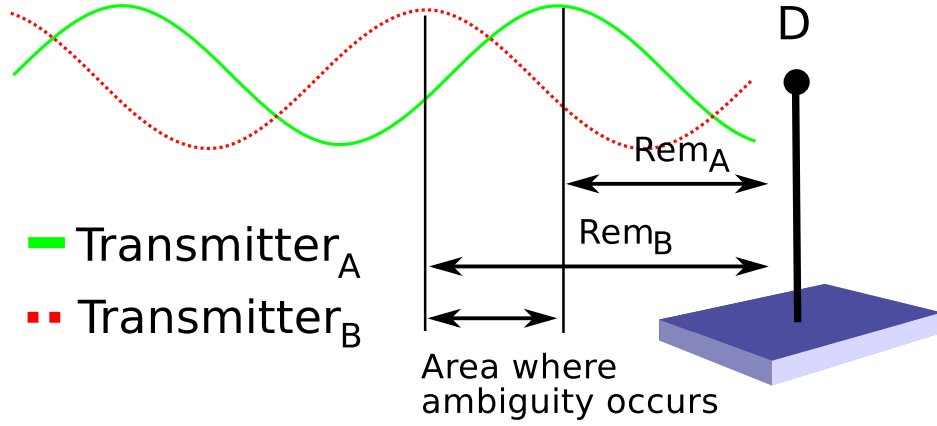
Figure 4.2: An illustration showing the area where ambiguity occurs as well as $Rem_A$ and $Rem_B$

The next step in the investigation is to substitute (4.8) and (4.9) into the equation for the phase offset of the interference signal measured at node D (4.4). Doing so results in 4.10 and 4.11.

$$\varphi_{D_{measured}} = -2\pi \left( \frac{Rem_A}{\lambda_A} - \frac{Rem_B}{\lambda_B} \right) \tag{4.10}$$

$$\varphi_{D_{unambiguous}} = -2\pi \left( \left( k_{AD}\lambda_A + \frac{Rem_A}{\lambda_A} \right) - \left( k_{BD}\lambda_B + \frac{Rem_B}{\lambda_B} \right) \right) \tag{4.11}$$

Rearranging (4.11) results in (4.12).

$$\varphi_{D_{unambiguous}} = -2\pi \left( \left( \frac{Rem_A}{\lambda_A} - \frac{Rem_B}{\lambda_B} \right) + \left( (k_{AD}\lambda_A - k_{BD}\lambda_B) \right) \right) \tag{4.12}$$

Now it can be seen that if the values of $k_{AD}$ and $k_{BD}$ are the same, the second term in (4.12) cancels out almost completely. Resulting in $\varphi_{D_{measured}} \approx \varphi_{D_{unambiguous}}$. This can be said on the condition that the signals from the two transmitter nodes are in the same $k^{th}$ wavelength and the frequency separation between the two signals is in the order of kilohertz, as is a requirement of RIPS [7]. The difference between the unambiguous and the ambiguous phases at receiver D is defined in (4.13).

$$Error = k \left( \lambda_A - \lambda_B \right) \tag{4.13}$$

Where $k$ applies to each of the signals from A and B since $k_{AD}$ and $k_{BD}$ are equal in such a case. If this condition is met at both receivers the ambiguous q-range resulting

from a RIPS measurement will have a value that is close to that of the true unambiguous q-range. Therefore the seemingly correct q-ranges that are observed in figure 4.1 are still ambiguous but close to being correct.

The findings made can be summarised as follows: A special case of q-range ambiguity has been identified were ambiguous q-ranges have values that are close to those of the correct unambiguous q-ranges. This effect occurs when the signals from the two transmitters are in the same $k^{th}$ wavelength and the frequency separation between the two transmitted signals is less than $\lambda_c$.

The signals from the two transmitters will only be in the same $k^{th}$ wavelength if the distance between the the two transmitters is smaller than the wavelengths of the signals used. As the distance between the transmitter nodes increases the bands where q-range ambiguity occurs in the conventional sense, such as shown in figures 4.1 and 4.2 will increase in width. When the distance between the transmitter nodes becomes larger than the wavelengths of the signals used, the bands merge and this special case ceases to occur.

## 4.4   Exploitation of Special Case of Q-range Ambiguity

This special case of q-range ambiguity can be exploited to solve q-range ambiguity. The ambiguous q-ranges that occur in this special case, have errors (defined in (4.13)), that are so small that they could possibly be used directly without any alteration. There is however still the problem that occurs when transmitter frequencies are in different $k^{th}$ wavelengths, resulting in conventionally ambiguous q-ranges that cannot be used directly. Therefore such cases need to be identified.

This can be done by exploiting the situation in which this special case of q-range ambiguity occurs. When the two transmitter frequencies are in different wavelengths at the receiver, the value of the q-range jumps by a value essentially equal to $\lambda_C$. This

jump can be identified in any situation if it causes the q-range value to exceed the limits of values that are possible for a q-range. If hyperbolic trilateration is used to solve q-ranges obtained by using this method, the limit is defined as (4.14).

$$[-d_{AB} + d_{BC} - d_{AC}; d_{AB} + d_{BC} - d_{AC}]\epsilon R \qquad (4.14)$$

The proof of this limit is given in chapter 3. The special case of q-range ambiguity identified in this section relies on transmission frequencies with wavelengths that are larger than the distance between the two transmitters. If one of the receivers is also placed close to the two transmitters such as is the case in figure 4.2, the range of possible q-range values can be limited in such a way that the jumps in q-range values will exceed the limits of values that are possible for q-ranges and will therefore be identifiable.

Once this occurs an alternative transmitter frequency can be used in the RIPS measurement. This alternative frequency must be of such a nature that it still replicates the special case of q-range ambiguity, but possesses a wavelength that causes conventional ambiguity to occur in bands that do not overlap those of the frequency used in the previous measurements. It should be noted that the ambiguity bands of any two viable frequencies will overlap at some stage. But the frequencies can be chosen in such a way that they do not overlap for a distance equal to the maximum communication distance of the nodes. Hence forth this solution to q-range ambiguity is referred to as Same $k$, since it relies on signals being in the same $k^{th}$ wavelength.

## 4.5 Chapter Conclusion

In this chapter a possible alternative method for solving q-range ambiguity was developed. This was done by using a brute force method to investigate where q-range ambiguity occurs. From this unexpected results were obtained. Patterns in these unexpected results patterns were identified and these patterns were explained on the basis of the theory behind RIPS. From the knowledge gained a special case of q-range ambiguity was identified and a possible method of using this case to solve q-range ambiguity was presented.

# Chapter 5

# Conceptual Design

*In this chapter the knowledge gained in chapters 2 and 3 is used to design a generic node. This node will be designed to take advantage of using RIPS in conjunction with multiple antennas, that are able to transmit and receive independently to determine the positions of other nodes in the network. The design process is started by choosing a method of processing measured q-ranges. The choice of method then determines the antenna configuration that is to be used. A method of solving q-range ambiguity is also chosen. Possible ranges of operating frequencies are identified and finally a high level functional flow for the conceptual system is given.*

## 5.1   Motivation

In section 1.2 RIPS was identified as having overheads in terms of co-operation between nodes. The implementation of RIPS on a single node through the use of multiple antennas was identified as a possible solution to these overheads. This is due to the idea that the antennas would act as individual nodes do in RIPS. This would lessen the need for co-operation between nodes. Such an implementation of RIPS would also reduce the number of q-ranges required to localise a NOI, due to the distances separat-

ing the antennas on the device being constant and therefore known. For these reasons a conceptual design for such a node is created in this chapter.

## 5.2   Choice of Q-Range Processing Method

In section 3.3, three possible methods of processing q-ranges into usable NOI positions were investigated. The advantages and disadvantages of these three methods are now discussed and a choice of method that will be used is then made.

### 5.2.1   Numeric Solution

This method is used successfully in [26], but this is in a case where the position of the NOI is limited to a specific range. This makes it possible to work around the problem of choosing a starting point for the numeric algorithm. In the context of this dissertation the position of the NOI cannot be bounded in such a way, since it can be placed anywhere on a two dimensional plane.

### 5.2.2   Genetic Algorithm

The genetic algorithm circumvents the pitfalls of choosing a correct starting point by effectively using multiple starting points. However, genetic algorithms are computationally demanding and thus take time to process q-range values. Therefore such a solution is not well suited for real time localisation. It also requires a large population of q-range values to function, each provided by a RIPS measurement [25]. This is in conflict with the motivation for implementing RIPS on a single wireless node, which was given in section 1.2.

### 5.2.3 Hyperbolic Trilateration

This method is the only analytical solution. It is less hardware intensive and also eliminates the need to guess a starting point. There are two drawbacks to this method that were identified in section 3.3.1, in terms of ambiguity and sensitivity. This method sometimes returns ambiguous results for the position of the NOI.

This problem can be solved by using positions determined by another one of the exact same devices designed in this conceptual design. The positions from the two devices can then be compared. If one of the devices localised an unambiguous position this position is accepted as correct. If both devices localised the NOI ambiguously, the position that occurs in both sets of ambiguous positions is accepted as correct. This would only require the exchange of localised positions by the two devices. No further co-operation would be required.

Hyperbolic trilateration also becomes more sensitive when the NOI is not surrounded by the anchor nodes [25], such as would be the case in the implementation of RIPS on a single node. However it is not known how much this sensitivity would affect the accuracy of such a system. Although there are disadvantages to its use, hyperbolic trilateration is identified as the only viable q-range processing method. Hyperbolic trilateration is chosen for the conceptual design.

## 5.3 Antenna Configuration

The choice of hyperbolic trilateration in section 5.2 determines the choice of antenna configuration, in terms of the number of antennas that are to be used. Since hyperbolic trilateration uses three anchor nodes, it makes sense to use three antennas on the conceptual device. These three antennas would then act as anchor nodes for hyperbolic trilateration. The choice of hyperbolic trilateration also determines the placement of these antennas in relation to each other. According to [25], positioning anchor nodes

at ninety degree angles relative to each other minimises the area where q-range ambiguity occurs. Therefore such a placement is used for the three antennas on the device. The resulting antenna placement is illustrated in figure 5.1.
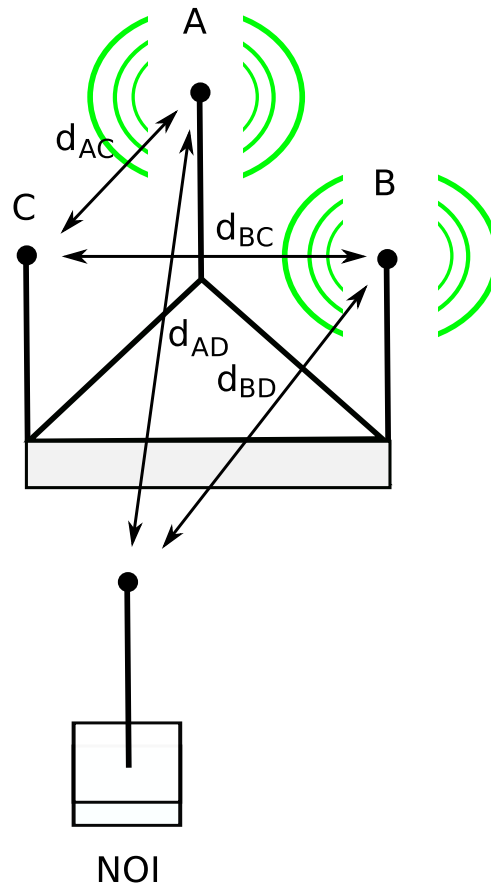


Figure 5.1: An illustration of the conceptual design

Another issue addressed in this section of the conceptual design is the distance separating the antennas. Since RIPS relies on distances between nodes (antennas in this case), the distance separating them could have an impact on the functionality of the device. Therefore the distances separating the antennas will not be constrained yet at this stage. The effects of different distances will be tested and from the results obtained interpretations will be made that will determine the choice of antenna separation.

## 5.4   Method of Q-range Measurement

In a configuration as is illustrated in figure 5.1, only two antennas would transmit at a time, just like in a conventional RIPS measurement. The difference in this case would be that there would only need to be one actual receiver, the NOI. The NOI would act as a receiver, while the remaining antenna would be left idle. This antenna can be left idle since it is placed on the device. This means that the distances separating it from the other two transmitting antennas would be constant and known. Therefore the phase measurement that would be made at this antenna can simply be calculated theoretically. No actual phase measurement is required.

In order to make the relative phase measurements that RIPS relies on to calculate q-range values, the receiver nodes need to have a common reference of time. This is achieved through synchronisation. The device being developed in this conceptual design would also need to be able to synchronise in such a manner. In this case, time synchronisation would be between the device and the NOI. The NOI can then send a timestamp back to the device after making a phase measurement along with its measured phase value. This timestamp would indicate at which time the NOI made the measurements and can then be used by the device to theoretically calculate the phase that would be measured at the idle receiver at that time.

## 5.5   Q-range Ambiguity Solution

In section 3.2.1 the TAC q-range solution was discussed and in chapter 4, Same *k* was developed as an alternative to TAC. Both of these methods rely on multiple measurements using different frequencies. However, they function in very different ways. TAC relies on multiple measurements to find the true unambiguous q-range as a value that occurs in each measurement's set of possible q-range values. This method cannot function with just a single measurement and can require as many as 16 measurements to

solve a single q-range [29].

Same $k$ has not been tested yet and will therefore be investigated as well. This method is constrained to operating frequencies that have wavelengths in the order of metres with differences between the frequencies used in separate measurements in the order of tens of megahertz. This method can function with only a single measurement and only requires additional measurements when the NOI is in a position where the signals from the transmitters are in different $k^{th}$ wavelengths. Both of these methods will be considered and tested in a simulation.

## 5.6    Generation of Linearly Independent Q-ranges

As previously shown in section 3.3.1, hyperbolic trilateration requires two linearly independent q-ranges to function. These two q-ranges ($d_{ABCD}$ and $d_{ACBD}$), are generated by using different combinations of transmitters and receivers. The generation of these two q-ranges by the device can be explained by referring to figure 5.2. In figure 5.2 the three antennas are denoted as antennas A, B and C.
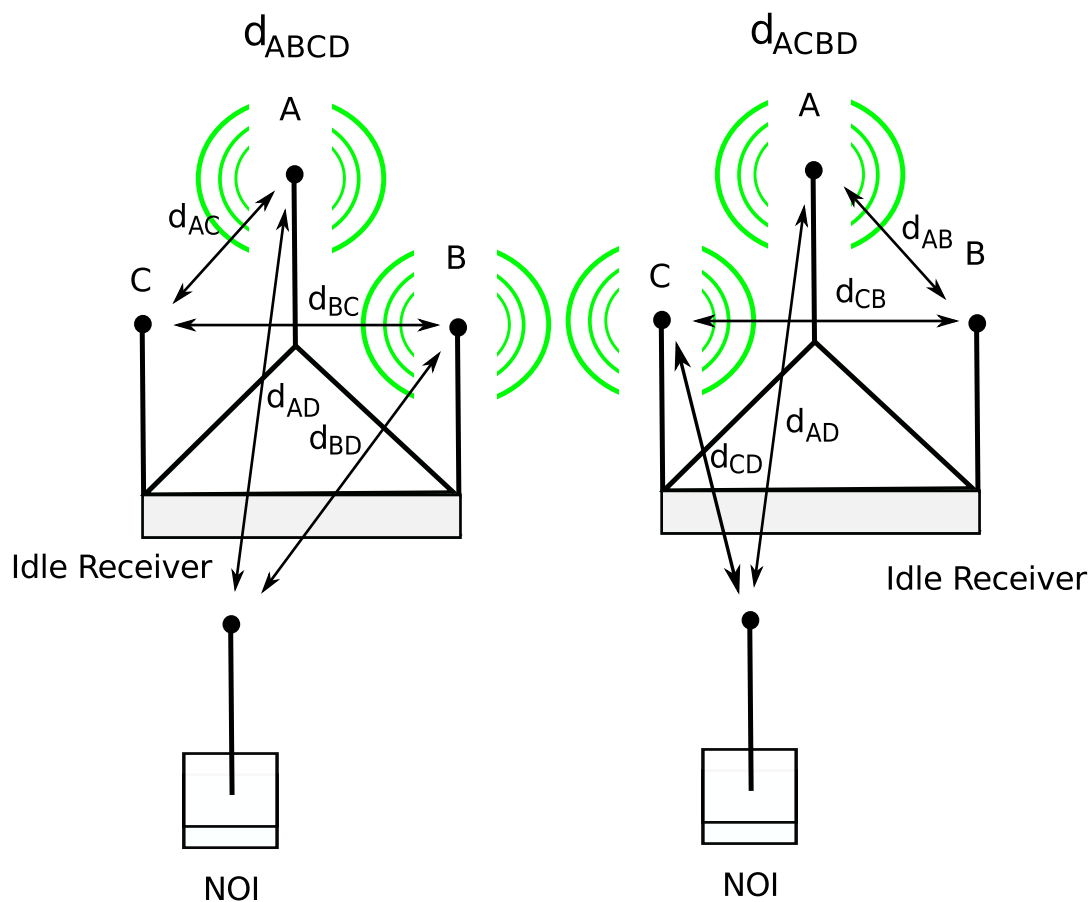
Figure 5.2: An illustration of how linearly independent q-ranges are generated

In order to generate $d_{ABCD}$, antennas A and B would be used as transmitters. Antenna C would be used as the idle receiver and the NOI would act as a receiver in the conventional sense. The second q-range $d_{ACBD}$, would be generated by having antennas A and C act as transmitters. Antenna B would now be used as the idle receiver and the NOI would remain in the role of a conventional receiver.

## 5.7 Operating Frequencies

Since the use of both solutions for q-range ambiguity will be investigated, different sets of operating frequencies are to be used, depending on what method is used to solve q-

range ambiguity. For TAC it is decided to use the 2.4 GHz and 5 GHz frequency ranges specified by the 802.11n standard [30]. The different frequencies used in measurements would then correspond with the channels defined for these frequency ranges in the standard. For Same *k* two frequencies will be used, namely 60 MHz and 70 MHz. The near-field effects that would be experienced by the device's antennas when using the 60 MHz and 70 MHz frequencies, are not considered in this research.

## 5.8   Hardware Requirements

The use of RIPS requires that the device be able to transmit sine wave signals from two antennas at a time while the third antenna stays idle. The frequencies of the signals transmitted by the two transmitters must differ, but only in the order of kilohertz. Therefore the device must be capable of finely tuning its operating frequency. In order to solve Q-range ambiguity the device must be able to make measurements using different frequencies. The antennas used on the device must have an omnidirectional propagation pattern. Finally, the device must be able the synchronise its reference of time with that of the NOI.

## 5.9   Functional Flow

A high level functional flow for the conceptual device is illustrated by figure 5.3. Each of the numbered steps in the functional flow are explained in the rest of this section.

## Step 1

Before the measurement can start the device and the NOI must be time synchronised. This step is needed for the device to use the timestamp sent with measurements from the NOI to compute the theoretical measured phase value at the idle receiver antenna.

## Step 2

The current transmitter antennas now transmit sine wave signals with frequencies differing in the order of kilohertz.

## Step 3

The NOI measures the phase offset value $\varphi$ of the interference signal.

## Step 4

The phase offset $\varphi$ of the interference signal measured at the NOI is transmitted by the NOI to the device along with a timestamp to indicate when the measurement took place.

## Step 5

The theoretical value of the phase offset $\varphi$ that would be measured at the idle antenna is calculated using the device's dimensions and the values of the transmission frequencies that were used for the time indicated by the timestamp received from the NOI.

## Step 6

The two phase offsets produced by steps 3 and 5 are then used to calculate the q-range value for the measurement.

## Step 7.1

If all frequencies in the range have been used for measurements the process can continue to the next step. Otherwise the steps 2 to 6 must be repeated until this condition is met.

## Step 7.2

The device moves on to the next transmitter frequency in the range.

## Step 8

Ambiguity in the q-range is now solved, using either TAC or Same $k$.

## Step 9.1

Hyperbolic trilateration is is used to solve q-ranges, thus two linearly independent q-ranges are required. This is done repeating the RIPS measurement using different combinations of transmitters and receivers. If two combinations of transmitting and idle antennas have been used the process can continue to the next step. Otherwise steps 2 to 8 must be repeated until this condition is met.

## Step 9.2

The combination of transmitters and receivers is changed in the following way. The idle receiver now becomes a transmitter and one of the transmitter antennas becomes the idle receiver.

## Step 10

The two unambiguous q-ranges can now be processed using hyperbolic trilateration into a position for the NOI.
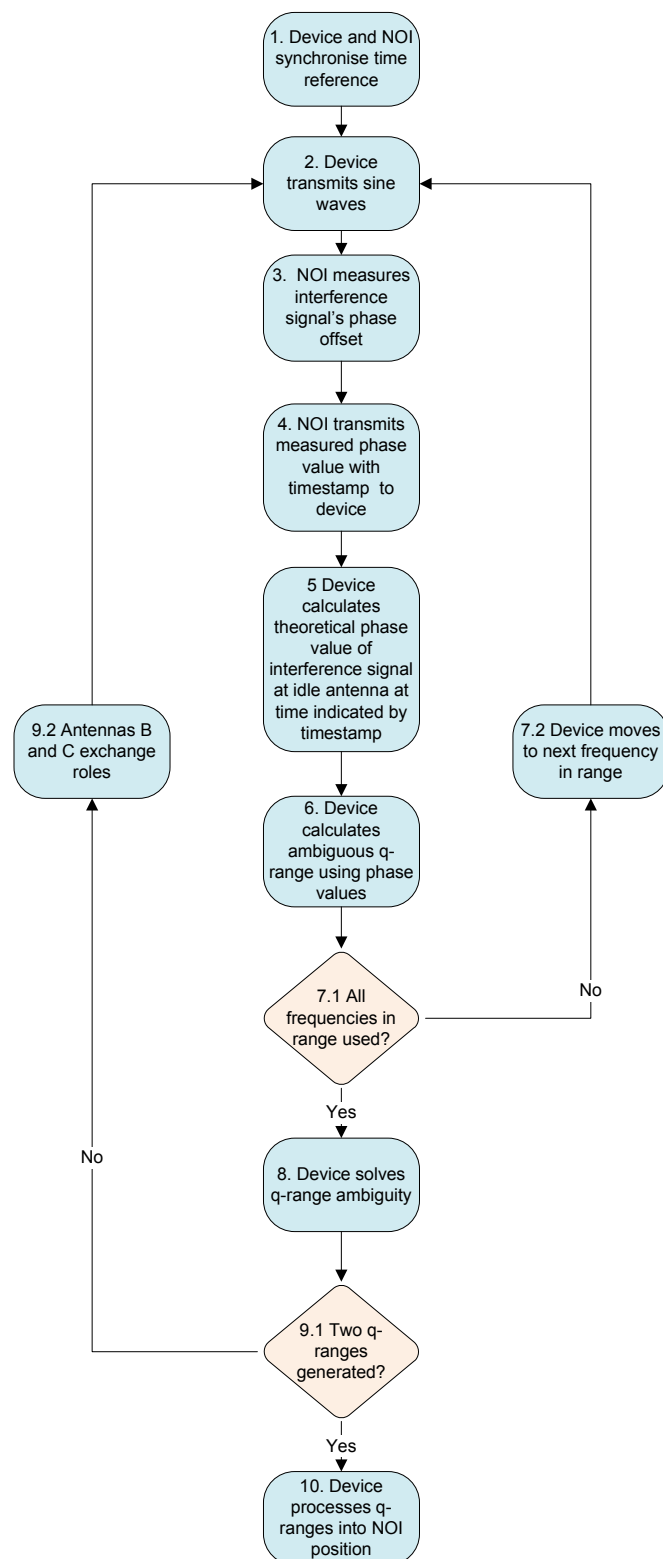
Figure 5.3: An illustration of the conceptual design's functional flow

## Conceptual System Example

The functional flow is further clarified through the use of an example. The scenario for this example is laid out as the following:

- The NOI is located at (12,7) on a two dimensional plane;

- A separation of 1 m is used between the antennas. The positions of the antennas that are denoted as A, B and C are then $Pos_A = (0,0)$, $Pos_B = (0,1)$ and $Pos_C = (1,0)$;

- The TAC is used to solve q-range ambiguity;

- Three operating frequencies are used from the 2.4 GHz range, 2.418 GHz, 2.438 GHz and 2.458 GHz;

- The transmission frequency separation is 1 kHz.

## Step 1

This step does not factor into this example. It simply involves making sure that the device and the NOI are working from the same reference time.

## Step 2

For this example antennas A and B are chosen as the first two transmitter antennas. Now the current two transmitter antennas each transmit an unmodulated sine wave at frequencies that differ by the frequency separation of 1 kHz for this case. The first operating frequency is 2.418 GHz, thus antenna A will transmit at 2.418 GHz and antenna B will transmit at 2.4179999 GHz. The time at which transmission takes place must also be saved.

## Step 3

The NOI measures the interference signal at a frequency equal to the transmission frequency separation. The absolute phase offset of this interference signal is measured and the time at which the measurement was made is saved. The term absolute phase offset simply means the phase offset of the signal relative to a specific point in time. Using (4.2) this phase value, $\varphi_D$ is calculated as 1.008 rad. In a practical implementation this value will of course be subject to interference, which is not present in this theoretically calculated value.

## Step 4

The value of the phase offset measured by the NOI is now transmitted to the device along with the time at which the measurement took place.

## Step 5

The phase that would be measured at the idle receiver antenna C is now calculated theoretically by the device by using (4.2). For this case the value of the phase at C $\varphi_C$ is 2.1417 rad.

## Step 6

With $\varphi_C$ and $\varphi_D$ known the still ambiguous q-range can be calculated using (3.14). For this case the value of the still ambiguous q-range is 0.0224.

## Step 7

Now it must be checked whether all the frequencies in the range have been used. This is done in order to solve q-range ambiguity using TAC. There are still two frequencies in the range that have to be used. So steps 2 to 6 are repeated using 2.438 GHz and 2.458 GHz. The ambiguous q-ranges resulting from each of these measurements are 0.1525 and 0.1585.

## Step 8

Now the ambiguous q-ranges are solved using TAC. This involves using 3.16 to calculate each possible q-range for each measurement that was done with the limits in (3.35). For this scenario these limits for the value of $n$ are $[-6; 12]$ $n \epsilon N$. A section of the possible q-ranges is given in table 5.1.

Table 5.1: A table showing a section of the possible values for the q-range, with the true q-range shown in boldface

| Operating Frequency | n=5 | n=6 | n=7 | n=8 | n=9 | n=10 | n=11 |
|---|---|---|---|---|---|---|---|
| 2.418 GHz | 0.5183 | 0.6423 | 0.7663 | **0.8902** | 1.0143 | 1.1382 | 1.2622 |
| 2.438 GHz | 0.6443 | 0.7673 | **0.8902** | 1.0132 | 1.1362 | 1.2592 | 1.3821 |
| 2.458 GHz | 0.6463 | 0.7682 | **0.8902** | 1.0122 | 1.1342 | 1.2562 | 1.3781 |

The true unambiguous q-range value $d_{ABCD}$ for this scenario is 0.8902. This value is present in three sets of possible q-range values and is shown in boldface in table 5.1. The fact that it is present in all of the operating frequency's sets is how TAC solves this problem. In a practical implementation the table containing all possible q-range values would be searched using a algorithm to find the true q-range that occurs in each set.

**Step 9**

Steps two to nine are now repeated, using a different combination of transmitters and receivers in order to generate a new q-range $d_{ACBD}$ which is linearly independent from the previous one $d_{ABCD}$. This is done because hyperbolic trilateration, the method that is being used to process q-ranges into a NOI position requires two q-ranges that are calculated in this way. For this scenario antenna A continues to act as a transmitter and the NOI continues to act as a receiver, but antennas B and C exchange roles. Antenna B now acts as the idle receiver and antenna C acts as a transmitter. The value of the second q-range $d_{ACBD}$ is 1.2683 for this scenario.

**Step 10**

The two q-ranges, $d_{ABCD}$ and $d_{ACBD}$ are now fed into the algorithm for hyperbolic trilateration as given in subsection 3.3.1. The algorithm then determines the position of the NOI unambiguously as (12,7).

## 5.10   Chapter Conclusion

In this chapter a conceptual design was created for a device that would be able to independently locate other nodes in a network through the use of RIPS. Choices were made regarding what method of q-range processing would be used. From this choice the number of antennas to be used was derived as well as what the layout of these antennas would be. Hardware requirements were identified. The operation of the proposed system was presented in the form of a functional flow, which was explained further through the use of an example. Certain aspects such as what distance would separate the antennas, what q-range ambiguity solution would be used as well as the choice of operating frequency were left open for further investigation in this dissertation. In the next chapter, the detail design of a simulation model of the conceptual

design is presented.

# Chapter 6

# Detail Simulation Design

*In this chapter the design of the simulation model for the conceptual system is discussed. The simulation model's design is explained by firstly discussing the simulation model from the perspective of a high level overview. Next, the simulation model's design is broken down into lower level functional blocks, which are then discussed in further detail.*

## 6.1   Simulation Design

The simulation model is designed for implementation in MATLAB. This simulation model is designed with only Rician fading being taken into account. Hardware tolerances are not taken into account. A high level design of the simulation model can be seen in figure 6.1. This design segments the simulation into four discrete steps. Each of these four steps are now discussed in further detail.
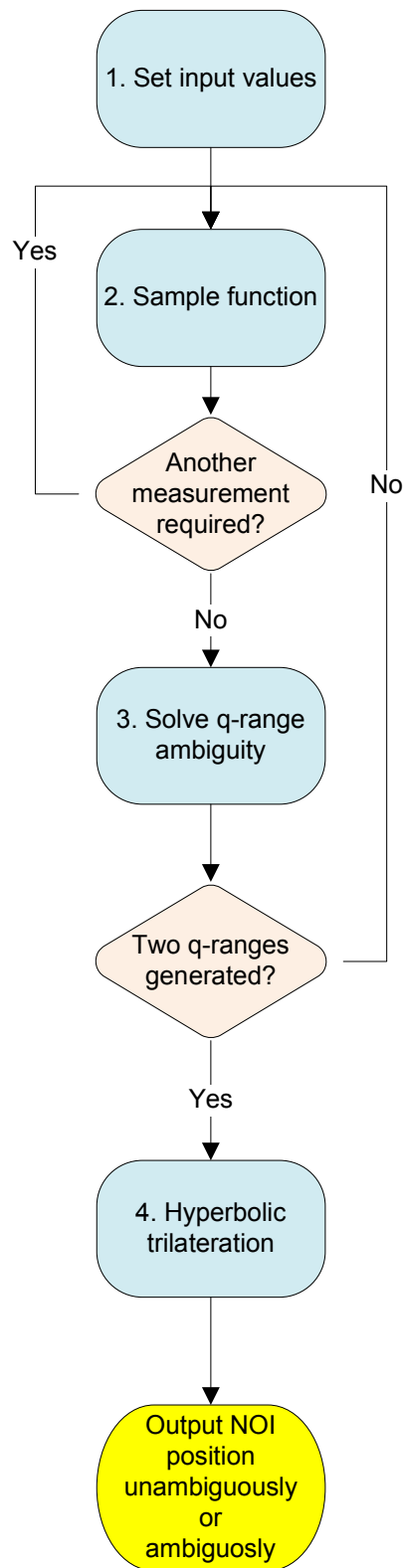
Figure 6.1: A high level design of the simulation model

### 6.1.1   Step 1: Simulation Model Inputs

In this step (step 1 in figure 6.1), all the values that are provided as inputs to the simulation model are set. The full list of inputs is given in table 6.1, along with descriptions of each input's purpose in the simulation model.

Table 6.1: List of inputs used in the simulation model

| Variable Name | Description |
| --- | --- |
| $F_A trans$ | Transmitted signal frequency from antenna A. |
| $F_B trans = F_A trans - Sigdiff$ | Transmitted signal frequency from antenna B. Derived from $F_A trans$ by subtracting $Sigdiff$. |
| $Sigdiff$ | Defines the frequency difference between $F_A trans$ and $F_B trans$. |
| $F_A$ | Mixed down version of the signal frequency from antenna A. |
| $F_B = F_A - Sigdiff$ | Mixed down version of the signal frequency from antenna B. Derived from $F_A$ by subtracting $Sigdiff$. |
| $F_C = \dfrac{F_A + F_B}{2}$ | Carrier frequency. Derived from transmitter frequencies. |
| $\lambda_C = \dfrac{C}{F_C}$ | Wavelength of the carrier frequency. |
| $samplerate$ | Receiver sample rate. |
| $samplelength$ | Length of time sampled. |
| $sampleres$ | The frequency resolution of the FFT |
| $bandsep$ | Separation between measurement frequencies. |
| $PosA$ | The position of antenna A in 2 dimensional Cartesian format. |
| $PosB$ | The position of antenna B in 2 dimensional Cartesian format. |
| $PosC$ | The position of antenna C in 2 dimensional Cartesian format. |
| $PosD$ | The position of the NOI in 2 dimensional Cartesian format. |

### 6.1.2   Step 2: Sample Function

The sample function (step 2 in figure 6.1), is called to generate a q-range. The q-ranges generated by this function are still ambiguous. Q-range ambiguity is solved in step

3. The variables listed in table 6.1 are all passed on to this function. This function is broken down further into steps that are shown in figure 6.2. These steps are explained in detail in the rest of this section.
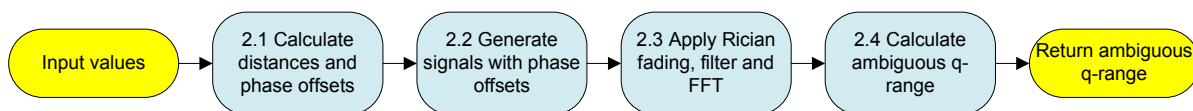


Figure 6.2: An illustration of the steps involved in the sample function

**Step 2.1**

In this step (step 2.1 in figure 6.2), the information regarding the positions of the antennas and the NOI is used to calculate the phase offsets of the transmitted signals at the receivers. This is done by calculating the distances between the antennas and the NOI and using this in conjunction with the wavelength of the signal in question. The calculations are given in algorithm 1. These calculations are repeated for distances $d_{AD}$ , $d_{BC}$ and $d_{BD}$.

---
**Algorithm 1** Step 2.1: Calculate phase offsets and distances
---
1: $d_{AC} = \sqrt{(posC_y - posA_y)^2 + (posC_x - posA_x)^2)}$

2: $phase_{AC} = -\pi\dfrac{Rem_{AC}}{\lambda_A} \rightarrow \{$Where $Rem_{AC}$ is the remainder of $\dfrac{d_{AC}}{\lambda_A}\}$

---

**Step 2.2**

Once all of the phase offsets have been calculated, the signal received by the NOI must be generated in this step (step 2.2 in figure 6.2). This is done by first generating a time series. The time series is an array that spans a length of time defined by the sample length input, at intervals defined by the sampling frequency. The signal is then created by determining the cosine function values for each value in the time series,

with the correct phase offset taken into account. Algorithm 2 shows this process for the interference signal measured at the NOI, in this case denoted as D.

---

**Algorithm 2** Step 2.2: Generate time series and signal at NOI

1: $t_C = 0 : \dfrac{1}{samplerate} : samplelength - \dfrac{1}{samplerate}$

2: $signal_D = cos(2\pi F_A t_D + phase_{AD}) + cos(2\pi F_B t_D + phase_{BD})$

---

**Step 2.3**

In this step (step 2.3 in figure 6.2), Rician fading is applied to the interference signal measured at the NOI (D), using the MATLAB `ricianchan` object. Next the interference signal is rectified using the MATLAB `abs` function. This is done in order to make the envelope frequency visible. The signal is then filtered using a low pass FIR filter created with the MATLAB `fir1` function. The cut off frequency of the filter is determined by the envelope frequency created by the interference signal. This filter is implemented in such a way that it does not have an affect on the phase of the signal, using the MATLAB `filtfilt` function. The FFT of the signal measured at the NOI is then calculated. All these steps are shown in algorithm 3.

---

**Algorithm 3** Step 2.3: Apply fading, rectify, filter, calculate FFT

1: $channel = ricianchan(samplelength, 0, 1000000)$

2: $signal_D = filter(channel, signal_D)$

3: $signal_D = abs(signal_D)$

4: $b = fir1(3, \frac{2Sigdiff}{samplerate/2})$

5: $signal_D = filtfilt(b, 1, signal_D)$

6: $n_{FFT} = 1/sampleres + 1/samplerate$

7: $fourier_D = fft(signal_D, n)$

---

**Step 2.4**

In this step (step 2.4 in figure 6.2), the value of the envelope signal's phase at node C is now calculated theoretically. The envelope signal's phase value measured at the NOI is calculated from the result of its measured signal's FFT. The difference of the interference signal's phase angles is then used to determine the ambiguous q-range as is shown in algorithm 4. Note that the phase value measured at the NOI is subtracted from the theoretically calculated phase value for antenna C.

---

**Algorithm 4** Step 2.4: Determining ambiguous q-range

1: $phase_C = phase_{AC} - phase_{BC}$

2: $phase_D = angle(fourier_D)$

3: $phase_{Dmeasured} = phase_D((fA - fB)/sampleres + 1)$

4: $phase_{ABCD} = phase_{Ccalulated} - phase_{Dmeasured}$

5: $q - range = phase_{ABCD}\dfrac{\lambda_C}{\pi}$

---

## 6.1.3   Step 3: Solution of q-range ambiguity

This step (step 3 in figure 6.1), is used to solve q-range ambiguity. In this step there is a choice between using either TAC or Same $k$, to solve q-range ambiguity. Therefore this step is further broken down as shown in figure 6.3.
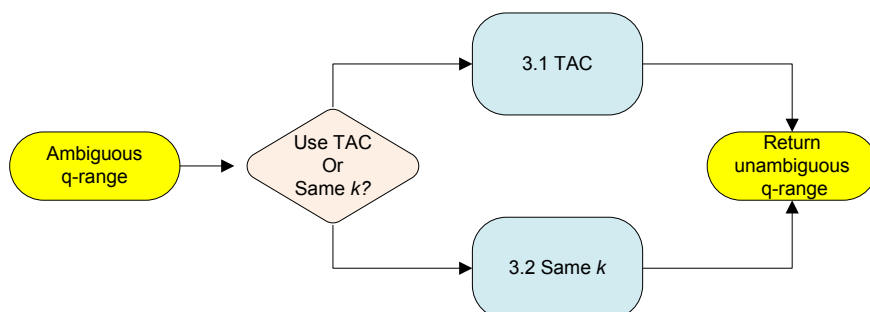


Figure 6.3: An illustration of two choices available for solving q-range ambiguity

**Step 3.1: TAC**

TAC is further broken down into steps, as can be seen in figure 6.4.
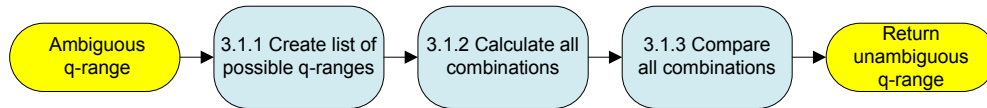


Figure 6.4: An illustration of the steps involved in TAC

**Step 3.1.1: Create List of Possible Q-ranges**

This step (step 3.1.1 in figure 6.4), creates a list of all the possible values for the ambiguous q-ranges that are obtained through using step 2 (the sample function) repeatedly.

This is done by firstly defining the range of possible q-range values, thereby creating a limit for the possible values of $n$. Now multiple measurements are made using step 2 (the sample function), multiple times. Each time a different frequency from a predefined set of transmitter frequencies is used. The ambiguous q-ranges obtained from these measurements are used in (3.16) to create a list of all possible q-ranges values for each transmitted frequency, with the values of $n$ that are possible used as bounds. The pseudo code for step 3.1.1 is given in algorithm 5.

---

**Algorithm 5** Step 3.1.1: Creation of a list of possible q-range values

---

1: $q_{min} = -d_{AB} + d_{BC} - d_{AC}$

2: $q_{max} = +d_{AB} + d_{BC} - d_{AC}$

3: $n_{min} = \frac{q_{min}}{\lambda_C} + 1$

4: $n_{max} = \frac{q_{max}}{\lambda_C} + 1$

5: **for** $i = 0$ to *measnum* **do**

6:     $qrangeAmbiguous = sample(variables)$

7:     $\lambda = \dfrac{C}{F_A transbandsep - \dfrac{sigdiff}{2}}$

8:     **for** $n = n_{min}$ to $n_{max}$ **do**

9:        $measTable(m + 1, n + nmax + 1) = qrangeAmbiguous + n\lambda$

10:    **end for**

11: **end for**

---

**Step 3.1.2: Calculate All Combinations**

This step (step 3.1.2 in figure 6.4), involves calculating all the combinations of values that are possible by taking a value from each measurement's set of possible q-range values. These combinations are all then stored in a table. One of these combinations then only contains values that are equal to the unambiguous q-range. These values are not exactly the same due to errors caused by sampling and Rician fading. The number of combinations can grow impractically large, as can be seen from equation 6.1.

$$n_{possible} = (abs(nmin) + nmax + 1)^{measnum} \tag{6.1}$$

Therefore only combinations are calculated that have values that that differ less than a specified maximum allowed value. By filtering the table of possible sets in such a way its size is easily controlled. The pseudo code for step 3.1.2 is shown in algorithm 6, which is a recursive function.

---

**Algorithm 6** Step 3.1.2: Calculation of all combinations

1:  *function combination*(*variables*)

2:  *global* = *keepercount keeper*

3:  *meascurrent* = *meascurrent* + 1

4:  **for** *n*1 = *nmin* to *nmax* **do**

5:      **if** *meascurrent* == 1 **then**

6:          *keepercurrent*(*meascurrent*) = *meastable*(*meascurrent*, *n* − *nmin* + 1)

7:          **if** *meascurrent* == *measnum* **then**

8:              *keeper*(*keepercount*, :) = *keepercurrent*

9:              *keeprercount* = *keepercount* + 1

10:         **end if**

11:         **if** *meascurrent* < *measnum* **then**

12:             *combination*(*variables*)

13:         **end if**

14:     **else** **if** *abs*(*meastable*(*meascurrent* − 1, *ncalled* − *nmin* + 1) − *meastable*(*meastable*, *n* − *min* + 1) < 0.01 **and** *meascurrent* <= *measnum* **then**

15:         *keepercurrent*(*meascurrent*) = *meastable*(*meascurrent*, *n* − *nmin* + 1)

16:         **if** *meascurrent* == *measnum* **then**

17:             *keeper*(*keepercount*, :) = *keepercurrent*

18:             *keeprercount* = *keepercount* + 1

19:         **end if**

20:         **if** *meascurrent* < *measnum* **then**

21:             *combination*(*variables*)

22:         **end if**

23:     **end if**

24: **end for**

**Step 3.1.3: Compare all Combinations**

The final step (step 3.1.3 in figure 6.4), finds the combination that has the smallest variance. This is simply done by going through all the combinations, calculating each combination's variance and keeping the combination with the smallest variance. The average value of this combination is then used as the true unambiguous q-range. The pseudo code for step 3.1.3 is given in algorithm 7.

---

**Algorithm 7** Step 3.1.3: Comparison of all Combinations

---

  $min = var(keeper(1,:))$

  **for** $k = 1$ **to** $keepercount - 1$ **do**

    **if** $var(keeper(k,:)) < min$ **then**

      $min = var(keeper(k,:))$

      $qrangeTrue = mean(keeper(k,:))$

    **end if**

  **end for**

---

**Step 3.2: Same $k$**

Same $k$ (step 3.2 in figure 6.3) is simpler to implement than TAC. Firstly a measurement is made using step 2 from figure 6.1, with a transmitter frequency of 60 MHz. The q-range value resulting from this measurement is then checked to see if it exceeds the bounds of possible q-range values. If it does not it is used without any alteration. If it does exceed these bounds, a new measurement is made using a transmitter frequency of 70 MHz. For Same $k$ q-range ambiguity occurs in circular bands around the transmitter antenna. These bands have a maximum width equal to the distance separating the two transmitter antennas and occur at intervals equal to the wavelength of the transmitter frequency. By correctly choosing the transmitter frequencies that are used so that all of them do not overlap at once for the maximum communication range an unambiguous q-range can always be obtained. The pseudo code for Same $k$ is shown in algorithm 8.

---

**Algorithm 8** Step 3.2: Same $k$

---

$qrange = sample(variables)$

**if** $qrange < min$ **or** $qrange > max$ **then**

   $F_A trans = newfreq$

   $F_B trans = F_A trans - Sigdiff$

   $qrange = sample(variables)$

**end if**

---

## 6.1.4   Step 4: Hyperbolic Trilateration

This step (step 4 in figure 6.1), processes the q-ranges into usable NOI positions. Hyperbolic trilateration is used to process the measured q-ranges into an actual NOI position. This method requires two q-ranges to function. The algorithm is given in algorithm 9 and is based on the version of hyperbolic trilateration discussed in section 3.3.1.

---

**Algorithm 9** Step 4: Hyperbolic Trilateration

---

1: **function** $posStruct = trilat(d_{ABCD}, d_{ACBD}, PosA, PosB, PosC)$

2: $d_{AC} = \sqrt{(posC_y - posA_y)^2 + (posC_x - posA_x)^2}$

3: $d_{BC} = \sqrt{(posC_y - posB_y)^2 + (posC_x - posB_x)^2}$

4: $d_{AB} = \sqrt{(posB_y - posA_y)^2 + (posB_x - posA_x)^2}$

5: $m1 = d_{AC} - d_{BC} + d_{ABCD}$

6: $m2 = d_{AB} - d_{CB} + d_{ACBD}$

7: $m = [m1; m2]$

8: $s = [PosB_x, PosB_y; PosC_x, PosC_y]$

9: $z = 0.5[PosB_x^2 + PosB_y^2 - m1^2; PosC_x^2 + PosC_y^2 - m2^2]$

10: $A = s^-1z$

11: $B = s^-1m$

12: $Ans = B'B$

13: **if** $Ans < 1$ **then**

14:   $d_{AD} = \dfrac{\sqrt{(A'B)^2 - (B'B - 1)} + A'B}{1 - B'B}$

15:   $PosD = A + Bd_{AD}$

16: **end if**

17: **if** $Ans > 1$ **then**

18:   $d_{AD1} = \dfrac{-\sqrt{(A'B)^2 - (B'B - 1)} - A'B}{B'B - 1}$

19:   $d_{AD2} = \dfrac{\sqrt{(A'B)^2 - (B'B - 1)} - A'B}{B'B - 1}$

20:   $PosD_1 = A + Bd_{AD1}$

21:   $PosD_2 = A + Bd_{AD2}$

22: **end if**

---

## 6.2   Chapter Conclusion

In this chapter a detail design was presented for a simulation model of the conceptual design presented in chapter 5. This detail design was presented in the form of a high level overview which was then broken down into sections that were presented

by means of pseudo code algorithms. Before this simulation model can be used in experiments it must first be verified and validated. This is the focus of chapter 7.

# Chapter 7

# Validation and Verification

*In this chapter the simulation model presented in chapter 6, is validated and verified. This is done in three stages. Firstly, the basic theory that the simulation is based on, the simulation's logic, causal- and mathematical-relationships as well as assumptions made are validated. Next, the implementation of the simulation is verified by showing that the outputs of each of its steps are correct. Lastly, the simulation model's outputs are validated by showing that they are accurate enough for the purposes of this dissertation.*

Before the simulation model can be used in experiments, it must first be validated and verified. This is done to ensure that the results obtained from the experiments can be trusted. The process of validation and verification followed in this chapter is based on an article written specifically on the validation and verification of simulation models [12]. This paper divides the process of the validation and verification of a simulation model into three parts:

- Conceptual model validation;

- Computerised model verification;

- Operational validation.

The term conceptual model can be described as the simulation model before it has been implemented on a computer. It encompasses all of the theories and assumptions that the model is based on, as well as the manner in which these theories and assumptions are logically linked together to create the simulation model. Validating the conceptual model entails proving that the theories used are correct and correctly implemented, showing that the assumptions that were made are reasonable and that the logic, causal- and mathematical-relationships are reasonable for the intended purpose of the simulation model. [12]

Computerised model verification is the process of testing whether the conceptual model has been correctly programmed on a computer. In [12], a distinction is made between the verification of implementations in simulation languages such as MATLAB and the verification of implementations in high level programming languages such as C++ and FORTAN.

Verification of simulation languages entails checking if the functions and models of the simulation language can be accepted as correct and whether the simulation model is programmed correctly. When a high level language is used then it should be checked for proper software engineering techniques such as structured programming, program modularity and object oriented design. Simulation models written in high level languages must also be tested to verify that the model is programmed correctly. [12]

Finally, operational validation involves proving that the simulation model's outputs are accurate enough for its intended purpose [12].

These steps are now followed to validate and verify the simulation model described in chapter 6.

## 7.1 Conceptual Model Validation

In this section the ideas behind the simulation model before implementation are validated. This section is further divided into sections for theories, assumptions and finally logic, mathematical- and causal-relationships.

### 7.1.1 Theorems

The four theorems that are validated concern the working of RIPS with the first three of these provided in [7] and the final provided in [21].

Theorem 1: Let $f_B < f_A$ be two close carrier frequencies with $\delta = (f_A - f_B)/2\delta << f_B$ and $2\delta < f_{cut}$. Furthermore assume that a node receives the radio signal
$$s(t) = a_A cos(2\pi f_A t + \varphi_1) + a_B cos(2\pi f_B t + \varphi_2) + n(t)$$
where $n(t)$ is Gaussian noise. Then the filtered RSSI signal $r(t)$ is periodic with a fundamental frequency of $f_A - f_B$ and absolute phase offset $\varphi_A - \varphi_B$. [7]

The proof for this theorem is given in [7]. It can be shown that the simulation conforms to the requirement set by this theorem by referring back to table 6.1. In table 6.1 the transmission frequency of antenna B is defined as $f_B = f_A - 2\delta$, this is in line with the requirements of $f_B < f_A$ and $\delta = (f_A - f_B)/2$. Since $f_A$ is in the range of either gigahertz or megahertz and $\delta$ is in the range of kilohertz the requirement of $\delta << f_B$ is also met.

Theorem 2: Assume two nodes A and B transmit pure sine waves at two close frequencies $f_A > f_B$ such that $f_A - f_B < f_{cut}$ and two other nodes C and D measure the filtered RSSI signal. Then the relative phase offset of the signals received at nodes C and D is then
$$2\pi \left( \frac{d_{AD} - d_{AC}}{\lambda_A} + \frac{d_{BC} - d_{BD}}{\lambda_B} \right) (mod 2\pi) \text{ [7]}$$

The proof of this theorem is given in [7]. The requirements are the same as those of the previous theorem and have already been shown to have been met.

Theorem 3: Assume that two nodes A and B transmit pure sine waves at two close frequencies $f_A > f_B$ and two other nodes C and D measure the filtered RSSI. If $f_A - f_B < 2$ kHz and $d_{AC}, d_{AD}, d_{BC}, d_{BD} < 1$ km then the relative phase offset of the signals measured at nodes C and D is.

$$2\pi \frac{d_{AD} - d_{BD} + d_{BC} - d_{AC}}{\lambda_{carrier}} (mod2\pi)$$

where $\lambda_{carrier}$ is the wavelength of the frequency $f_{carrier} = \frac{f_A + f_B}{2}$. [7]

The proof of this theorem is given in [7]. In the simulation the difference between the two transmitted frequencies $\delta$ can be set to any value and can therefore simply be given any value that complies with the requirement of $\delta < 2$ kHz set in this theorem. The theorem also requires that distances between the nodes, or in this case antennas be less that 1 km. The idea for this dissertation is to use antennas mounted on the same device as nodes. The distances separating the antennas has been left open for investigation, but it can be safely assumed to be less than 1 km. In practice the maximum localisation range achieved by RIPS thus far is 160 m [8]. Therefore this requirement is also met. The rest of the requirements are the same as those of the previous two theorems and have already been shown to have been met.

The next theorem concerns how combinations of nodes are chosen to create sets of linearly independent q-ranges.

Theorem 4: The dimension of the vector space spanned by the measurements $d_{ABCD}$ on a set of $n$ nodes, $n > 3$ is $n(n-3)/2$ [21].

Thus in the case of the conceptual device where there are three antennas and one NOI $n$, equals four. According to the theorem this means that is possible to make two lin-

early independent q-range measurements. The proof for theorem 4 is provided in [21]. The choice of which antennas are used to transmit or receive can be made by referring to the proof of this theorem. In the proof all possible combinations of nodes for q-ranges are divided into classes. For this case only classes zero and one apply. These classes are defined as

$$Class0 : \{012D|2 < D\} \text{ containing } n - 3 \text{ elements;}$$
$$Class1 : \{0B1D|1 < B < D\} \text{ containing } (n - 2)(n - 3)/2 \text{ elements; [21]}$$

Using these classes only two combinations of nodes are possible, $d_{ABCD}$ and $d_{ACBD}$. These are the combinations chosen in the conceptual design.

Thus proofs of the theorems used have been provided and it has been shown that these theorems are applied correctly and are therefore valid in the simulation model.

## 7.1.2 Assumptions

In the simulation model two assumptions are made. Firstly, it is assumed that the transmitted signals propagate at the speed of light in free space. Defined as

$$c = 299{,}792{,}458 \text{ m/s}$$

Since the signal passes through air this is a good approximation [15]. Therefore this assumption can be seen as reasonable.

The second assumption made is that Rician fading would apply in the case being studied. Rician fading models multipath fading with a dominant line of sight component [31]. In other words the signal travels along a direct path from transmitter to receiver. This is important because the phase shifts in RIPS are defined by assuming that the measured signal travelled along a straight path.

Thus it can be concluded that the assumptions made for this simulation are reasonable for the intended purpose of the simulation model and are therefore valid.

### 7.1.3   Logic, Causal- and Mathematical-Relationships

The first step in the conceptual model is to define all the variables used in the model. This is done according to the requirements of the theorems discussed in section 7.1.1. The next step is given in algorithm 1 of chapter 6. In the first line, the positions of the antennas and NOI are used to calculate the distances that make up the q-range. The formula used is the standard formula to calculate distance between two points in a two dimensional Cartesian space given the positions of the points. The distances calculated are then used along with the wavelengths of the two transmitted frequencies to calculate the absolute phase offsets at the receiving NOI and antenna in line 2 of the algorithm. The formula used works by calculating the remainder from diving the distance between the transmitting antenna and receiving antenna/node by the wavelength of the transmitted frequency. This remainder value is then divided by the wavelength in question, giving the proportion of the wavelength that was completed. The result of this is then multiplied by $-\pi$ to transform it into radians. A value of one $\pi$ is used instead of two because the FFT function used later on only returns phase angle values up until $\pi$. This is compensated for when the still ambiguous q-range is calculated from the relative phase offset between the two receivers by dividing the relative phase offset by $\pi$ instead of $2\pi$.

The next step is shown in algorithm 2 of chapter 6. In the first line a time series is created. The separation of points in this time series represents period of the sampling frequency used and its length represents the sample time. In the second line the calculated phase values are then used to define a mixed down version of the interference signal measured at the NOI, the values of which are calculated for each point in the time series. This formula for the mixed down version of the signal is given in [7]. In

this formula it is assumed that the mixing did not have an effect on the phase offsets and since this formula comes from a published, peer reviewed paper it can be accepted as reasonable.

Once the interference signal at the NOI has been calculated this signal is subjected to Rician fading, rectified and filtered. The FFT of the signal measured at the NOI is then calculated. This is done as shown in algorithm 3 of chapter 6. All of this is done using verified MATLAB functions.

In line one of algorithm 4 of chapter 6, the phase of the envelope signal at the idle receiver is calculated theoretically. The envelope signal's phase measured at the NOI is calculated from the signal's FFT in lines two to three. Now that the absolute phase of the interference signal at each of the receivers has been measured, the relative phase offset is calculated by simply calculating difference between the phases. As shown in line four of algorithm 4. In the fifth line the still ambiguous q-range is calculated using the relative phase offset. The formulas used for these calculations have been taken from [7], a published peer reviewed article and can therefore be accepted as correct.

Now the ambiguity in the q-range must be solved. The simulation model is able to do this in two ways, either by using TAC given in [8] or by using Same *k* given in [28]. Both of these methods are discussed in chapters 3 and 4

If TAC is used, the previous steps are repeated a number of times using a different transmission frequency each time and recording each iteration's ambiguous q-range value. Once this has been done all the possible values of each q-range are calculated and stored as a matrix. The limit of possible values for a case with three stationary measurement points in RIPS is defined and proven in section 3.3.1 of chapter 3 and implemented in algorithm 5. This limit is used to calculate all the possible values for each q-range given the wavelength of the carrier signal as shown in lines one to four of algorithm 5. All the sets of possible values for each measurement's q-range are then compared as shown in algorithm 6. This algorithm compiles a list of sets of values,

one from each measurement that differ by less than a specified maximum difference. This difference is used to filter the number of combinations of q-ranges values that are generated. This is necessary, since calculating every possible combination would be too computationally demanding. Once this list has been compiled it is searched for the combination of q-range values that has the smallest variance in algorithm 7. There is of course a chance that there could be more than one value occurring in each set, possibly resulting in incorrect yet similar q-range values having the smallest variance. However, if several measurements are made the chances of this are unlikely [8].

Same $k$ is simpler. It is shown in algorithm 8 of chapter 6. In line one of the algorithm the q-range is checked so see if it is within the limits of possible values defined in 3.3.1 of chapter 3. If it is within these bounds it is used without any alteration. If it is outside these bounds the measurement is repeated using another transmitter frequency with a wavelength that is of such a nature that its ambiguity areas as defined in chapter 4, do not overlap with those of the previous transmitter frequency used. The new q-range resulting from this is then used without any alteration.

The entire process up until now is repeated twice each time with a different combination of transmitters and receivers as defined by theorem 4. These two q-ranges are then processed using hyperbolic trilateration as shown in algorithm 9. Hyperbolic trilateration is a well known method of processing localisation data [16] and this algorithm has been tested in two peer reviewed and published papers [24, 25]. Therefore the logic, mathematical- and causal-relationships that the algorithm is comprised of can be viewed as sound. The algorithm is fed two linearly independent q-ranges according to the algorithms requirements and therefore the algorithm's incorporation into the simulation model can be seen as reasonable for the intended purpose of the model.

**Conclusion**

In this section the conceptual model has been validated. The theory on which the simulation model is based has been shown to be true and correctly implemented. The assumptions that are made have been shown as reasonable as well as the simulation model's logic, mathematical- and causal-relationships. Therefore it can be concluded that the conceptual model is valid according to the requirements set in [12].

## 7.2   Computerised Model Verification

The computerised model is verified by checking if it was programmed correctly in line with what was set out in the conceptual model [12]. In this section this is done by testing each algorithm presented in chapter 6 to see whether the algorithm's outputs correlate with what can be be expected according to the conceptual design. The inputs and their values are listed in table 7.1 and were defined according to table 6.1 in chapter 6.

Table 7.1: List of input values used

| Variable Name | Value |
|---|---|
| $C$ | 299,792,458 m/s |
| $F_A trans$ | 5.180 GHz |
| $F_B trans$ | $F_B trans = F_A trans - Sigdiff$ |
| $Sigdiff$ | 1.990 kHz |
| $F_A$ | 30 kHz |
| $F_B$ | $F_B = F_A - Sigdiff$ |
| $F_C$ | $F_C = \dfrac{F_A + F_B}{2}$ |
| $\lambda_C$ | $\lambda_C = \dfrac{C}{F_C}$ |
| $samplerate$ | 100 kHz |
| $samplelength$ | 4 ms |
| $sampleres$ | 10 Hz |
| $bandsep$ | 20 MHz |
| $measnum$ | 6 |
| $PosA$ | (0,0) |
| $PosB$ | (0,1) |
| $PosC$ | (1,0) |
| $PosD$ | (5,5) |

## Algorithm 1

The outputs generated by the computer implementation of algorithm 1 are shown in figure 7.1. The results of calculating these outputs by hand using the formulas used in algorithm 1, are shown in table 7.2. By comparing the values in figure 7.1, with those in table 7.2 the computer implementation of algorithm 1 is verified as correct. The differences in the values can be explained as the result of different methods of rounding being used.
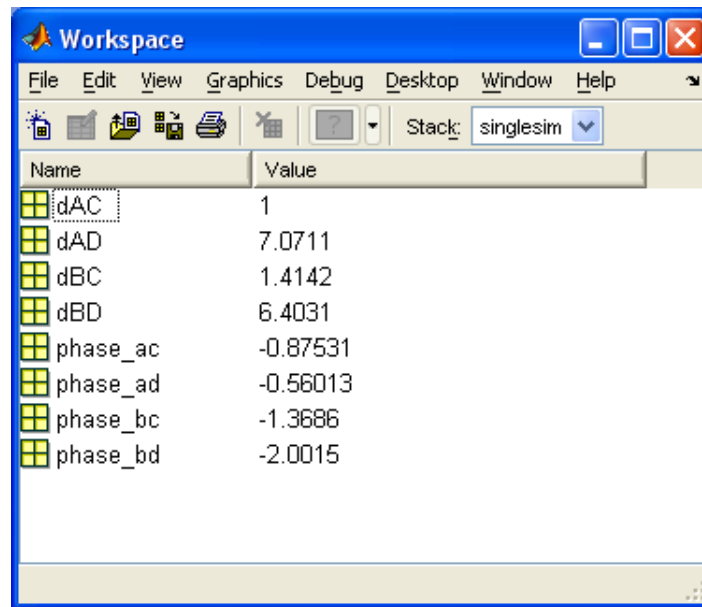
Figure 7.1: Simulation model outputs for algorithm 1

Table 7.2: Expected outputs for algorithm 1

| Variable Name | Value |
|---|---|
| dAC | 1 |
| dAD | 7.071 |
| dBC | 1.414 |
| dBD | 6.403 |
| phase_ac | -0.875 |
| phase_ad | -0.556 |
| phase_bc | -1.368 |
| phase_bd | -2.000 |

## Algorithm 2

The output generated by the computer implementation of algorithm 2 is shown in figure 7.2. In this figure the envelope frequency is seen to present at 1.990 kHz in its still unrectified form, having both positive and negative amplitudes. This is the output that is expected from the correct implementation of algorithm 2. The shape of the signal in the output can be further verified by referring to images of the unrectified envelope frequency shown in [7, 8]. This output correlates with expected results as

well as images given in [7,8] and can therefore be verified as correct.
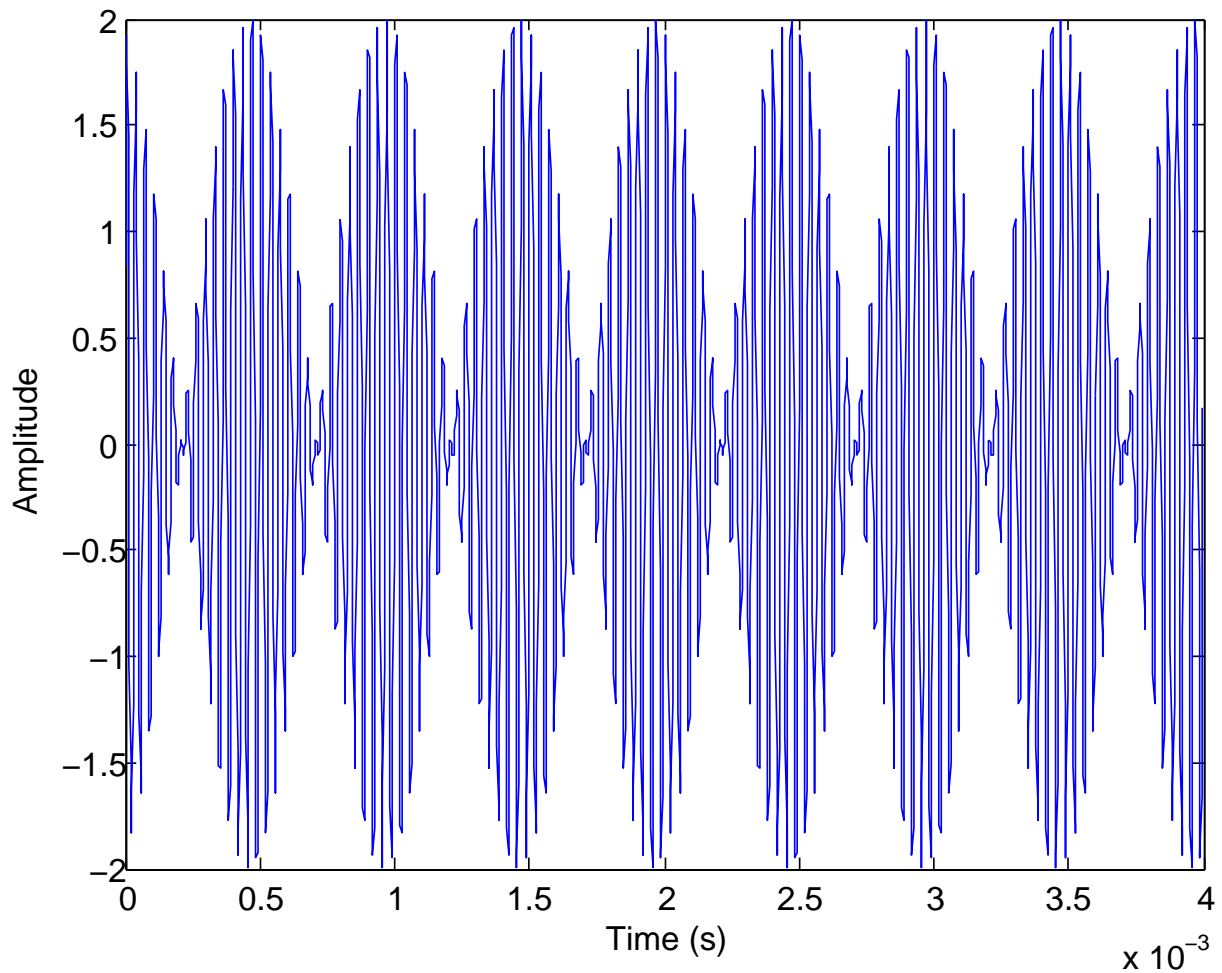


Figure 7.2: Simulation model outputs for algorithm 2

## Algorithm 3

The output generated by the computer implementation of the first five lines of algorithm 3 is shown in figure 7.3. The output shows that the first part of the algorithm behaves as expected. By looking at the amplitude of the signal it can be seen that the fading that was applied had an effect. The shape of the waveform is what can be expected from rectification and the blank areas at the base of each waveform shows that the filter worked correctly. This part of the implementation can be verified as correct.
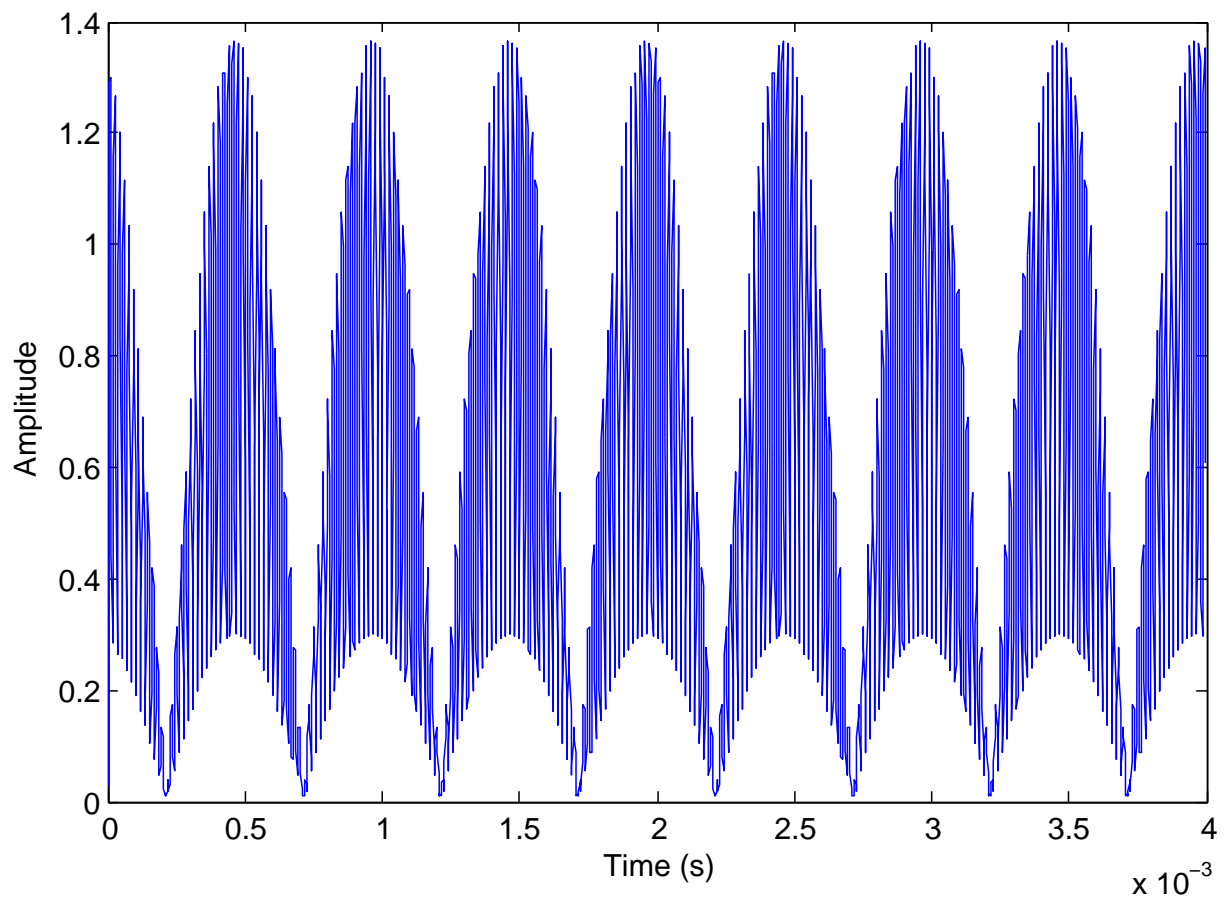
Figure 7.3: Simulation model outputs for the first five lines of algorithm 3

The output of the FFT function (line seven in algorithm 3) is shown in figure 7.4. This shows the envelope frequency present at 1.990 kHz, where it should be according to RIPS literature [7, 8]. The large component at the beginning of the spectrum is caused by sampling. This output further verifies the implementation up until now as correct.
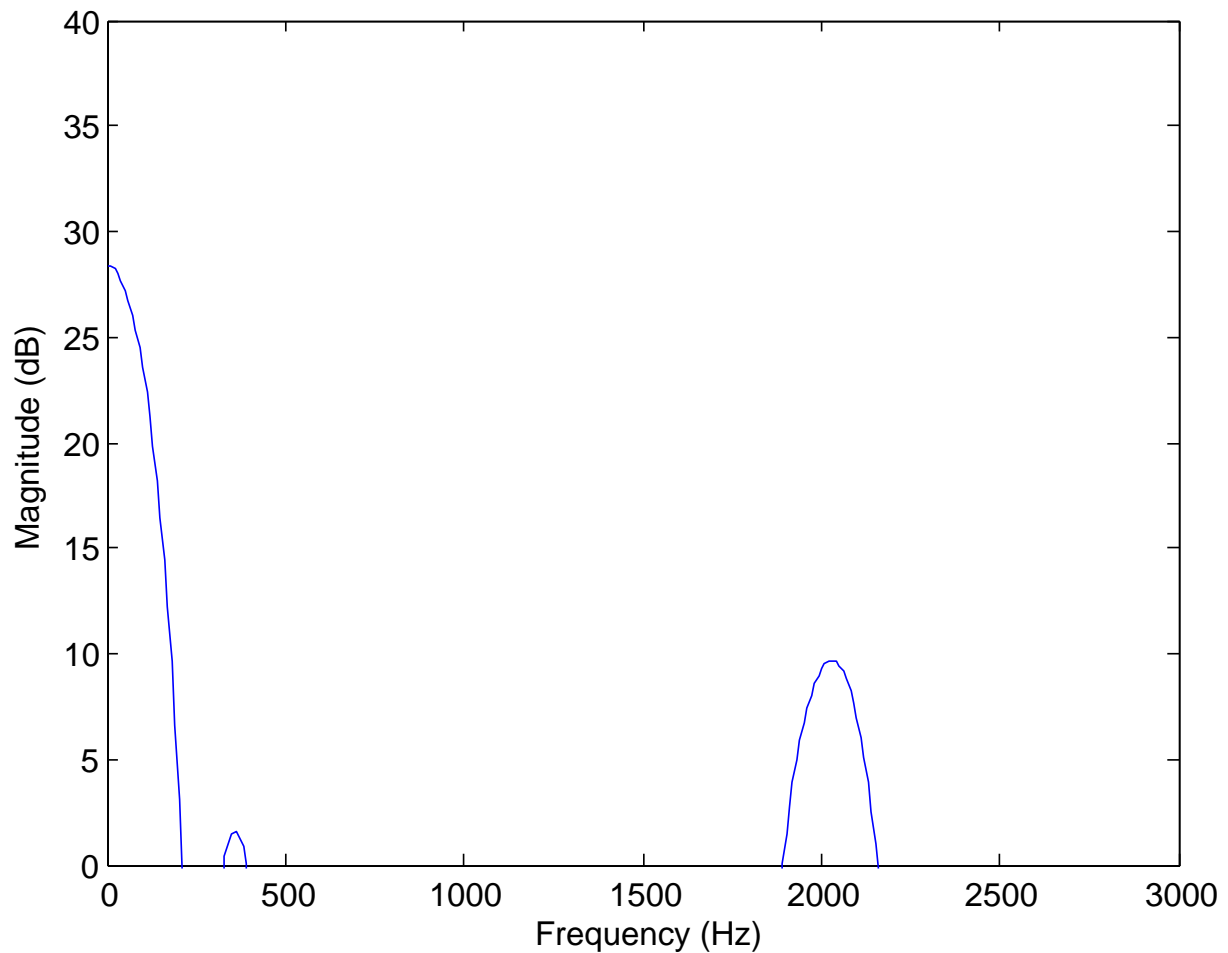
Figure 7.4: Magnitude plot of FFT from simulation model outputs for line seven in algorithm 3

## Algorithm 4

The output of the computer implementation of algorithm 4 is shown in figure 7.5. The results of calculating these outputs by hand using the formulas used in algorithm 4, are shown in table 7.3. By comparing the values in figure 4, with those in table 7.3, the computer implementation of algorithm 4 is verified as correct. The differences in the values can be explained as the result of different methods of rounding being used and the effects of sampling and Rician fading.
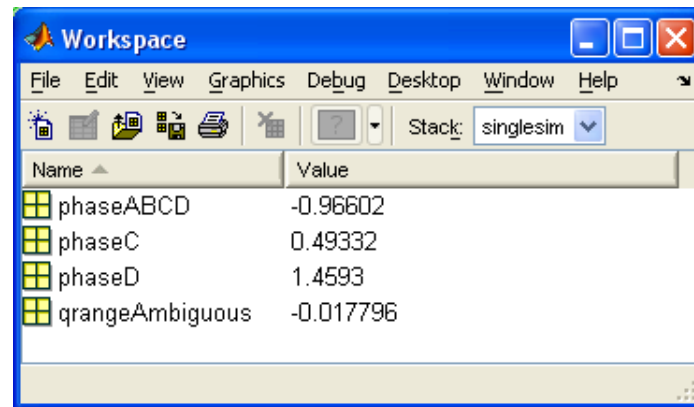
Figure 7.5: Simulation model outputs for algorithm 4

Table 7.3: Expected outputs for algorithm 4

| Variable Name | Value |
|---|---|
| phaseABCD | -0.949 |
| phaseC | 0.493 |
| phaseD | 1.443 |
| qrangeAmbiguous | 0.017 |

## Algorithm 5

The output of the computer implementation of algorithm 5 is shown in figure 7.6. The output of the first four lines of algorithm 5 calculated by hand are shown in table 7.4. The hand calculated output of the first four lines of algorithm 5 correlate with the output of the computer implementation. The differences between the values can be explained by different methods of rounding being used. The variable meastable1 is the list containing each measurement's set of possible q-range values. Using the number of measurements, given in table 7.1 as 6 with the range of possible values for $n$ the correct dimensions for this list can be calculated. With a range of possible values for $n$ from -11 to 25, there are 37 possible q-range values for each measurement (zero is also counted). With six measurements and 37 possible q-range values for each measurement, the dimensions of the list should be $6 \times 37$. This correlates with the dimensions of meastable shown in figure 7.6.
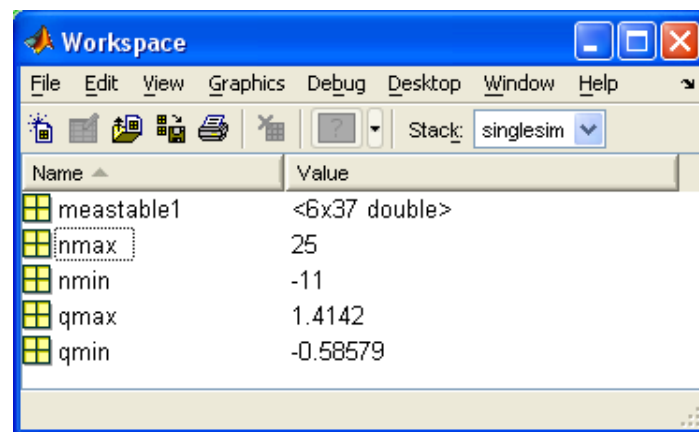
Figure 7.6: Simulation model outputs for algorithm 5

Table 7.4: Expected outputs for the first four lines of algorithm 5

| Variable Name | Value |
|---|---|
| nmax | 25 |
| nminC | -11 |
| qmax | 1.4142 |
| qmin | -0.5858 |

A section of the table's contents are shown in figure 7.7. The possible q-range value all differ by multiples of $\lambda_C$, which is correct. The unambiguous q-range value has a value of 1,082,157, when calculated by hand using the definition of the q-range given in (3.13). This value can be seen can be seen in column 31 of all six the measurements except for the second where it can be found at column 30.
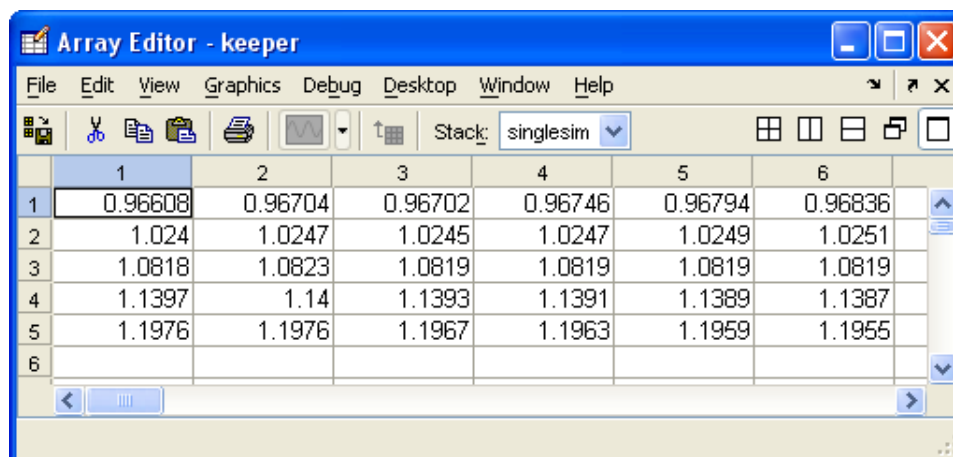
| | 27 | 28 | 29 | 30 | 31 | 32 | 33 | 34 | 35 |
|---|---|---|---|---|---|---|---|---|---|
| 1 | 0.85033 | 0.9082 | 0.96608 | 1.024 | 1.0818 | 1.1397 | 1.1976 | 1.2555 | 1.3133 |
| 2 | 0.90938 | 0.96704 | 1.0247 | 1.0823 | 1.14 | 1.1976 | 1.2553 | 1.313 | 1.3706 |
| 3 | 0.85216 | 0.90959 | 0.96702 | 1.0245 | 1.0819 | 1.1393 | 1.1967 | 1.2542 | 1.3116 |
| 4 | 0.85303 | 0.91024 | 0.96746 | 1.0247 | 1.0819 | 1.1391 | 1.1963 | 1.2535 | 1.3107 |
| 5 | 0.85395 | 0.91095 | 0.96794 | 1.0249 | 1.0819 | 1.1389 | 1.1959 | 1.2529 | 1.3099 |
| 6 | 0.8548 | 0.91158 | 0.96836 | 1.0251 | 1.0819 | 1.1387 | 1.1955 | 1.2523 | 1.309 |
| 7 | | | | | | | | | |

Figure 7.7: Simulation model's contents of the meastable variable from algorithm 5

These outputs are correct thus the implementation of algorithm 5 can be verified as correct.

## Algorithm 6

The output of the implementation of algorithm 6 is given in figure 7.8. It shows the contents of the table generated by algorithm 6. The sets of q-range values are all valid combinations and all the values contained in the sets differ by less than the maximum allowed difference specified in algorithm 6. The unambiguous q-range can be seen in row 3. This correlates with what is expected from algorithm 6. This output is correct and this algorithm can therefore be validated as being correct.
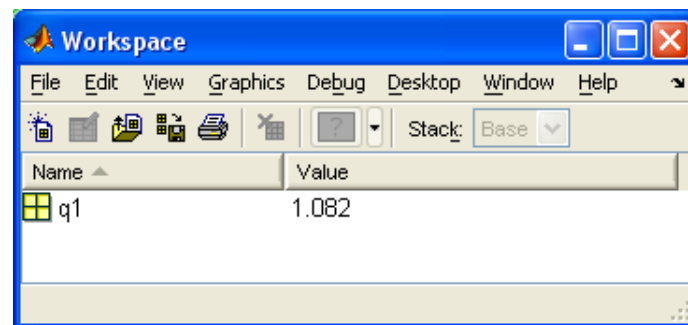
Figure 7.8: Simulation model's contents of the keeper variable from algorithm 6

## Algorithm 7

Algorithm 7 only has a single output, the true unambiguous q-range. This output is given in figure 7.9.



Figure 7.9: Simulation model outputs for algorithm 7

This value correlates with the value of the q-range calculated by hand, which is 1,082,157. Therefore the implementation of algorithm 7 can be verified as being correct.

## Algorithm 8

Same $k$ functions in a different manner from TAC. Because of this a slightly different set of input values are required. A list of input values used for this test is given in table 7.5.

Table 7.5: List of input values used for Same $k$

| Variable Name | Value |
|---|---|
| $C$ | 299,792,458 m/s |
| $F_A trans$ | 60 MHz |
| $F_B trans$ | $F_B trans = F_A trans - Sigdiff$ |
| $Sigdiff$ | 1.990 kHz |
| $F_A$ | 30 kHz |
| $F_B$ | $F_B = F_A - Sigdiff$ |
| $F_C$ | $F_C = \dfrac{F_A + F_B}{2}$ |
| $\lambda_C$ | $\lambda_C = \dfrac{C}{F_C}$ |
| $samplerate$ | 100 kHz |
| $samplelength$ | 4 ms |
| $sampleres$ | 10 Hz |
| $bandsep$ | 10 MHz |
| $PosA$ | (0,0) |
| $PosB$ | (0,1) |
| $PosC$ | (1,0) |
| $PosD$ | (5,5) |

The *measnum* variable is omitted from this list because it does not apply for Same $k$. The q-range value output by the computer implementation of algorithm 8 is shown in figure 7.10.
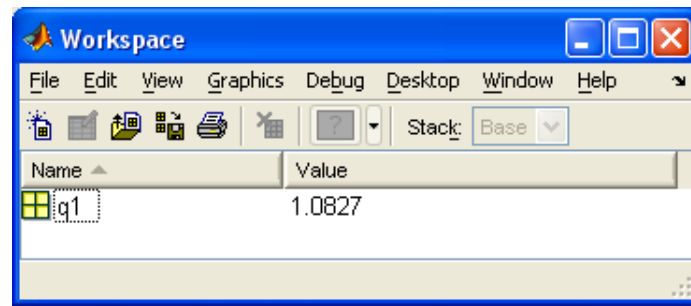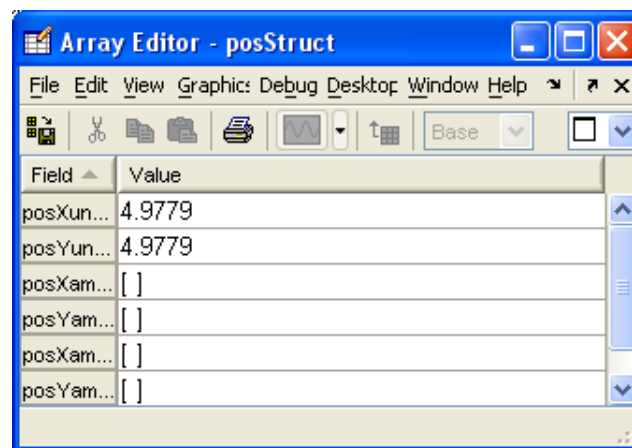
Figure 7.10: Simulation model outputs for algorithm 8

When this output is compared to the value of the q-range calculated by hand which is 1,082,157, there is a slight error in the output of the implementation of algorithm 8. However it is small enough for the output to be accepted as correct. Thus the implementation of algorithm 8 can be verified as correct.

## Algorithm 9
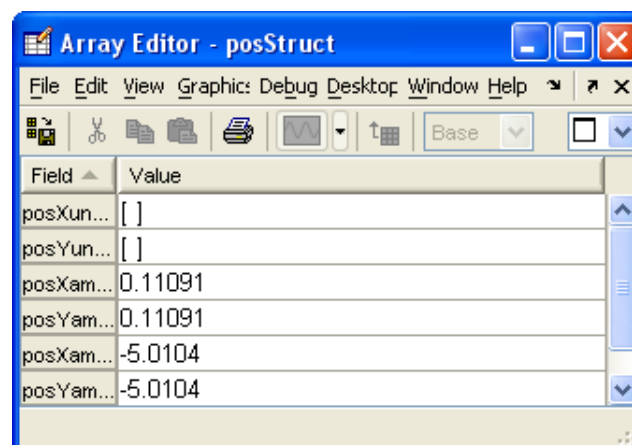
Q-ranges produced using TAC are used to test this algorithm. The algorithm for hyperbolic trilateration algorithm 9 only has a single output, the position of the NOI. This position can either be obtained unambiguously resulting in a single position being returned, or ambiguously resulting in two possible positions being returned. The output resulting from the input values given in table 7.1 is given in figure 7.11.

Figure 7.11: Simulation model outputs for algorithm 9

The position given in the output has a 7 cm error, but is otherwise correct. The error is the result of inaccuracy cased by sampling as well as a small phase shift caused by filtering and can be expected. Therefore this output can be accepted as correct. In order to verify that the algorithm functions correctly in the case of an ambiguous result it was tested using a NOI position that would result in an ambiguous result. A position of $(-5, -5)$ was used. The output from this test is given in figure 7.12.



Figure 7.12: Simulation model outputs for algorithm 9 from a NOI position resulting in ambiguity

The output given in figure 7.12 shows two positions, one correct and one incorrect.

This is what is expected of a correctly functioning implementation of algorithm 9. The implementation of this algorithm can therefore be verified as correct.

All of the algorithms that make up the simulation model have been correctly implemented in MATLAB. The computerised model verification is complete as the MATLAB implementation of the simulation model has been verified as correct.

## 7.3 Operational Validation

The purpose of the simulation model in this dissertation is to provide a means of testing how a single node can use RIPS for localisation. This simulation model does exactly this. It can therefore be concluded that the model is accurate enough for its intended purpose and therefore operationally validated according to the requirements set out in [12].

## 7.4 Chapter Conclusion

In this chapter the simulation model that was presented in chapter 6 was validated and verified. This was done according to the process given in [12].

The conceptual model of the simulation model was validated by proving that the theory that it is based on is correct and has been applied correctly, as well as proving that the assumptions that are made are reasonable for the intended purpose of the simulation model. Next the simulation model's logic, mathematical- and causal-relationships were proven to be sound and reasonable for the intended purpose of the simulation model.

The simulations model's implementation in MATLAB was verified as being correct by checking if each of its algorithms functioned correctly. This was done by checking it

the outputs produced by the algorithms correlated with what could be expected from the input values that were used.

Finally, the simulation model was proven to be operationally valid by showing that it was in line with what was stated in the research goal given in chapter 1. The simulation model has been verified and validated and can now be used in experimentation.

# Chapter 8

# Experimental Methodology

*In chapter 7, the simulation model designed in chapter 6 was validated and verified. In this chapter experiments are developed for the simulation model to be used in. These experiments will investigate the effects of specific system attributes on the performance of the system. This is done with the aim of possibly observing patterns from these effects that can be be interpreted by referring back to the fundamental theory that the system is based on. These insights will eventually be used to make conclusions about the proposed system's viability.*

## 8.1 Experimental Methodology

The simulation model designed in chapter 6 will be used to investigate the effects of the following system attributes on the accuracy of the system:

- The position of the NOI;

- The distance between the antennas;

- The operating frequency used;

- The method of solving q-range ambiguity.

The effect of the position of the NOI relative to the device will be investigated by varying its position over the axis intersections of a m×m two dimensional grid and attempting to localise it at each position. The positions in this grid are spaced in intervals of 1 m. This distance is chosen because the distances between nodes in a wireless ad-hoc network would definitely be greater than 1 m and therefore the resolution is fine enough. This overcompensation in resolution will be useful in studying the effect of the NOI position on localisation accuracy.

Antenna configuration will be tested by varying it in terms of distances that the other two antennas are placed from the "central" antenna which is placed at the origin (position (0,0)) of the two dimensional Cartesian space.

Three distances are used, 1 m, 0.5 m and 10 cm. The 1 m separation is chosen in order to investigate the effects of a large separation between the antennas. The 10 cm separation is chosen in order to investigate a small separation and the 0.5 m separation is chosen as an intermediary between the previous two separations. The antenna configuration is also chosen in such a way that it is slightly asymmetric. This is done because it has been found to increase accuracy in RIPS [26]. This asymmetry is achieved by slightly varying the distance between the "central" antenna and one of the other antennas, as can be seen from the antenna positions given in table 8.1.

In experiments using TAC to solve q-range ambiguity, two different frequency ranges will be tested. The 2.412/2.452 GHz and 5.180/5.320 GHz ranges are chosen as given in the 802.11n standard [30]. These frequency ranges were identified during the conceptual design in chapter 5. Both frequency ranges will be tested for three different antenna configurations, with the NOI being moved over an m×m grid for each experiment. The process to be followed in experiments using TAC is shown in figure 8.1.
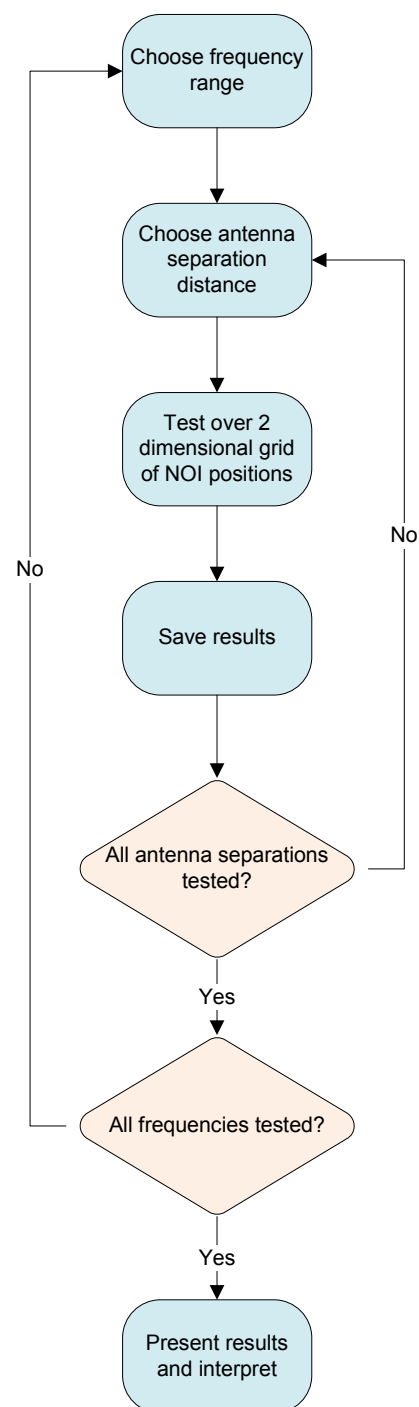
Figure 8.1: An illustration of the process followed for experiments using TAC

Finally, an experiment will be done using Same $k$, developed in chapter 4. Only one experiment will be done using Same $k$. This experiment is not meant to investigate the

effects of using different antenna separations and operating frequencies as will be the case in the other six experiments. The purpose of this experiment will only be to investigate the effects of using Same $k$ to solve q-range ambiguity on localisation accuracy.

Once again the position of the NOI is moved over a m × m grid. For this experiment only one antenna configuration will be tested. The use of Same $k$ requires different operating frequencies to be used, therefore the two operating frequencies to be used in this experiment are 70 MHz and 60 MHz. Same $k$ requires two operating frequencies to function, therefore these two operating frequencies are used in a single experiment. The process to be followed in the experiment using Same $k$ is shown in figure 8.2. The values of variables investigated for each experiment are shown in table 8.1.
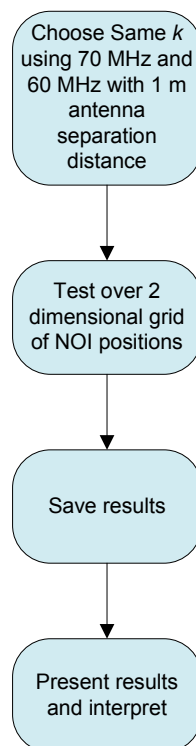


Figure 8.2: An illustration of the process followed for the experiment using Same $k$

Table 8.1: Attribute combinations to be used in the simulation experiments

| Frequencies Used | Antenna Positions |
|---|---|
| 60 MHz, 70 MHz | $Pos_A$= (0,0) $Pos_B$= (0,1) $Pos_C$=(0.9,0) |
| 2.412/2.452 GHz with 20 MHz spacings | $Pos_A$= (0,0) $Pos_B$= (0,1.11) $Pos_C$=(1,0) |
| 2.412/2.452 GHz with 20 MHz spacings | $Pos_A$= (0,0) $Pos_B$= (0,0.55) $Pos_C$=(0.5,0) |
| 2.412/2.452 GHz with 20 MHz spacings | $Pos_A$= (0,0) $Pos_B$= (0,0.11) $Pos_C$=(0.1,0) |
| 5.180/5.320 GHz with 20 MHz spacings | $Pos_A$= (0,0) $Pos_B$= (0,1.11) $Pos_C$=(1,0) |
| 5.180/5.320 GHz with 20 MHz spacings | $Pos_A$= (0,0) $Pos_B$= (0,0.55) $Pos_C$=(0.5,0) |
| 5.180/5.320 GHz with 20 MHz spacings | $Pos_A$= (0,0) $Pos_B$= (0,0.11) $Pos_C$=(0.1,0) |

For the experiments the following general assumptions are made:

- That there is line of sight between the device's antennas and the NOI;

- That Rician fading with a K factor of 9 dB, applies for the channel;

- That there is no additional radio interference;

- That hardware tolerances in terms of transmission frequency accuracy are negligible.

## 8.2 Chapter Conclusion

In this chapter, system attributes to be investigated were identified and the methodology for the experimental evaluation of the simulation model was presented. Assumptions made for these experiments were also given. Results from these experiments are presented in the following chapter, chapter 9.

# Chapter 9

# Simulation Results and Observations

*In this chapter the results for the experiments that were developed in chapter 8 are shown and observations are made from these results. The experiments are divided into three sections. The first two sections make use of TAC to solve q-range ambiguity, with the first section using the 5 GHz frequency range and the second using the 2.4 GHz frequency range. In the final section Same k is used to solve q-range ambiguity.*

The results presented in the first two sections (section 9.1 and section 9.2), were obtained by using TAC to solve q-range ambiguity. These two sections are divided into groups for each frequency range, with every antenna configuration tested for each of the frequency range. The results presented in section 9.3 were obtained by using Same $k$ to solve q-range ambiguity. For every experiment a graphic representation of the experiment's results is given in the form of a two dimensional map. These maps show the different NOI positions used in the experiments and the localisation results obtained for those NOI positions. There is a differentiation between the different localisation results in terms of whether they were determined ambiguously or unambiguously. This ambiguity is due to the use of hyperbolic trilateration to process q-ranges into NOI positions which in some cases results in two possible positions for the NOI. Unambiguously obtained NOI positions are shown as red circles, while correct NOI

positions obtained ambiguously are shown as black circles. Incorrect NOI positions obtained ambiguously are shown as blue circles.

Determining which one of the two NOI positions obtained from an ambiguous result is the correct one is done by comparing these two positions with the actual position of the NOI. The position that is the closest to the actual position of the NOI is then accepted as the correct position. This is done with the assumption that the incorrect ambiguously obtained NOI position can be identified with co-operation from another conceptual device. This was stated as a possible solution for the ambiguity sometimes occurring in the NOI position retuned by hyperbolic trilateration in section 5.2.3.

The incorrect ambiguously obtained NOI positions were therefore not taken into account when calculating the localisation accuracy standard deviation, maximum error and mean error given for the results of each experiment. This also applies to the histogram of errors per localisation attempt accompanying the results of each experiment.

The error in localisation accuracy for each individual localisation attempt was calculated as the difference in distance between the actual NOI position and the localised NOI position. This is in line with the definition of accuracy given in section 2.1.1. Finally, it should be noted that the positions of the antennas shown in the figures accompanying experiments 2, 3, 5 and 6 are not to scale for illustrative purposes.

## 9.1   5.180/5.320 GHz

This section makes use of TAC as shown in algorithms 5, 6 and 7 to solve q-range ambiguity. For the frequency range used, 6 different measurements were made to determine a q-range, each using a different frequency. Since two q-ranges are required for the hyperbolic trilateration given in algorithm 9 that was used, this equals 12 RIPS measurements per localisation attempt. The 6 measurement frequencies are separated by 20 MHz and are listed in table 9.1 alongside their corresponding channel numbers

as defined in the IEEE 802.11n standard [30]. This frequency range was chosen for investigation in chapter 5.

Table 9.1: Frequencies used for measurements in the 5.180/5.320 GHz range

| Channel Number | Frequency |
|:---:|:---:|
| 36 | 5.180 GHz |
| 40 | 5.200 GHz |
| 44 | 5.220 GHz |
| 48 | 5.240 GHz |
| 52 | 5.260 GHz |
| 56 | 5.280 GHz |

**Experiment 1**

This experiment was done using the variable values shown in table 9.2. The results for this experiment are given in table 9.3 and graphically illustrated in figures 9.1 and 9.2.

Table 9.2: Values assigned to variables for experiment 1

| Variable Name | Assigned Value |
|:---:|:---:|
| Measurement Frequency Separation | 20 MHz |
| Number of Measurements per q-range | 6 |
| Antenna Configuration | $Pos_A$= (0,0) $Pos_B$= (0,1.11) $Pos_C$=(1,0) |
| Grid Size | 20 m×20 m |

The results for experiment 1 given in table 9.3 show that the position of the NOI was determined to within an average error of 0.035 m for all NOI positions that were tested. There was a standard deviation of 0.132 m from the average error and the maximum error was 1.989 m. There is a large difference between the average and maximum error.

Table 9.3: Results for experiment 1

| Attribute | Value |
|:---:|:---:|
| Average Error | 0.035 m |
| $\sigma$ | 0.132 m |
| Maximum Error | 1.989 m |

By referring to figure 9.1 it can be seen that this large deviation is caused by a small

number of NOI positions. This observation is verified by the histogram in figure 9.2 as well as the standard deviation of 0.132 m. In figure 9.2 it can be seen that the majority NOI positions return small errors relative to the maximum error. The maximum error is shown to be an outlier.
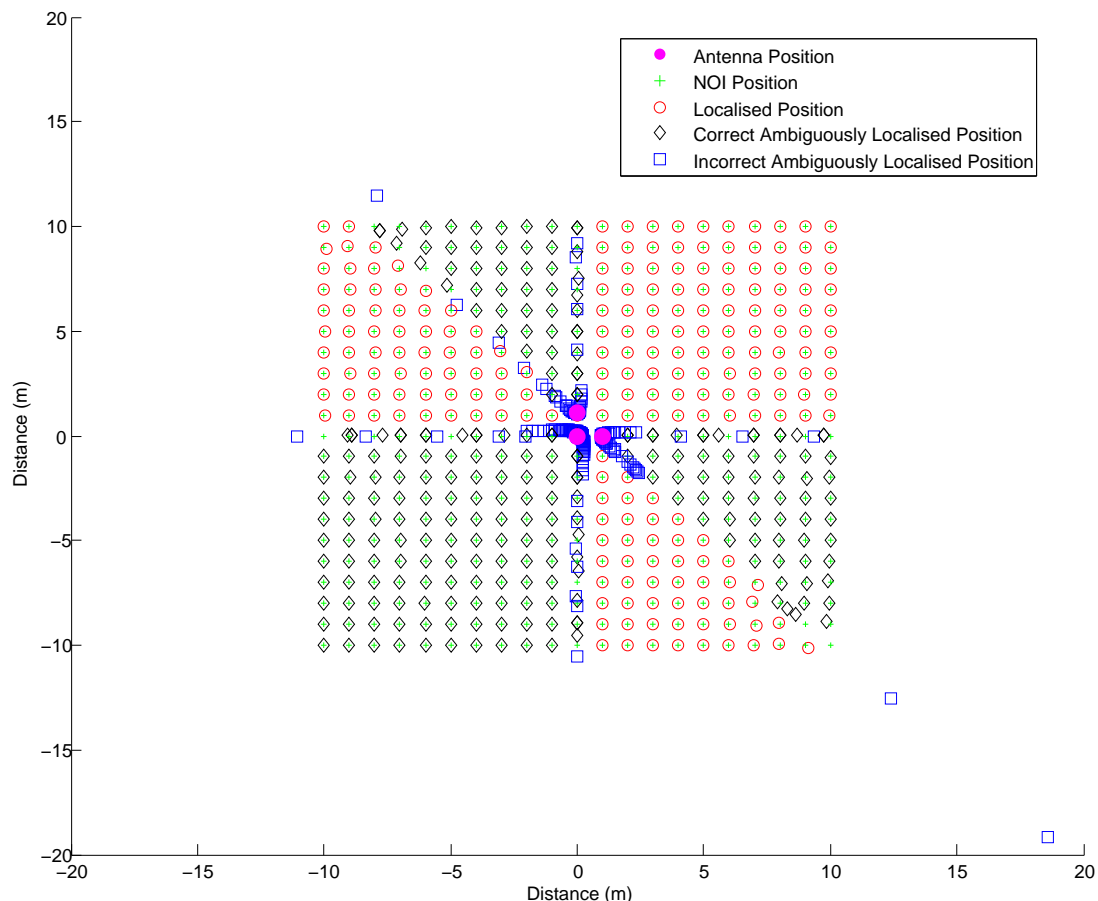


Figure 9.1: Results for experiment 1

The localised positions with large errors relative to the average error are all located on the extended lines intersecting two antennas. For the three antenna design that was used there are three such lines. These lines can be seen as the extended sides of a triangle created by using the three antenna positions as corners. When the NOI is positioned on one of these lines the localisation accuracy decreases sharply.
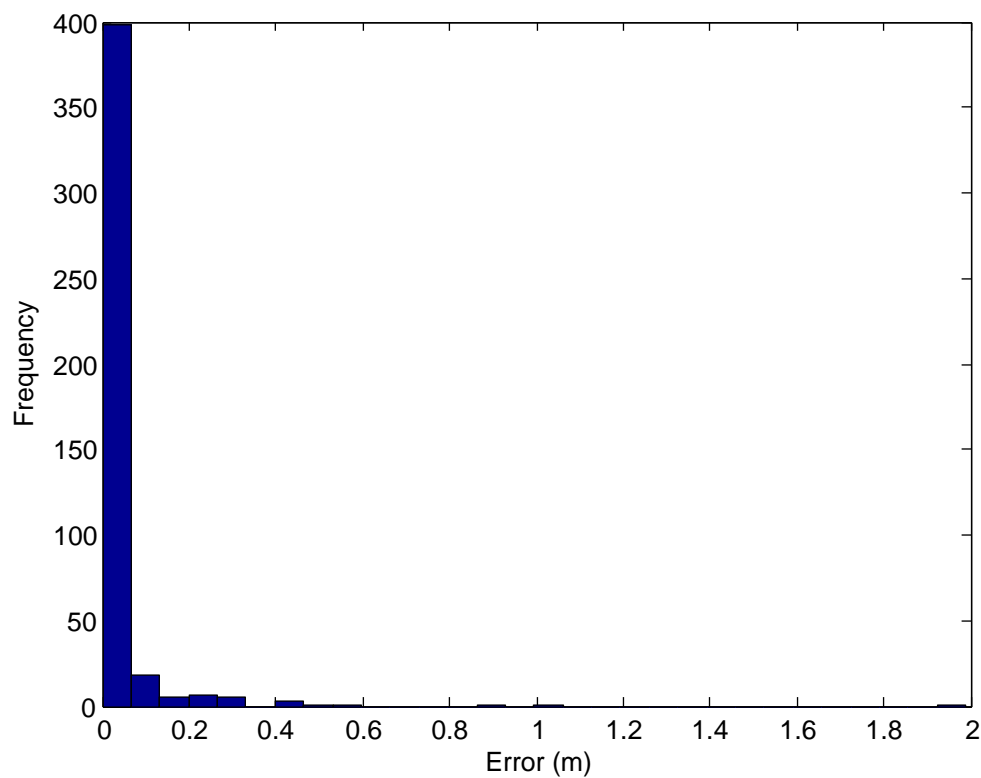
Figure 9.2: Histogram of localisation errors for experiment 1

The results for localisation attempts for positions that are not on one of these lines seem to be more accurate. This is the same for results obtained both unambiguously and ambiguously. It can be seen that the incorrect ambiguous results are located close to the positions of the antennas and are also visible to a lesser degree along the extended lines connecting the antennas.

**Experiment 2**

This experiment was done using the variable values shown in table 9.4. The results for this experiment are given in table 9.5 and graphically illustrated in figures 9.3 and 9.4.

Figure 9.3: Results for experiment 2

Table 9.4: Values assigned to variables for experiment 2

| Variable Name | Assigned Value |
| --- | --- |
| Measurement Frequency Separation | 20 MHz |
| Number of Measurements per q-range | 6 |
| Antenna Configuration | $Pos_A$= (0,0) $Pos_B$= (0,0.55) $Pos_C$=(0.5,0) |
| Grid Size | 20 m×20 m |

In experiment 2 an average error of 0.115 m was achieved with a standard deviation of 0.370 m. The maximum error was 3.539 m. The results for experiment 2 show the same patterns as observed in experiment 1. Again there is a large difference between the maximum and average error given in table 9.5 and again this seems to correlate with the position of NOI relative to the antenna positions, as can be observed in figure 9.3. The one difference that can be observed between these results and those for experiment

1 is an increase in the average error, standard deviation and maximum error.

Table 9.5: Results for experiment 2

| Attribute | Value |
|---|---|
| Average Error | 0.115 m |
| $\sigma$ | 0.370 m |
| Maximum Error | 3.539 m |

The histogram of measurement errors given in figure 9.4 shows that the maximum error is once again an outlier. It also shows that more values have retuned larger error values, when compared to the histogram of the result for experiment one, shown in figure 9.2. This is confirmed by the value of the standard deviation, which is now 0.370 m. Since the only variable that was changed for this experiment is the antenna configuration, it is possibly the cause. Once again the incorrect ambiguously obtained NOI positions all appear in positions that are close to the antennas or on the extended lines connecting them.
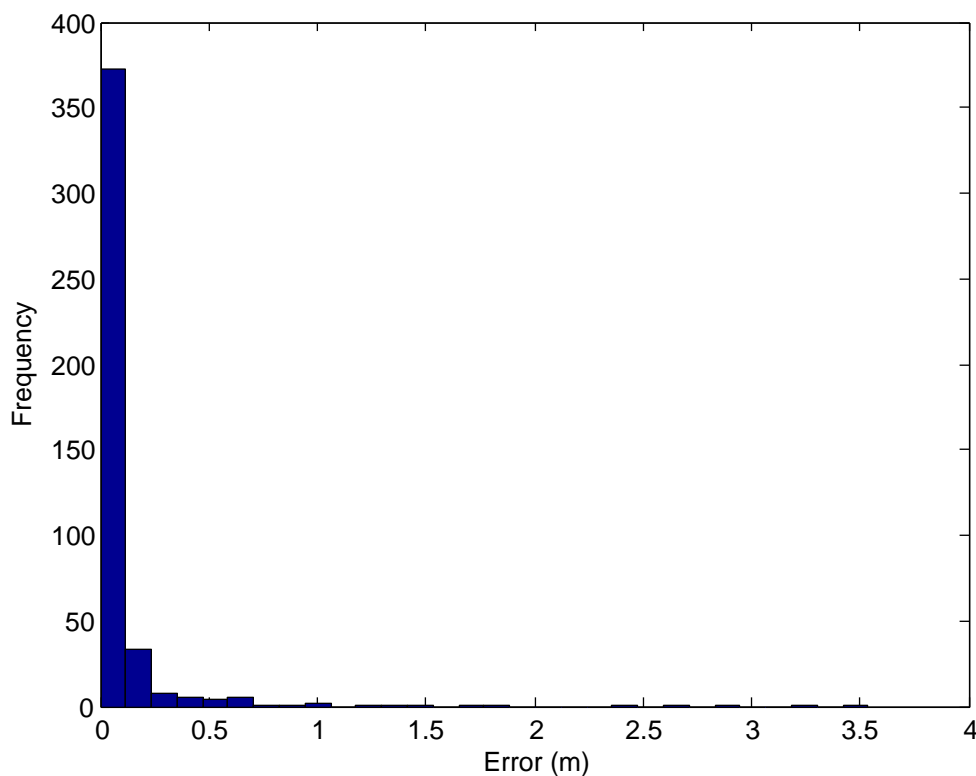


Figure 9.4: Histogram of localisation errors for experiment 2

**Experiment 3**

This experiment was done using the variable values shown in table 9.6. The results for this experiment are given in table 9.7 and graphically illustrated in figures 9.5 and 9.6.
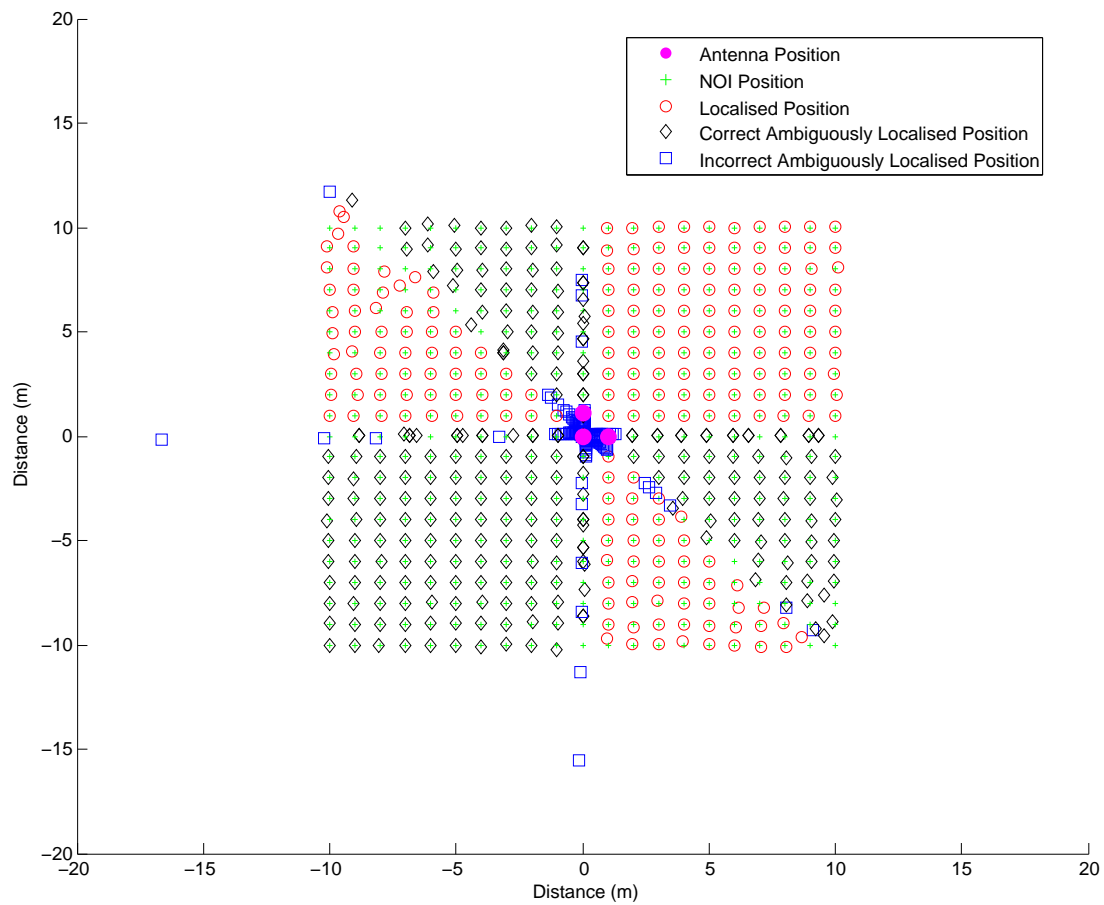
Table 9.6: Values assigned to variables for experiment 3

| Variable Name | Assigned Value |
|---|---|
| Measurement Frequency Separation | 20 MHz |
| Number of Measurements per q-range | 6 |
| Antenna Configuration | $Pos_A$= (0,0) $Pos_B$= (0,0.11) $Pos_C$=(0.1,0) |
| Grid Size | 20 m×20 m |
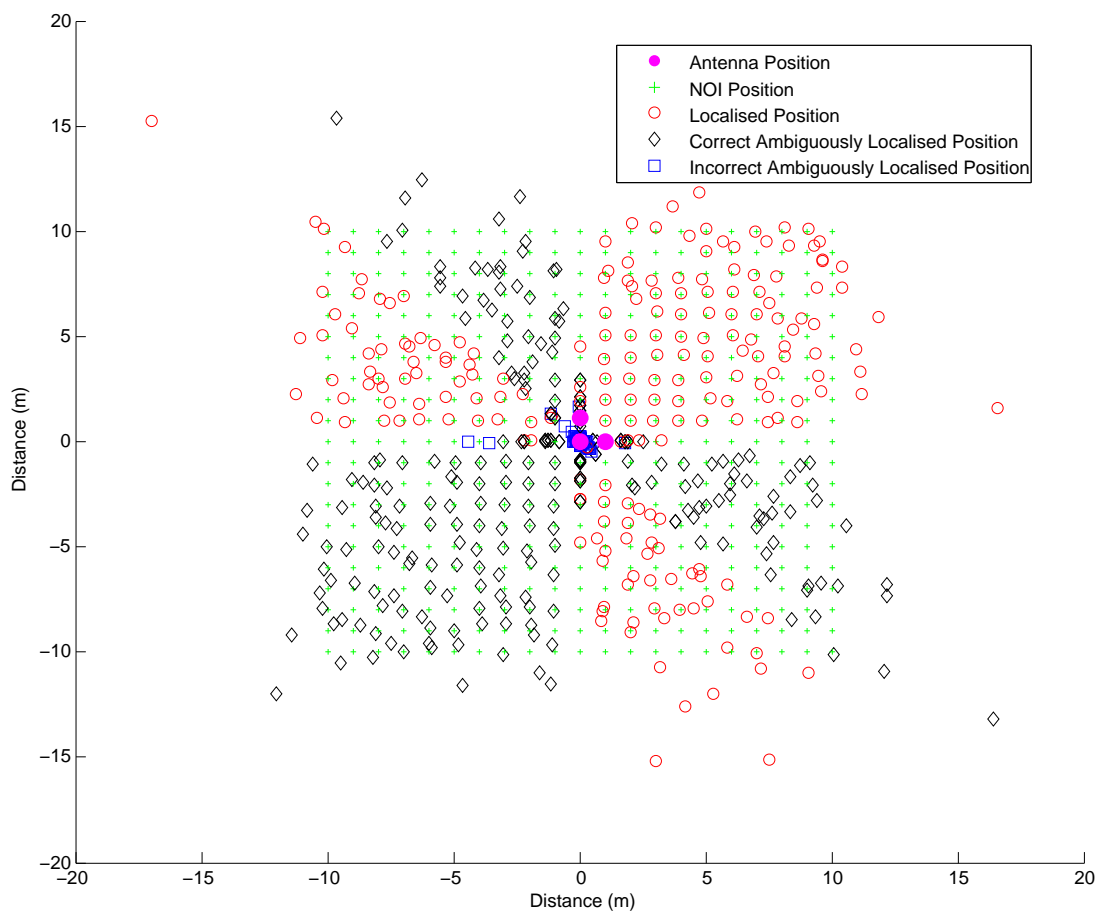


Figure 9.5: Results for experiment 3

In this experiment the average error,standard deviation and maximum error given in table 9.7 have increased sharply in comparison to those of experiments 1 and 2. When

figure 9.5 is observed it can be seen that the measured positions do not correlate with the true NOI positions.

Table 9.7: Results for experiment 3

| Attribute | Value |
|---|---|
| Average Error | 1.348 m |
| $\sigma$ | 2.225 m |
| Maximum Error | 15.215 m |

The histogram of localisation errors, given in figure 9.6, shows that a greater number of NOI positions now result in greater errors. This is confirmed by the increased standard deviation, which has now increased from 0.370 m in experiment 2 to 2.225 m in experiment 3. As in experiment 2 the only variable that was changed was the antenna configuration. Thus this must be the cause of the increase in the size of localisation errors. The incorrect ambiguously obtained NOI positions are all located either close to the device or on the extended lines connecting its antennas. In figure 9.5 it can also be seen that the errors in measurement seem to increase with the distance between the device and the NOI.
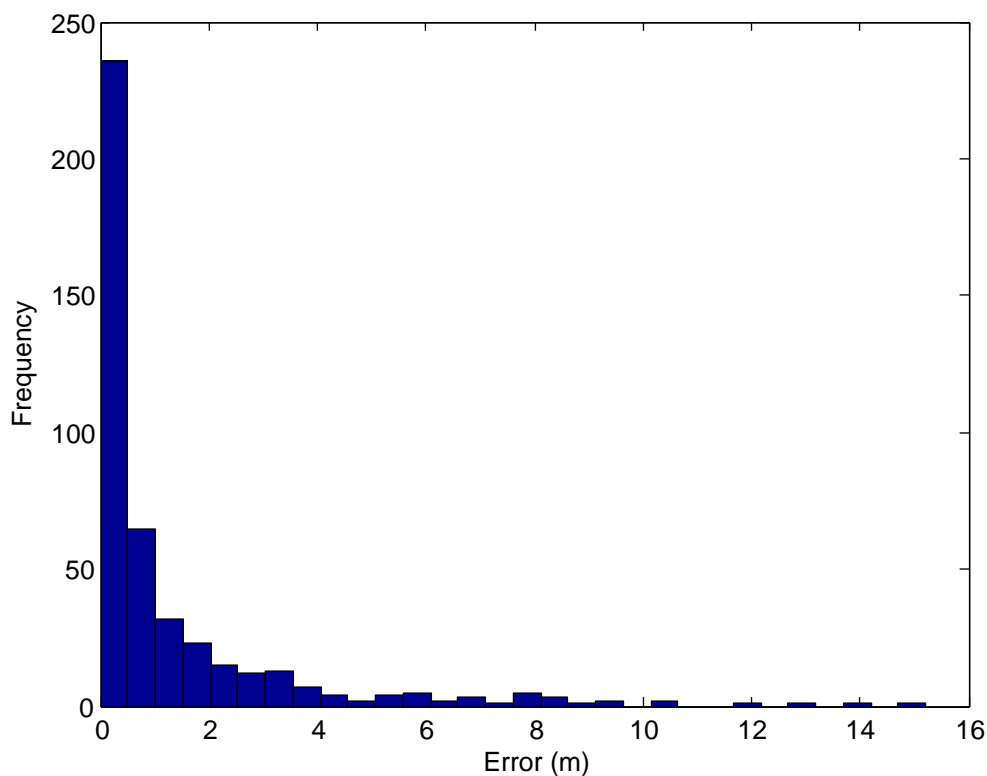
Figure 9.6: Histogram of localisation errors for experiment 3

## 9.2   2.412/2.452 GHz

The frequency range used in this section was chosen according to the frequency channels defined for the 2.4 GHz band in the 802.11 standard [30], as was chosen for investigation in chapter 5. The different channel frequencies are used to solve q-range ambiguity by using TAC , as shown in algorithms 5, 6 and 7. For this frequency range, three different measurements were used to determine a q-range. Since two q-ranges are required for the hyperbolic trilateration that was used to solve the q-ranges, 6 RIPS measurements are required per localisation attempt. The 3 frequencies used for measurements are separated by 20 MHz and are listed in table 9.8 alongside their corresponding channel numbers.

Table 9.8: Frequencies used for measurements in the 2.412/2.452 GHz range

| Channel Number | Frequency |
| --- | --- |
| 1 | 2.412 GHz |
| 5 | 2.432 GHz |
| 9 | 2.462 GHz |

**Experiment 4**

This experiment was done using the variable values shown in table 9.9. The results for this experiment are given in table 9.10 and graphically illustrated in figures 9.7 and 9.8. These results are similar to those obtained for experiment 1, which used the same antenna configuration. The larger errors occurred on the extended lines connecting the antennas, with accuracy appearing to increase when NOI positions were are not placed on these lines.

Table 9.9: Values assigned to variables for experiment 4

| Variable Name | Assigned Value |
| --- | --- |
| Measurement Frequency Separation | 20 MHz |
| Number of Measurements per q-range | 3 |
| Antenna Configuration | $Pos_A$= (0,0) $Pos_B$= (0,1.11) $Pos_C$=(1,0) |
| Grid Size | 20 m×20 m |

The average error, standard deviation and maximum error are given in table 9.10. The average error of 0.088 m does not differ by much from that of experiment 1, which was 0.035 m. The maximum error on the other hand, has almost doubled. Increasing from 1.989 m in experiment 1 to 3.579 m in experiment 4. There was also an increase in the standard deviation when compared to experiment 1, which was 0.132 m while the standard deviation in experiment 4 is 0.273 m.

Table 9.10: Results for experiment 4

| Attribute | Value |
| --- | --- |
| Average Error | 0.088 m |
| $\sigma$ | 0.273 m |
| Maximum Error | 3.579 m |
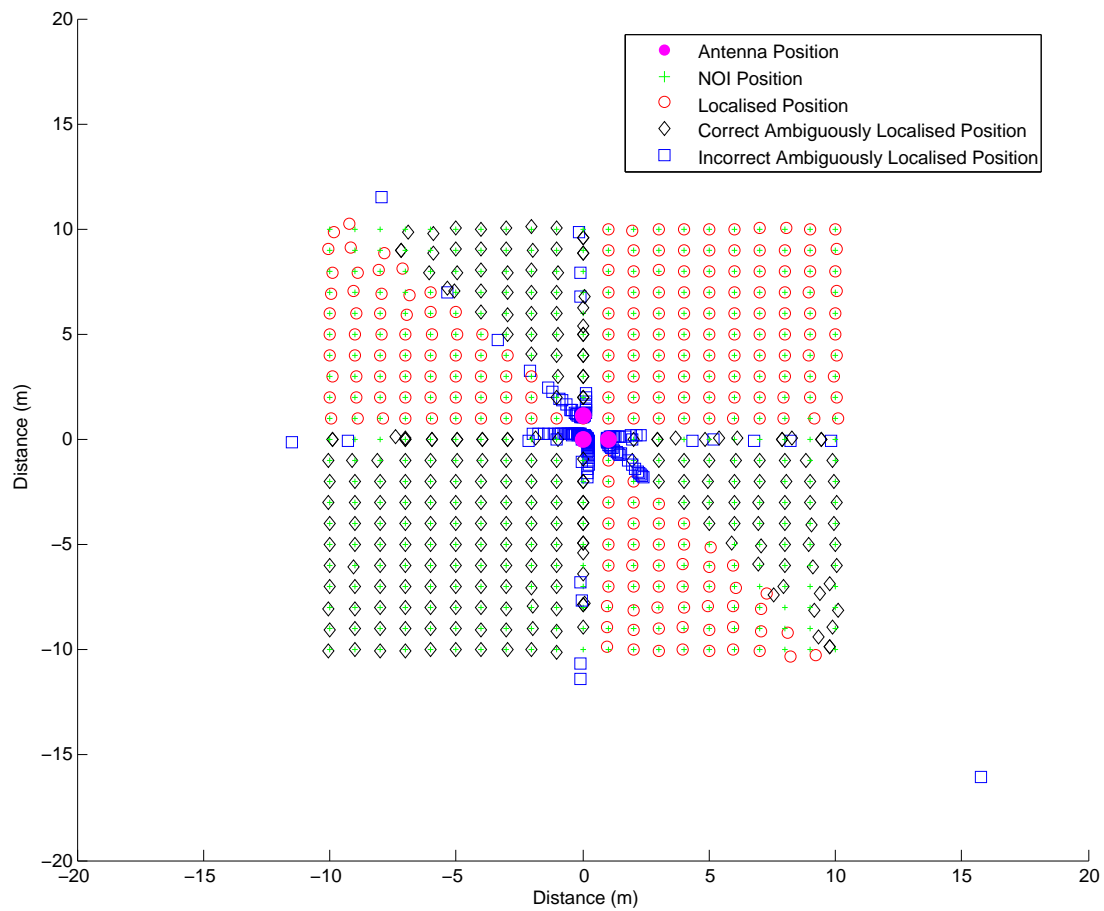
Figure 9.7: Results for experiment 4

The histogram of localisation errors given in figure 9.8, shows that the the majority of NOI positions resulting in error values close to the average error. This is confirmed by the standard deviation of 0.273 m. Finally, it is once again observed that the majority of the incorrect ambiguously obtained NOI positions are located close to the antennas, with the remainder being found on the extended lines connecting the antennas.

Figure 9.8: Histogram of localisation errors for experiment 4

**Experiment 5**

This experiment was done using the variable values shown in table 9.11. The results for this experiment are given in table 9.12 and graphically illustrated in figures 9.9 and 9.10.

Table 9.11: Values assigned to variables for experiment 5

| Variable Name | Assigned Value |
|---|---|
| Measurement Frequency Separation | 20 MHz |
| Number of Measurements per q-range | 3 |
| Antenna Configuration | $Pos_A$= (0,0) $Pos_B$= (0,0.55) $Pos_C$=(0.5,0) |
| Grid Size | 20 m×20 m |

In this experiment, results are similar to those of experiment 2, in which the same antenna configuration was used. The average error, standard deviation and maximum

errors are all given in table 9.12. These are larger than those for experiment 4 given table 9.12. Therefore, once again the antenna configuration used in this experiment seems to have a negative effect on accuracy. When compared with the results of experiment 2, which used the same antenna separation distance, the average error, standard deviation and maximum error values have all increased. This is similar the the comparison of the results for experiment 1 given in table 9.3 and those of experiment 4 given in table 9.10, which also shows the experiment using the 2.4 GHz band to result in increased errors.
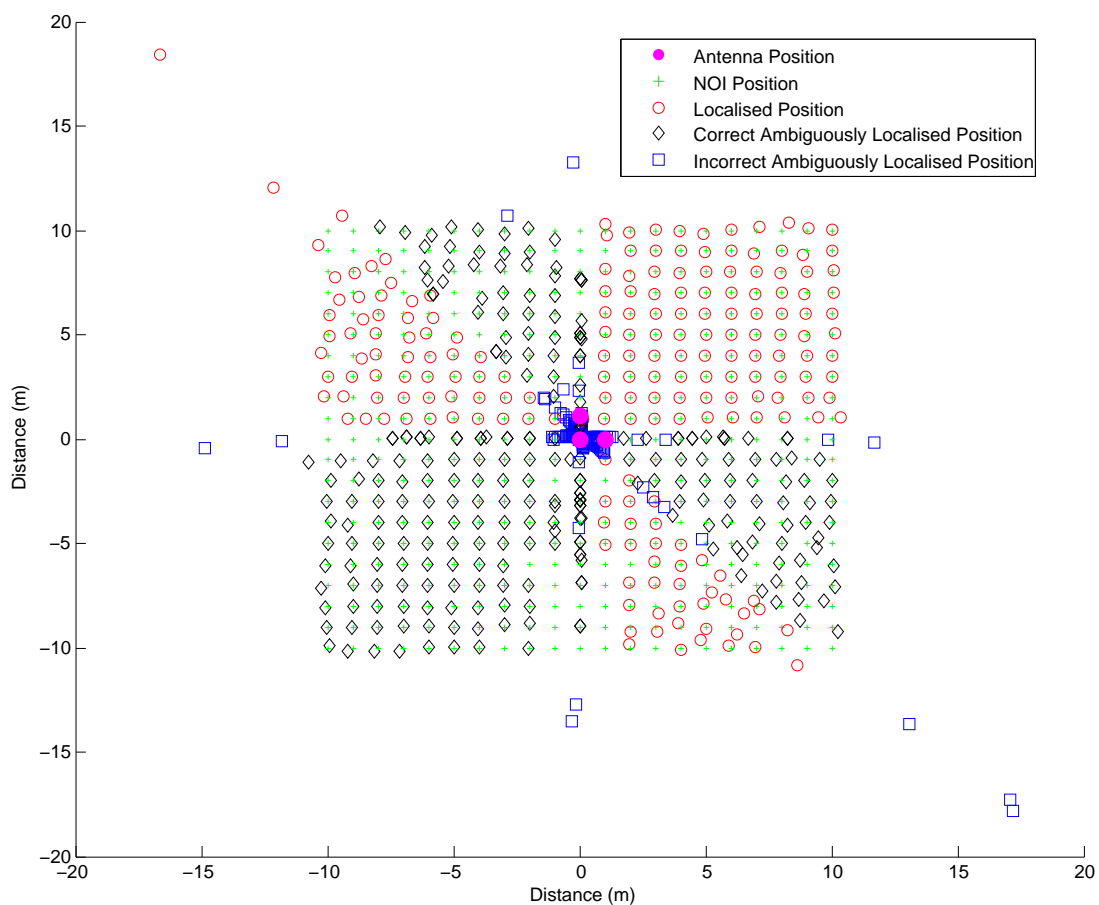


Figure 9.9: Results for experiment 5

Table 9.12: Results for experiment 5

| Attribute | Value |
| --- | --- |
| Average Error | 0.545 m |
| $\sigma$ | 1.585 m |
| Maximum Error | 12.804 m |

It is once again observed that the majority of the incorrect ambiguously obtained NOI positions are located close to the receivers. In figure 9.9 the incorrect ambiguously obtained NOI positions are mostly located close to the antennas and to a lesser extent on the lines connecting the antennas. However, there are now some instances where the the incorrect ambiguously obtained NOI positions are not located on these lines. As in experiment 3 it seems that the the error in localisation increases with distance. The histogram for the error values for this experiment given in figure 9.10, shows that the maximum error is caused by outlier values, this is confirmed by the standard deviation of 1.585 m.

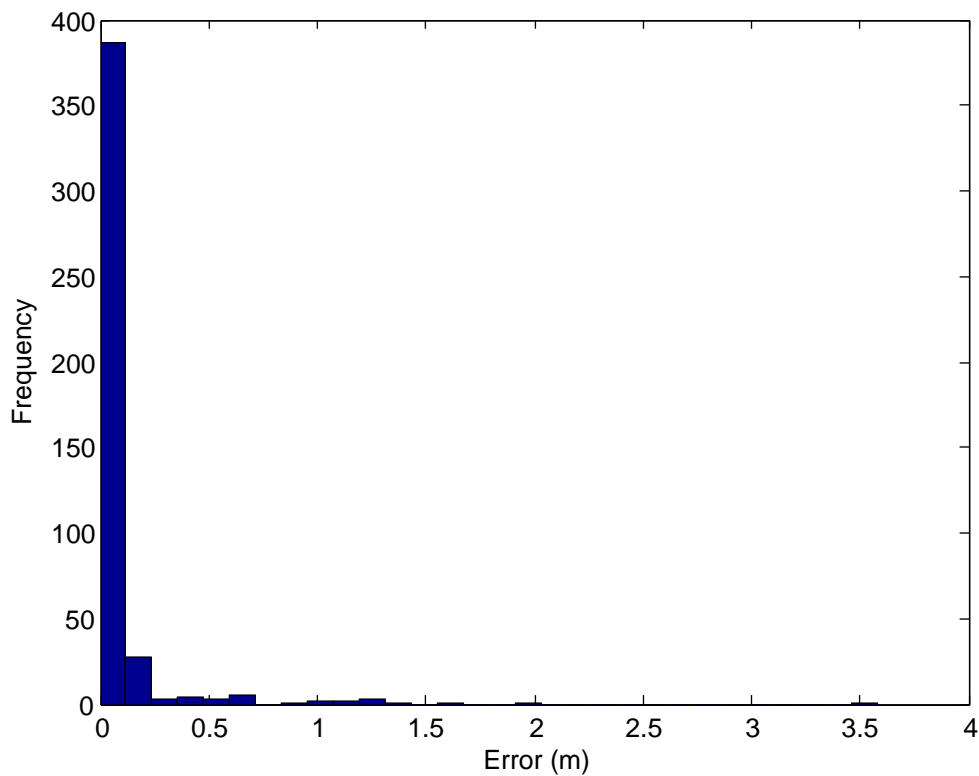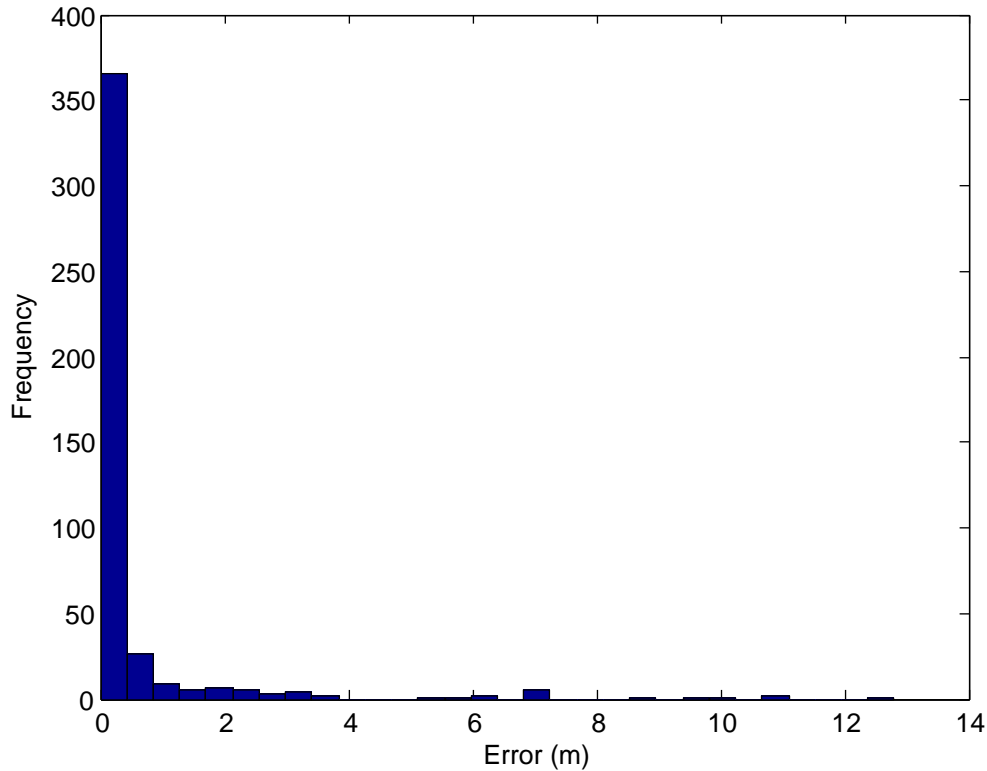

Figure 9.10: Histogram of localisation errors for experiment 5

**Experiment 6**

This experiment was done using the variable values shown in table 9.13. The results for this experiment are given in table 9.14 and graphically illustrated in figures 9.11 and 9.12.

Table 9.13: Values assigned to variables for experiment 6

| Variable Name | Assigned Value |
|---|---|
| Measurement Frequency Separation | 20 MHz |
| Number of Measurements per q-range | 3 |
| Antenna Configuration | $Pos_A$= (0,0) $Pos_B$= (0,0.11) $Pos_C$=(0.1,0) |
| Grid Size | 20 m×20 m |
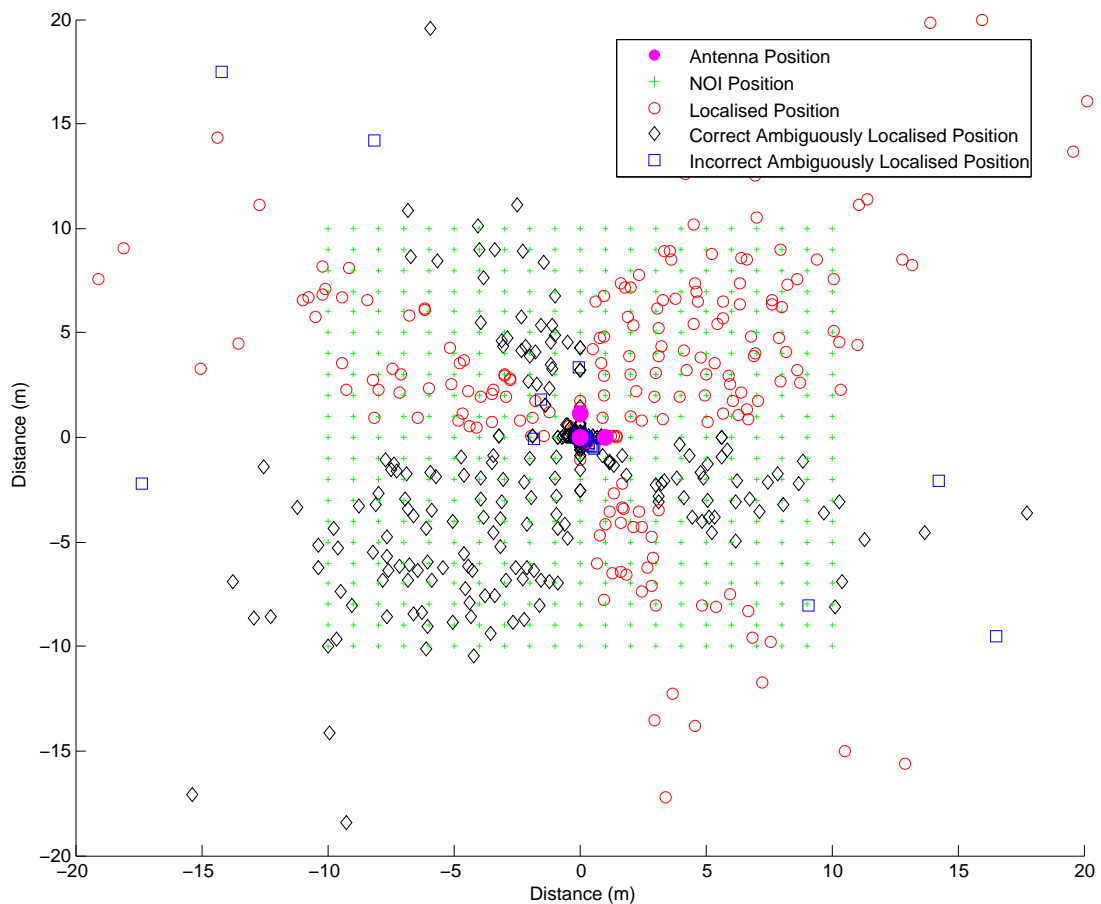


Figure 9.11: Results for experiment 6

The average error, standard deviation and maximum error given in table 9.14 are

greater than those produced in all previous experiments, including those of experiment 3. In figure 9.11 it is once again observed that the majority of incorrect ambiguously obtained NOI positions are located close to the antennas. However as is the case in experiment 5 some of these positions are now not placed on the lines connecting the antennas. As in experiments 3 and 5, errors also seem to increase with the distance between the NOI and the device.

Table 9.14: Results for experiment 6

| Attribute | Value |
|---|---|
| Average Error | 4.699 m |
| $\sigma$ | 18.037 m |
| Maximum Error | 335.819 m |

The histogram of this experiment's localisation errors given in figure 9.12, show that the maximum error of 335.819 m, is an outlier. This is confirmed by the standard deviation of 18.037 m. However this standard deviation also shows that a number of localisation attempts resulted in errors that are larger than the average error of 4.699 m.
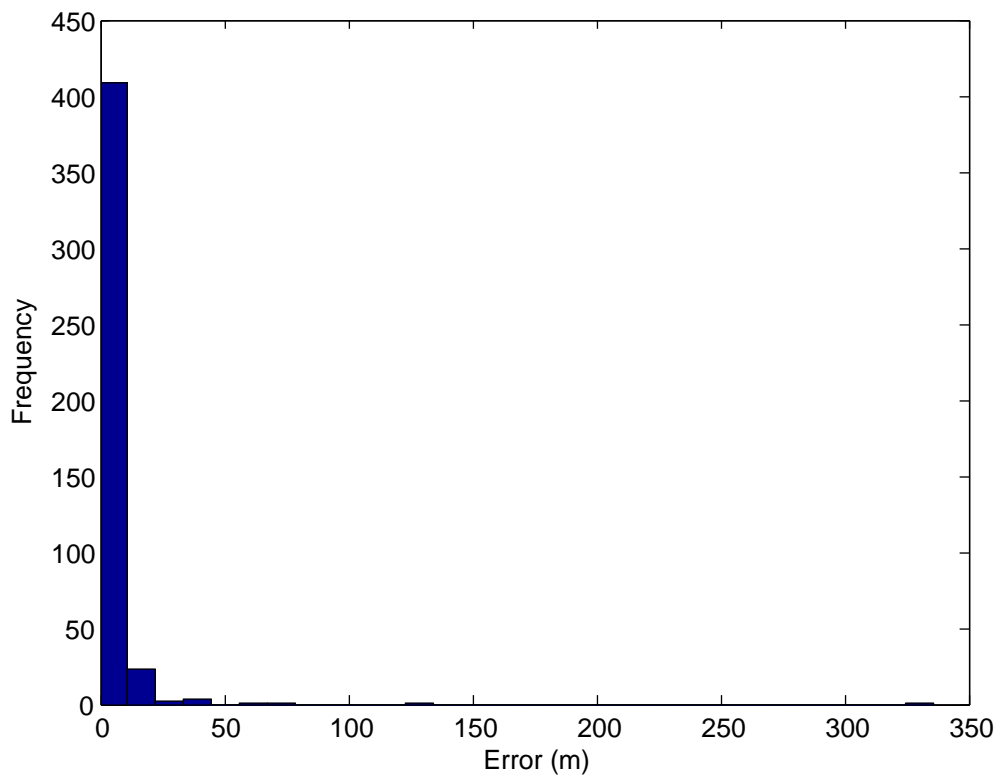
Figure 9.12: Histogram of localisation errors for experiment 6

## 9.3   Same $k$

The following experiment was done using Same $k$ to solve q-range ambiguity. For this method a maximum of two RIPS measurements are required per q-range. These two measurements are made using transmitter frequencies of 60 MHz and 70 MHz. Since hyperbolic trilateration is still used and two q-ranges are therefore required for localisation, this means that four RIPS measurements are required per localisation attempt. This method makes use of transmitter frequencies that are much lower than those used in the previous two experiments. This is due to the q-range ambiguity solution used here requiring transmitter signals with wavelengths in the order of metres.

## Experiment 7

This experiment was done using the variable values shown in table 9.15. The results for this experiment are given in table 9.16 and graphically illustrated in figures 9.13 and 9.14.

Table 9.15: Values assigned to variables for experiment 7

| Variable Name | Assigned Value |
|---|---|
| Measurement Frequency Separation | 10 MHz |
| Number of Measurements per q-range | 2 |
| Antenna Configuration | $Pos_A$= (0,0) $Pos_B$= (0,1) $Pos_C$=(0.9,0) |
| Grid Size | 20 m×20 m |

The results illustrated in figure 9.13 clearly show that the use of this method has a negative effect on the accuracy of the system. This occurred even though the antenna configuration used, was similar to one that yielded much better results in experiments 1 and 4.
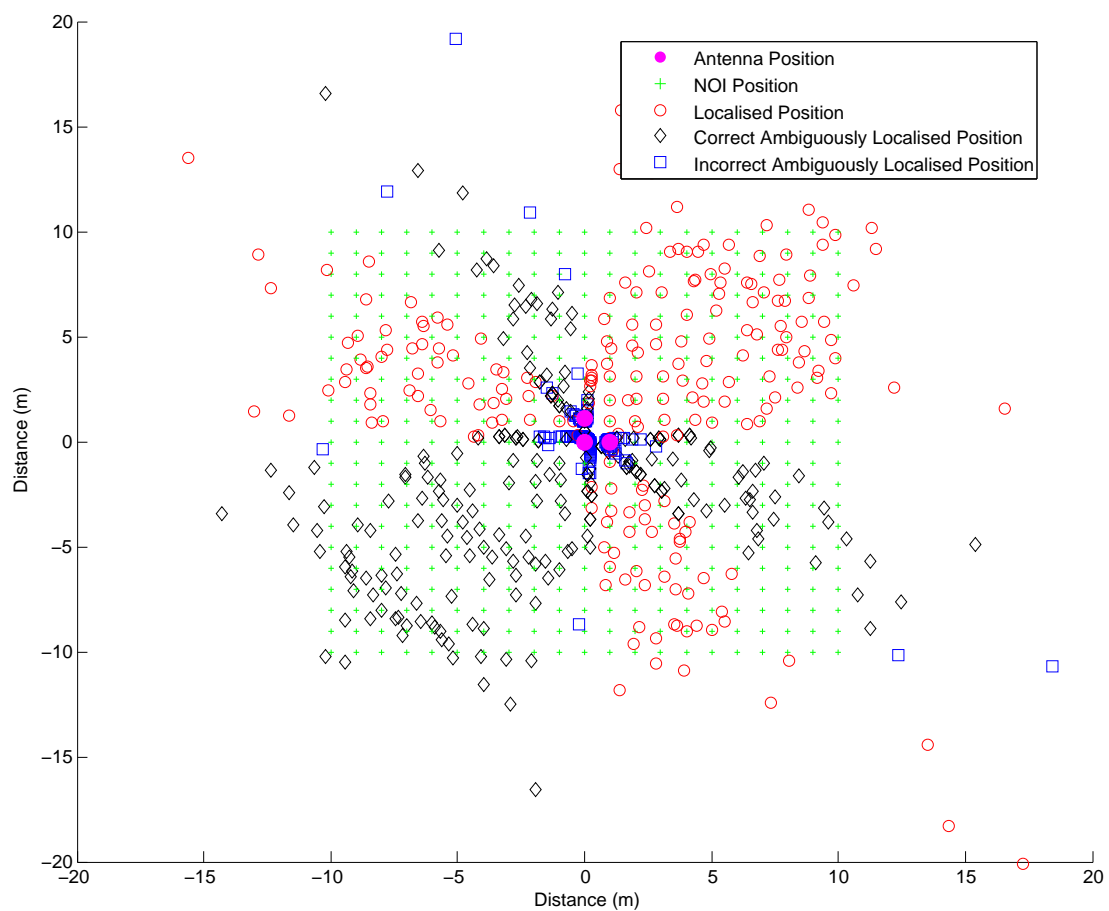
Figure 9.13: Results for experiment 7

The results for this experiment given in table 9.16 show a maximum error of 403.856 m. This is the greatest maximum error of any experiment done. This maximum error is shown to be an extreme outlier in the histogram of localisation errors given in figure 9.14. This is confirmed by the standard deviation of 20.245 m. The average error of this experiment was 3.672 m

Table 9.16: Results for experiment 7

| Attribute | Value |
|---|---|
| Average Error | 3.672 m |
| $\sigma$ | 20.245 m |
| Maximum Error | 403.856 m |
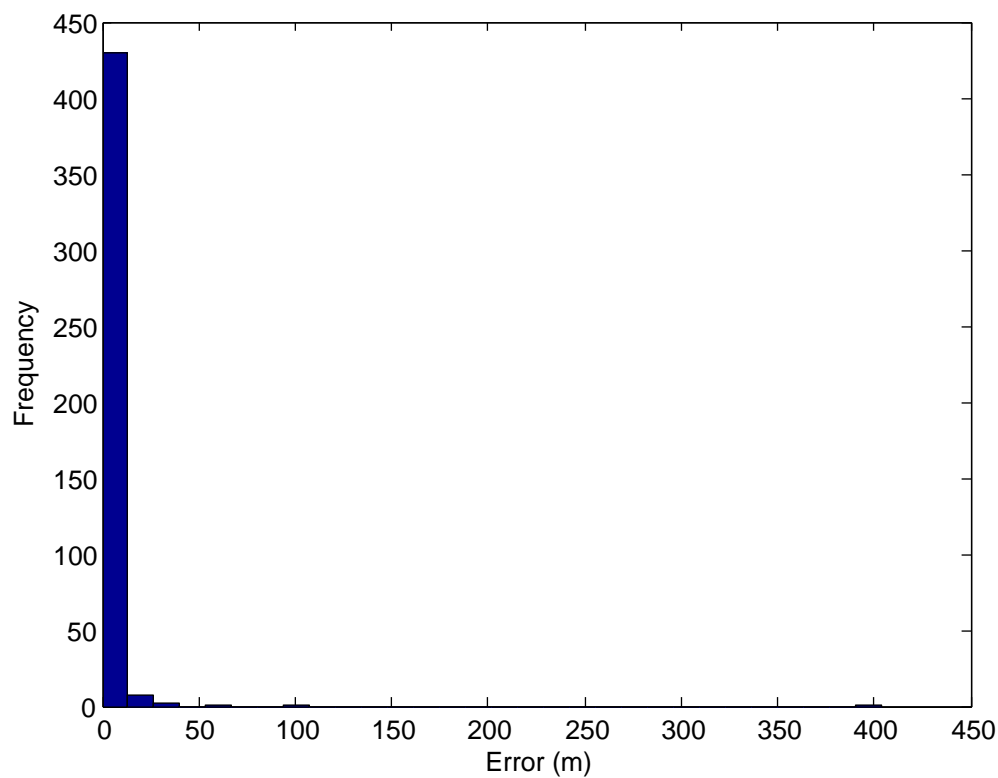
Figure 9.14: Histogram of localisation errors for experiment 7

## 9.4   Chapter Conclusion

In this chapter the results obtained for experiments done using the simulation model were given. These experiments investigated the impact that three variables have on the working of the conceptual design. These variables are:

- The position of the NOI;

- The distance between the antennas;

- The operating frequency used;

- The method of solving q-range ambiguity.

Firstly, is was observed that the position of the NOI relative to the device does have an effect on the system's accuracy. When the NOI is placed in a position which aligns with two of the device's antennas the accuracy of localised positions decreased. It was also seen that the further the NOI is placed from the device, the less accurate localisation became.

The distance between the antennas was also observed to affect accuracy. Experiments 1 and 4 which tested the largest antenna separations, resulted in the greatest accuracy being achieved. The experiments that tested the smallest antenna separation, experiments 3 and 6, resulted in the greatest errors. Therefore it was observed that larger distances separating the antennas resulted in greater accuracy.

With regards to operating frequency it was observed that lower frequencies resulted in decreased accuracy. This can be seen by comparing the results for experiments that used the same antenna separation and q-range ambiguity solution but different operating frequencies. Such comparisons can be made between experiments 1 and 4, 2 and 5, 3 and 6. In each of these comparisons its observed that the use of a higher operating frequency resulted in greater accuracy.

It was observed that experiments 1 and 4 that used TAC and a large antenna separation, resulted in greater accuracy than experiment 7 which used Same $k$ along with a similar antenna separation. It should be noted that this could be caused by the low frequencies that are a requirement of Same $k$, since it was observed that low frequencies resulted in lower accuracy.

Finally, it was observed that there is possibly a pattern in the incorrect ambiguously obtained NOI positions. These positions seemed to group around the antennas and appeared to a lesser extent on the lines connecting the antennas. This pattern could possibly be used as a means of identifying the incorrect ambiguously obtained NOI positions resulting from hyperbolic trilateration.

# Chapter 10

# Interpretation

*In this chapter interpretations are made from the results and observations presented in chapter 9. Interpretations are organised according to the three variables that were tested, namely NOI position, transmission frequency and antenna configuration. Results and observations obtained from experiments done using Same k are also interpreted.*

## 10.1   NOI Position

It was observed in chapter 9 that the position of the NOI has an effect on the accuracy of the system. Firstly, it was observed that when the NOI position aligns with any two of the device's antennas the system's accuracy degrades. Secondly it was observed that accuracy degrades when the NOI moves further from the the device. These two observations are now explained.

### 10.1.1   Alignment With Antennas

The decrease in accuracy occurring when the NOI aligns with two antennas can be explained by referring back to hyperbolic trilateration, which was studied in sections 2.1.3 and 3.3.1. This is done by looking at what the hyperbolas look like in cases where the NOI aligns with two antennas. There are three possibilities for this, if the antennas are named A, B and C, these cases are:

- Alignment with antennas A and B;

- Alignment with antennas A and C;

- Alignment with antennas B and C.

Now each of these cases are investigated by placing the NOI in three different positions, each conforming to the cases identified and then examining how the hyperbolas defined by such a case behave.

**Alignment with antennas A and B**

It can be seen from figure 10.1 that the hyperbolas in this case are becoming close to parallel. Therefore any change in the hyperbolas due to errors in the q-range values defining them would have a greater effect on where they intersect and therefore the resulting NOI position.
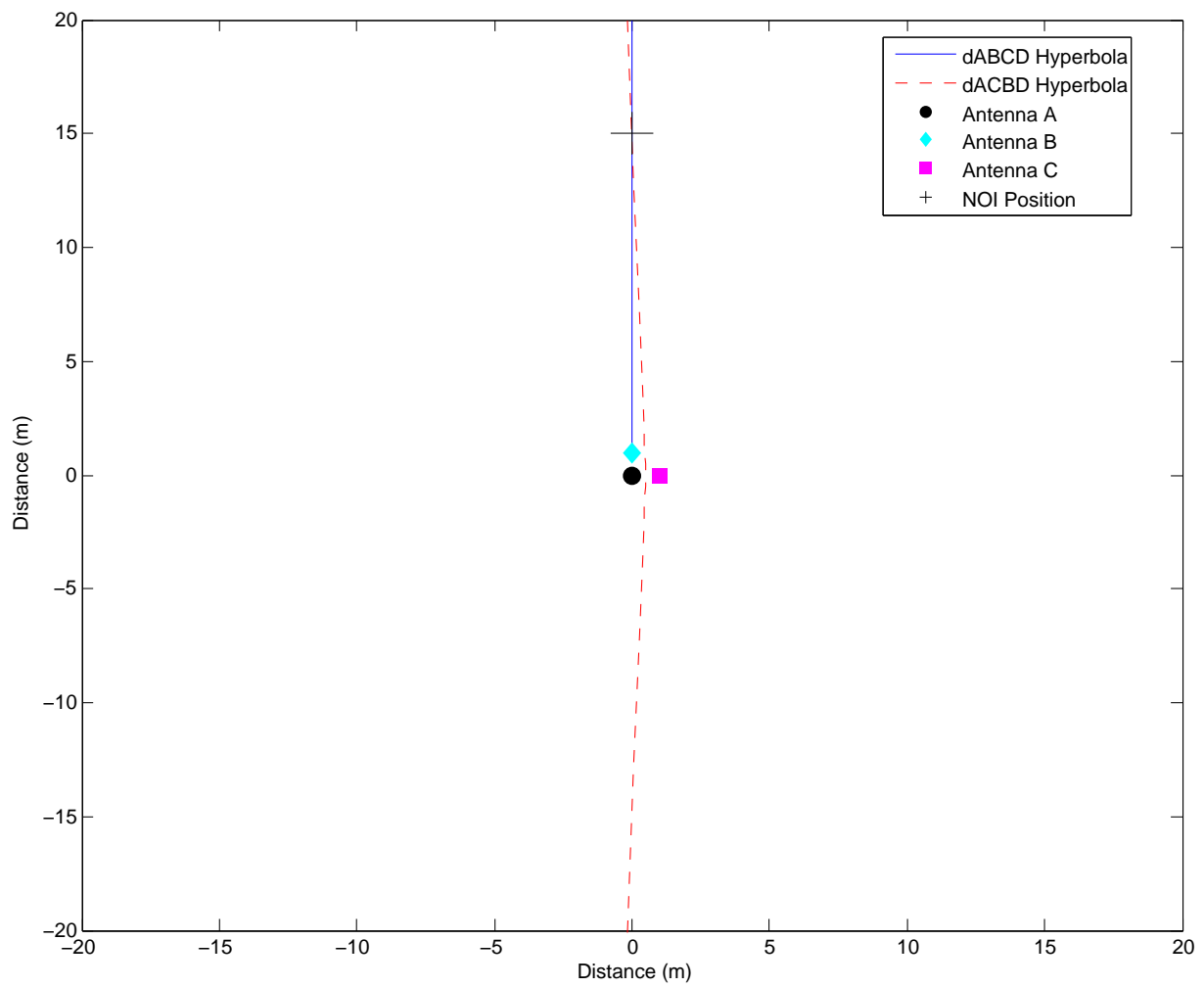
Figure 10.1: An illustration of hyperbolic trilateration when the NOI aligns with antennas A and B

**Alignment with antennas A and C**
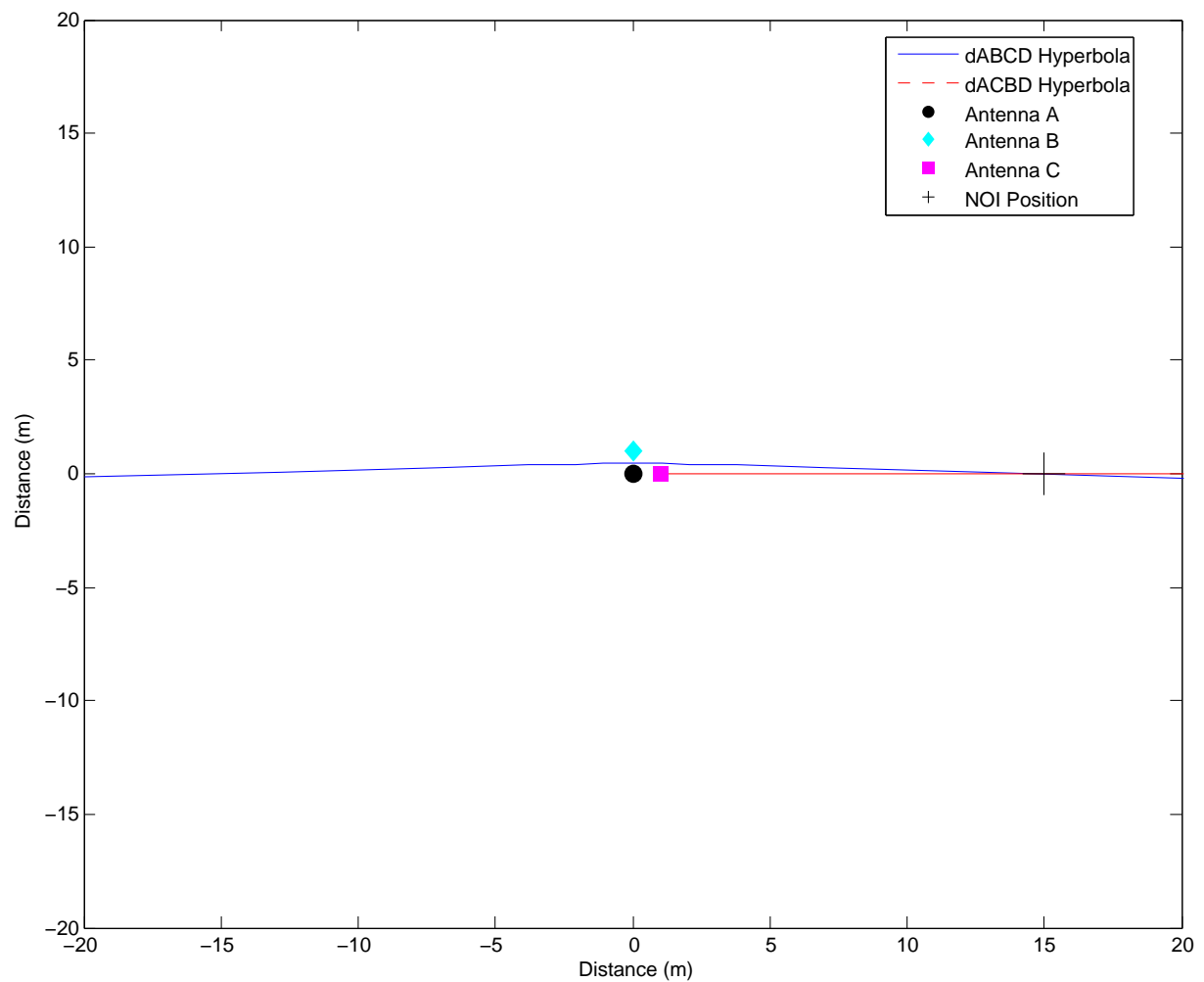


Figure 10.2: An illustration of hyperbolic trilateration when the NOI aligns with antennas A and C

Once again it can be seen from 10.2 that the hyperbolas are once more close to parallel, resulting in the same increased sensitivity to errors in q-range values.

**Alignment with antennas B and C**
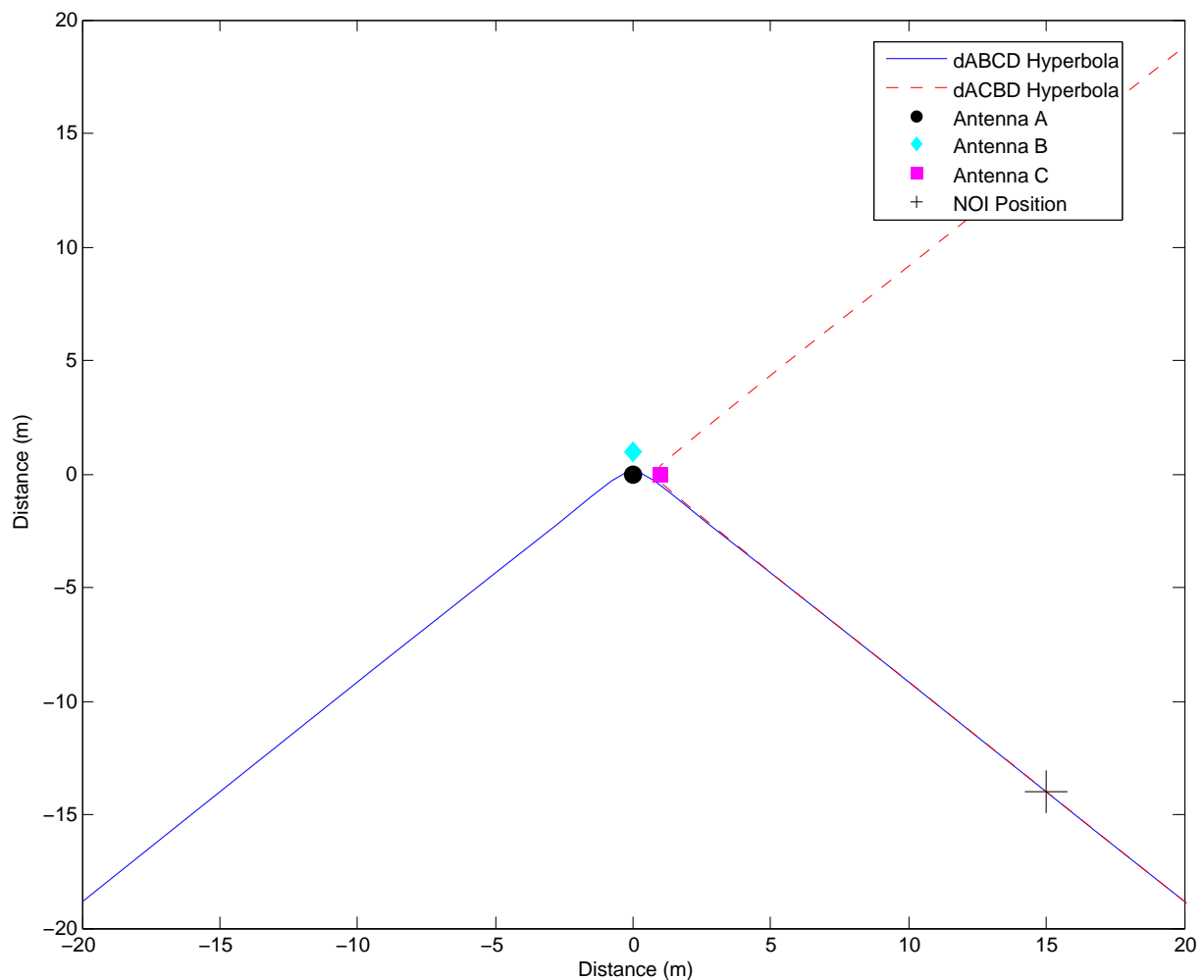


Figure 10.3: An illustration of hyperbolic trilateration when the NOI aligns with antennas B and C

The result in this case, shown in figure 10.3 is the same as that of the previous two. The hyperbolas are close to parallel, resulting in greater sensitivity to errors in q-range values. It can therefore be concluded that the decline in accuracy occurring when the NOI aligns with two antennas is caused by the hyperbolas in hyperbolic trilateration being close to parallel. This results in greater sensitivity to errors in q-range values.

### 10.1.2 Distance Between NOI and Device

It was also observed that measurements become less accurate as the NOI moves further away from the device. This can be explained by referring back to chapter 3. In chapter 3 it is stated that the range of possible q-range values is limited by (3.18). The range was also defined specifically for the case of hyperbolic trilateration in (3.35). A limited range of possible q-range values does not imply a limited number of q-range values. Since q-ranges are real values there are an infinite number of q-range values within a bound range, but this means that an ever increasing resolution is needed. This makes the system sensitive to errors. The distribution of q-ranges $d_{ABCD}$ is given in the form of a contour plot in figure 10.4.
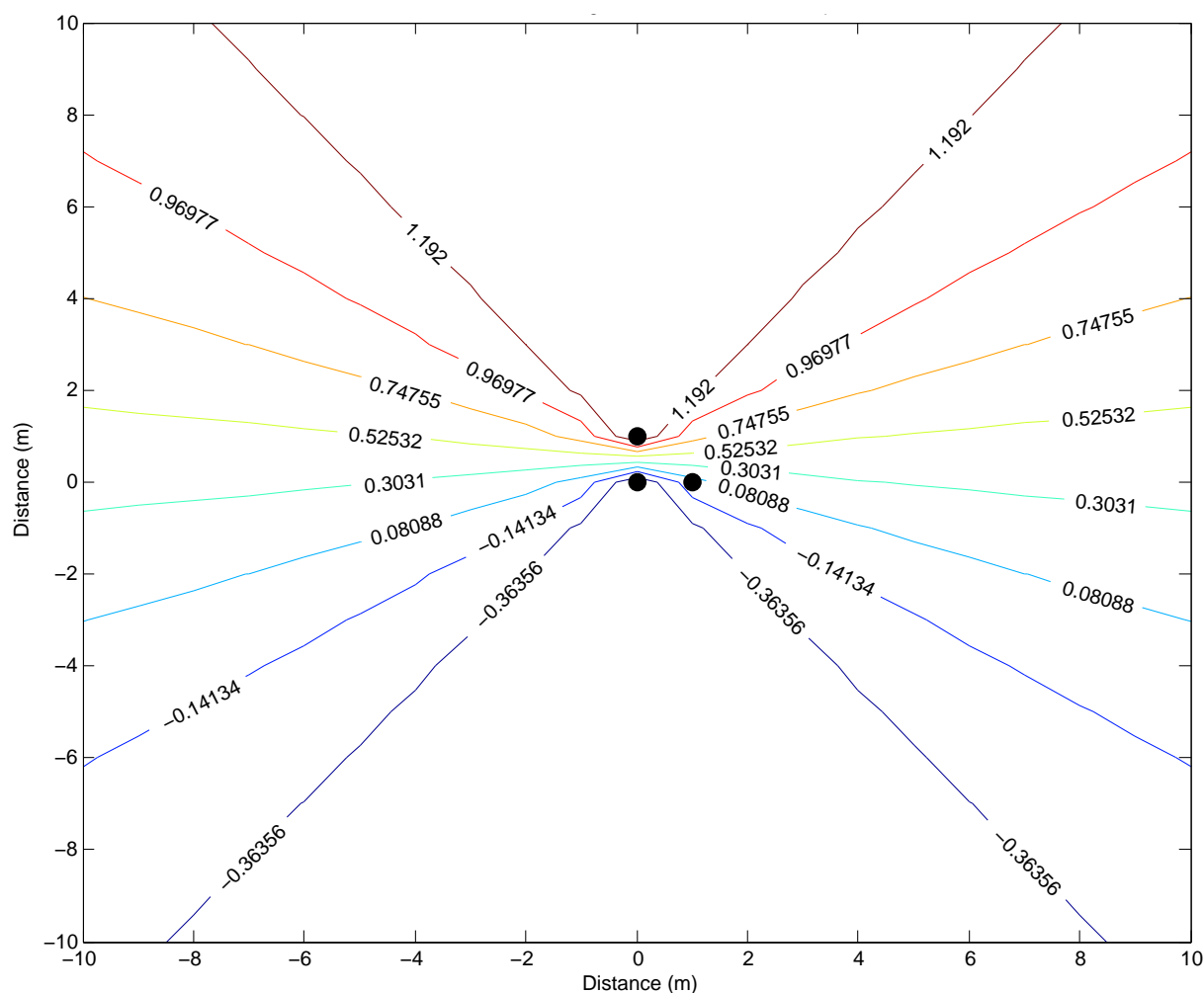


Figure 10.4: A contour plot of the distribution of q-range values

By referring to figure 10.4 it can be seen that the q-range values are very diverse close the the device while diversity decreases as the NOI moves further from the device. When a smaller range of q-range values has to be used to describe a larger area, a finer decimal resolution needs to be used. This causes the system to be more sensitive to errors in areas where the range of possible q-range values decreases.

## 10.2 Frequency

From results presented in chapter 9 it was observed that the use of higher frequencies resulted in greater accuracy. There are two possible reasons for this. The first can be explained by referring back to (3.16).

$$d_{ABCD} = \varphi_{ABCD}\frac{\lambda_c}{2\pi} + n\lambda_c, n\epsilon Z \tag{3.16}$$

Signals with higher frequencies have shorter wavelengths as can be seen from (10.1) [32].

$$\lambda = \frac{C}{f} \tag{10.1}$$

This means that more wavelengths are likely to be completed by the time the signal reaches the NOI. Therefore the value of $n$ in (10.2) is higher. This idea can be substantiated by defining a maximum value for the ambiguous q-range. This is done by first referring to the definition of the relative phase offset measured between the two receivers in RIPS, as given by (3.15).

$$\varphi_{ABCD} = \varphi_C - \varphi_D \tag{3.15}$$

Where $\varphi_{ABCD}$ is the relative phase offset between the two receivers and $\varphi_C$ and $\varphi_D$ are the individual phases measured at each receiver. This definition can be expanded as shown in (10.2).

$$\varphi_{ABCD} = (\varphi_{AC} - \varphi_{BD}) - (\varphi_{AD} - \varphi_{BD}) \tag{10.2}$$

Where $\varphi_{AC}$ and $\varphi_{BC}$ are the phase values of the signals transmitted by nodes A and B at receiver C. $\varphi_{AD}$ and $\varphi_{BD}$ are the phase values of these same signals measured at

receiver D. It can be seen that $\varphi_{ABCD}$ is at a maximum if $\varphi_{AC} = 2\pi\ rad$, $\varphi_{BC} = 0\ rad$, $\varphi_{AD} = 0\ rad$ and $\varphi_{BD} = 2\pi\ rad$. The maximum value of $\varphi_{ABCD}$ is then equal to $4\pi\ rad$. The value of the ambiguous q-range can then be calculated in (10.3).

$$\nu_{ABCD} = \varphi_{ABCD} \frac{\lambda_c}{2\pi} \tag{10.3}$$

Where $\nu_{ABCD}$ is the ambiguous q-range and $\lambda_C$ is the carrier frequency. The maximum value of the ambiguous q-range $\nu_{ABCD}$ is then equal to $\lambda_C$. If this maximum value is used in the definition of the unambiguous q-range (10.4),

$$d_{ABCD} = 2\lambda_C + n\lambda_C \tag{10.4}$$

It can be seen that as long as the limits of possible q-range values are large enough to allow large values of $n$, the ambiguous q-range forms a small part of the true q-range value in cases where the value of $n$ is large. For example, if the q-range has a maximum value in terms of metres and an operating frequency in the order of gigahertz is being used according to (10.1) the wavelength of the operating frequency is many times smaller than the maximum q-range in such a case. This allows the second term in (10.4) to make up the bulk of the q-range value in cases where the value of $n$ is large.

This means that the bulk of the unambiguous q-range's value is not subject to inaccuracy, as long as $n$ is determined correctly and there is no error in the transmission frequency. With the measured phase offset of the interference signal being responsible for any inaccuracies.

The second possible explanation for the increased accuracy of higher frequencies, is that the effect that errors in phase measurement have on the q-range value is dependent of the size of $\lambda_C$. With the effect of errors increasing with the value of $\lambda_C$. According to (10.1) wavelengths decrease as frequencies increase, therefore the errors of high frequency measurements have a smaller effect. This idea can be substantiated by altering (3.15) to include errors in the phase measurement at each receiver as is done in (10.5).

$$\varphi_{ABCD} = \varphi_C(1 + \epsilon_C) - \varphi_D(1 + \epsilon_D) \tag{10.5}$$

Where $\epsilon_C$ and $\epsilon_D$ are the measurement errors at receivers C and D respectively. If (10.5) is rearranged, both these errors can be denoted by a single term $\epsilon_{ABCD}$, that is defined in (10.6).

$$\epsilon_{ABCD} = \varphi_C \epsilon_C - \varphi_D \epsilon_D \tag{10.6}$$

This is then substituted into (10.3). The result of this is shown in 10.7

$$\nu_{ABCD} = \varphi_{ABCD}\frac{\lambda_C}{2\pi} + \epsilon_{ABCD}\frac{\lambda_C}{2\pi} \tag{10.7}$$

Finally, the result of (10.7) is substituted into the definition of the unambiguous q-range (3.16), that is shown rewritten using $\nu_{ABCD}$ in (10.8).

$$d_{ABCD} = \nu_{ABCD} + n\lambda_c \tag{10.8}$$

The result of this is shown in (10.9).

$$d_{ABCD} = \varphi_{ABCD}\frac{\lambda_C}{2\pi} + \epsilon_{ABCD}\frac{\lambda_C}{2\pi} + n\lambda_C \tag{10.9}$$

From (10.9) it can be seen that the size of the error $\epsilon_{ABCD}$ increases relative to the size of the q-range, when a lower operating frequency is being used. It should be noted that these effects might be offset by the fact that higher frequencies are more susceptible to fading due to smaller wavelengths in practical applications [32]. This means that lower frequencies could be more accurate in practical implementations. Using frequencies in the range of gigahertz also creates a problem for practical implementation, since hardware that functions at these frequencies is not able to tune their frequencies as finely [29]. This makes it difficult to achieve the small separation between transmitter frequencies required by RIPS.

## 10.3   Antenna Configuration

In chapter 9 it was observed that the antenna configuration had the greatest effect on the system's accuracy. Placing the antennas slightly asymmetrically improved accuracy, but the distance separating the antennas had the greatest effect. A Smaller distance separating antennas led to greater errors. This effect can be explained by looking

at the range of possible values the q-range can have. For a case where three antennas are stationary the range op possible values for q-range $d_{ABCD}$ (3.13) are defined in (3.35).

$$d_{ABCD} = d_{AD} - d_{BD} + d_{BC} - d_{AC} \qquad (3.13)$$

$$[-d_{AB} + d_{BC} - d_{AC}; d_{AB} + d_{BC} - d_{AC}]\epsilon R \qquad (3.35)$$

The last two terms in (3.13) are constant for all q-range values in the case of hyperbolic trilateration using RIPS and only change with antenna configuration. The first two terms form the difference in distance from antennas A and B to node D. Changes in the q-range value are caused only by the this difference in distance.

If the range of possible q-range values is worked out for an antenna configuration of $Pos_A = (0,0)$, $Pos_B = (0,1)$ and $Pos_C = (1,0)$, a range of $[-0.585; 1.414]$ is calculated. This means that all the possible positions of node D have to be described with this range of values. Since it is a range of real values there are an infinite number of values within the range, so it is possible to do this. However, this requires numbers with a finer resolution, making such q-ranges more susceptible to errors. The smaller the range of possible q-range values the more sensitive the system is to errors in q-range value. Since the size of the range is determined by the distance separating the antennas, with larger distances resulting in larger ranges, the antennas cannot be placed too close to each other.

## 10.4   Same *k*

The results from the experiment carried out using Same *k* to solve q-range ambiguity showed that this method resulted in lower accuracy when compared to results from experiments that used TAC. This was observed to be the case even with distances of metres separating the device's antennas. There are three factors that contribute to this. The first is that the q-range value returned by this method has an inherent error defined

by (4.13).

$$Error = n\left(\lambda_A - \lambda_B\right) \tag{4.13}$$

This value is small but since the q-range is already limited to such a small range of values, it has an effect.

The second factor is the fact that this method relies on the use of low frequencies in the order of tens of megahertz. This has already been interpreted as a drawback in section 10.2. With wavelengths in the order of meters the value of $n$ is likely to be small. This means that most of the q-range's value is subject to measurement errors. The third and final factor is that the range of possible q-range values for experiment 7, is bound by (3.35) to values in the range of $[-0.554; 1445]$. This is calculated using the antenna positions used in experiment 7, given as $Pos_A = (0,0)$, $Pos_B = (0,1)$ and $Pos_C = (0.9,0)$. The wavelengths of the transmission frequencies used in experiment 7 were, 4.996 m and 4.282 m. Thus the wavelengths used are large relative to the value of the q-range in all cases. This causes any error in measurement to have a greater effect on the value of the q-range. According to section 4.4, Same $k$ relies on the wavelengths of the transmission frequencies used to be greater than the maximum possible q-range value.

## 10.5   Pattern in Hyperbolic Trilateration Ambiguity

In chapter 9, a pattern was observed in the incorrect NOI positions returned in case of ambiguity in hyperbolic trilateration. This pattern could be used to identify the incorrect NOI position in such cases. However, no satisfactory explanation for this pattern can be found. Therefore this subject remains open to investigation.

## 10.6   Chapter Conclusion

In this chapter the observations made from results in chapter 9 were interpreted and explained. These interpretations are used in the next chapter to make conclusions regarding the viability of the conceptual system.

# Chapter 11

# Conclusions

*This chapter starts by giving a summary of the work that was done. In this summary the research goal and the objectives for achieving it are firstly reviewed. The process of how these objectives were met is then discussed. Finally, conclusions are drawn regarding the work done and recommendations are made for future work.*

## 11.1    Summary of Work Done

In chapter 1 a context for the work done in this dissertation was created in the form of a background. From this background a motivation for the research was derived. The motivation for the research was given as follows:

It was shown that RIPS imposes a lot of overhead in terms of the required co-operation between nodes when making a measurement. The number of RIPS measurements required to localise a node further increases this overhead. The implementation of RIPS on a single wireless node was then identified a possible solution to this problem. The concept behind this was that the device would possess multiple antennas

that would fulfil the role of individual nodes as in the conventional implementation of RIPS. This would reduce the required number of q-range measurements as well as the co-operation between nodes required to make these measurements. From this motivation the research problem and goal were defined as follows:

**Research Problem:** Investigation into the considerations and benefits of implementing RIPS on a single wireless node.

**Research Goal:** To develop a conceptual design for a node capable of implementing RIPS to localise other nodes with minimum co-operation and to test this system by means of simulation.

The different issues that needed to be addressed in order fulfil the research goal were identified as the following:

- A high level conceptual design of a node that is capable of localisation using RIPS with minimum co-operation from other nodes;

- A simulation model of the conceptual design;

- Determination of conceptual design viability through simulation.

These issues were then addressed in the following way:

In chapter 2, a literature study was done regarding localisation in general. This literature study covered the different methods of making localisation measurements as well as methods for processing localisation measurements into NOI positions. Useful applications that require localisation to function were also discussed to provide further background and motivation for the research.

The literature study was then continued in chapter 3 with an in depth study of RIPS.

The process and theory behind a RIPS measurement was discussed in detail. The problem of q-range ambiguity was identified and an existing method of solving this problem, referred to as TAC was discussed. Different methods of processing q-range values into NOI positions were then discussed.

In chapter 4, an alternative to the use of Test All Combinations (TAC) for solving q-range ambiguity was developed. This was done by firstly identifying a special case of q-range ambiguity in RIPS. A method dubbed Same $k$ was then proposed to solve the problem of q-range ambiguity by exploiting this special case of q-range ambiguity.

Chapter 5 focused on the development of a high level conceptual design of a node capable of implementing RIPS with minimum co-operation. In this chapter choices were made regarding the following aspects:

- The choice of method used to solve q-ranges;

- The number of antennas to be used and their layout;

- The methods of solving q-range ambiguity to be investigated further;

- The choice of operating frequency to be used in measurements, based on the method of solving q-range ambiguity.

Firstly, hyperbolic trilateration was chosen as the method of solving q-ranges after the advantages and disadvantages of all the available options were considered. The choice of hyperbolic trilateration then determined the number of antennas to be used as three. This was because hyperbolic trilateration requires three anchor nodes to function.

Ambiguity caused by hyperbolic trilateration is minimised when the three anchor nodes are at a ninety degree angle. Therefore the choice of antenna layout was also determined by the used of hyperbolic trilateration. The choice of distance between the antennas was left to be investigated through experiments using the simulation model.

It was also decided that the TAC and Same $k$ methods for solving q-range ambiguity would be investigated through experiments using the simulation model. Finally, a high level functional flow was given for the conceptual design that was created. This was then used in an example to explain how the conceptual device would function.

In chapter 6, a detail design of the simulation model was given. The processes of the simulation model were broken up into steps and presented in the form of a flow chart explaining the operation of the simulation model. Each of these steps were then discussed and pseudo code algorithms were given to show how they would be implemented. The simulation model was then implemented in MATLAB and validated and verified in chapter 7. This was done by using a process designed specifically for the validation and verification of simulation models given in [12].

In chapter 8, the experimental methodology was presented. The results from experiments done using the simulation model were given in chapter 9. The experiments were done by using the simulation model to localise a NOI over a grid of possible NOI positions. Seven experiments were done. Experiments 1 to 6 made use of TAC, while experiment 7 was done using Same $k$. Measurements were made in experiments 1 to 3 using the 5 GHz frequency range. In experiments 4 to 6 measurement were made using the 2.4 GHz frequency range. Two measurement frequencies, 60 MHz and 70 MHz were used in experiment 7.

Different antenna configurations were also tested. Experiments 1, 4 and 7 used antenna separation distances of 1 m. In experiments 2 and 5 antenna separation distances of 0.5 m were used. Antenna separation distances of 10 cm were used in experiments 3 and 6. For each experiment observations were made and from these observations patterns were identified regarding the conceptual system.

Finally, the observations made from the results were interpreted in chapter 10. Interpretations were made regarding the effects of the following variables:

- The position of the NOI relative to the localising node;

- The distance separating the antennas;

- The frequency used to make measurements;

- The q-range ambiguity solution used.

## 11.2   Concluding Remarks

### 11.2.1   On the Same $k$ Q-range Ambiguity Solution

Same $k$ was developed as an alternative to the use of TAC in solving q-range ambiguity. It promised to provide advantages over TAC in terms of the number of measurements and processing required, by requiring at most two RIPS measurements per q-range value at negligible additional processing overhead. However, the experimental results provided in chapter 9, showed that the use of Same $k$ results in a decrease in accuracy when compared to TAC. In section 10.4 it was shown that this decrease in accuracy was caused by a fundamental flaw in the design of Same $k$.

Same $k$ relies on the use of q-range limits that are smaller than the wavelength of the transmission frequency used. This causes errors in phase measurements to have a greater effect on the resulting q-range values. Therefore it can be concluded that Same $k$ is not a viable solution for q-range ambiguity.

## 11.2.2   On the Viability of the Conceptual Device

The aim of the conceptual device was to limit the co-operation required between nodes in order to localise a NOI using RIPS. This was done by having the antennas on a multiple antenna device act as independent nodes would in RIPS. In doing so the required co-operation is limited to co-operation between the device and the NOI, with the exception of cases where hyperbolic trilateration results in the NOI position being obtained ambiguously. In such a case, positions from another device would be required to identity the correct NOI position. This would only entail an exchange of localised positions, no synchronisation would be required.

In chapter 9, a pattern was observed in the incorrect NOI positions that were obtained ambiguously. This pattern can possibly be used to identify which of the positions in a case of position ambiguity caused by hyperbolic trilateration is indeed the correct one. However, no concrete explanation for this pattern could be found.

The experimental results provided in chapter 9, showed that the conceptual device could achieve average accuracies in the range of centimetres. However, this was for a case where only Rician fading and sampling errors had an effect on the measurements made by the system. It should be noted that no attempt was made to correct these errors. In [7], it was mentioned that higher level algorithms could be used to negate the effects caused by multipath effects such as Rician fading.

The conceptual device relies on its multiple antennas acting as individual nodes would in conventional RIPS. However, such a configuration causes the range of possible q-range values to be bound by the distances separating the antennas. This was shown to increase the sensitivity of RIPS to errors.

It was also shown in chapter 10, that the use of higher frequencies resulted in increased accuracy for the cases studied. However, the use of frequencies in the gigahertz range creates problems in RIPS with regard to the the 2 kHz maximum transmitter frequency

separation required by RIPS [7, 29]. This is because devices operating in the gigahertz range usually cannot tune their transmission frequencies finely enough. The increased sensitivity of these frequencies to fading and multipath could also present a problem in practical implementations.

However, it can still be concluded that the conceptual device would only be viable if the operating frequency and antenna separation are chosen in such a way that the transmitted signal's wavelength is small relative to the distances separating the antennas of the device. From the results of experiments presented in chapter 9, the relation between signal wavelength and antenna separation distance can be quantified as being 0.057:1 for experiment 1, which resulted in the greatest accuracy.

## 11.3   Recommendations for Future Work

The research done, highlighted the following issues that warrant further investigation:

- The improvement of the simulation model;

- The development and investigation of alternatives to TAC for solving q-range ambiguity;

- The investigation of the patterns observed in the incorrect NOI position returned by hyperbolic trilateration;

- The development and investigation of alternatives to hyperbolic trilateration for processing q-ranges;

- The investigation of existing technology that can be used to realise the conceptual system.

Firstly, the simulation model needs to be expanded to include additional sources of error that are specific to RIPS. The simulation model developed in chapter 6 only in-

cluded the effects of sampling and Rician fading. Other factors such as hardware tolerances in terms of timing and transmission frequency errors need to be included. In new literature presented in [33], an equivalent measurement noise model is derived for RIPS. This could be used to increase the accuracy of the simulation model in terms of measurement errors.

It was concluded that the Same $k$ method for solving q-range ambiguity proposed in this dissertation is not a viable solution for q-range ambiguity. The existing TAC method is computationally intensive, therefore an alternative to this method is still needed. New literature presented in [34], proposes two new methods for solving q-range ambiguity. Another new method, that the authors claim correctly uses Chinese Remainder Theorem, is presented in [35]. All of these methods warrant further investigation.

In chapter 9, patterns were observed in the incorrect position returned by hyperbolic trilateration in cases of ambiguity with regards to the localised NOI position. These patterns can possibly be used to solve the problem of ambiguity in hyperbolic trilateration by identifying incorrect results in such cases. However, this pattern could not be interpreted. Therefore an interpretation of these patterns that describes their cause and provides a measure of certainty about when and where they occur is still needed.

In chapter 10, the hyperbolic trilateration method used to process q-ranges into NOI positions was shown to posses increased sensitivity to errors in cases where the NOI aligns with the antennas of the conceptual device. This due to the design of the conceptual device requiring localisation to be performed on NOI positions which are outside of the triangle created by the three points of measurement (antennas) used. Alternative methods for processing q-ranges values are thus needed. In [33], a new alternative to hyperbolic trilateration is presented, this warrants further investigation.

Finally, an investigation must be made into existing hardware that could be used to realise the conceptual system. A paper written on implementing RIPS using an FPGA

in conjunction with a CC1000 chip [36], could provide a useful staring point for this.

# Bibliography

[1] C. Lemmon, S. M. Lui, and I. Lee, "Geographic forwarding and routing for ad-hoc wireless network: A survey," in *INC, IMS and IDC, 2009. NCM '09. Fifth International Joint Conference on*, aug. 2009, pp. 188 –195.

[2] K. Jones and L. Liu, "What where wi: An analysis of millions of wi-fi access points," in *Portable Information Devices, 2007. PORTABLE07. IEEE International Conference on*, May 2007, pp. 1 –4.

[3] A. Nayak and I. Stojmenovic, *Wireless Sensor and Actuator Networks(Algorithms and Protocols for Scalable Coordination and Data Communication)*. Wiley, 2010.

[4] J. Hightower and G. Borriello, "Location systems for ubiquitous computing," *Computer*, vol. 34, no. 8, pp. 57 –66, aug 2001.

[5] J. Hightower, C. Vakili, G. Borriello, and R. Want, "Design and calibration of the spoton ad-hoc location sensing system," August 2001.

[6] C. D. Whitehouse, D. Culler, K. Pister, S. R. Date, C. D. Whitehouse, and C. D. Whitehouse, "The design of calamari: an ad-hoc localization system for sensor networks," Tech. Rep., 2002.

[7] M. Maroti, B. Kusy, G. Balogh, P. Volgyesi, A. Nadas, K. Molnar, S. Dora, and A. Ledeczi, "Radio interferometric geolocation," in *in Proc. ACM 3rd Conference on Embedded Networked Sensor Systems (SenSys'05)*, November 2005, paper link. [Online]. Available: http://www.truststc.org/pubs/148.html

[8] B. Kusy, A. Ledeczi, M. Maroti, and L. Meertens, "Node-density independent localization," in *Information Processing in Sensor Networks, 2006. IPSN 2006. The Fifth International Conference on*, 0-0 2006, pp. 441 –448.

[9] R. Huang, G. Zaruba, and M. Huber, "Complexity and error propagation of localization using interferometric ranging," in *Communications, 2007. ICC '07. IEEE International Conference on*, june 2007, pp. 3063 –3069.

[10] J. Li, J. Conan, and S. Pierre, "Using antenna array in multipath environment for wireless sensor positioning," in *Vehicular Technology Conference, 2006. VTC-2006 Fall. 2006 IEEE 64th*, sept. 2006, pp. 1 –4.

[11] J. Mietzner, R. Schober, L. Lampe, W. Gerstacker, and P. Hoeher, "Multiple-antenna techniques for wireless communications - a comprehensive literature survey," *Communications Surveys Tutorials, IEEE*, vol. 11, no. 2, pp. 87 –105, quarter 2009.

[12] R. Sargent, "Validation and verification of simulation models," in *Simulation Conference, 2004. Proceedings of the 2004 Winter*, vol. 1, dec. 2004, pp. 2 vol. (xliv+2164).

[13] J. Zheng and A. Jamalipour, *Wireless Sensor Networks a Networking Perspective*, J. Zheng and A. Jamalipour, Eds. Wiley, 2009.

[14] C. V. David Munoz, Frantz Bouchereau and R. Enriquez, *Position Location Techniques and Applications*. Academic Press, 2009.

[15] C. Haslett, *Essentials of Radio Wave Propagation*, S. D. W. Webb, Ed. Cambridge University Press, 2008.

[16] A. Bensky, *Wireless Positioning Technologies and Applications*. Artech House, 2008.

[17] L. Godara, "Application of antenna arrays to mobile communications. ii. beamforming and direction-of-arrival considerations," *Proceedings of the IEEE*, vol. 85, no. 8, pp. 1195 –1245, aug 1997.

[18] D. Mohapatra and S. Suma, "Survey of location based wireless services," in *Personal Wireless Communications, 2005. ICPWC 2005. 2005 IEEE International Conference on*, jan. 2005, pp. 358 – 362.

[19] F. Hansen and V. Oleshchuk, "Location-based security framework for use of handheld devices in medical information systems," in *Pervasive Computing and Communications Workshops, 2006. PerCom Workshops 2006. Fourth Annual IEEE International Conference on*, march 2006, pp. 5 pp. –569.

[20] A. Kaya, A. Zengin, and H. Ekiz, "Comparison of the beacon-less geographic routing protocols in wireless sensor networks," in *Wireless Communications and Mobile Computing Conference (IWCMC), 2011 7th International*, july 2011, pp. 1093 –1098.

[21] L. Lambert Meertens, "The dimension of the vector spanned by sets of radio-interferometric measurements," Kestrel Institute, Tech. Rep., 2005.

[22] C. Wang, Q. Yin, and W. Wang, "An efficient ranging method for wireless sensor networks," in *Acoustics Speech and Signal Processing (ICASSP), 2010 IEEE International Conference on*, march 2010, pp. 2846 –2849.

[23] B. Kusy and J. Sallai, "Analytical solution for radio-interferometric localization of mobile sensors," December, 2006 2006. [Online]. Available: http://w3.isis.vanderbilt.edu

[24] X. Wang, B. Moran, and M. Brazil, "Hyperbolic positioning using rips measurements for wireless sensor networks," in *Networks, 2007. ICON 2007. 15th IEEE International Conference on*, nov. 2007, pp. 425 –430.

[25] B. La Scala, X. Wang, and B. Moran, "Node self-localisation in large scale sensor networks," in *Information, Decision and Control, 2007. IDC '07*, feb. 2007, pp. 188 –192.

[26] S. J. de Wet, "Development of a system for tracking objects in a confined space," Master's thesis, Faculty of Electric, Electronic and Computer Engineering, North-West University: Potchefstroom Campus, 2007.

[27] M. Srinivas and L. Patnaik, "Genetic algorithms: a survey," *Computer*, vol. 27, no. 6, pp. 17 –26, jun 1994.

[28] D. van der Merwe, M. Grobler, and M. Fereirra, "A study of q-range ambiguity in the radio interferometric positioning system," in *Telecommunications (ICT), 2011 IEEE 18th International Conference on*, May 2011, pp. 452–459.

[29] B. Dil and P. Havinga, "A feasibility study of rip using 2.4 ghz 802.15.4 radios," in *Mobile Adhoc and Sensor Systems (MASS), 2010 IEEE 7th International Conference on*, 2010, pp. 690 –696.

[30] *IEEE Standard for Information Technology-Telecommunications and Information Exchange Between Systems-Local and Metropolitan Area Networks-Specific Requirements - Part 11: Wireless LAN Medium Access Control (MAC) and Physical Layer (PHY) Specifications*, IEEE Std., 2009.

[31] G. Stuber, *Principles of mobile communication*, 2nd ed., G. Stuber, Ed. Kluwer Academic Publishers, 2002.

[32] R. Blake, *Wireless Communiction Technology*, S. Clark, Ed. Delmar Thompson Learning, 2001.

[33] Y. Cheng, X. Wang, T. Caelli, X. Li, and B. Moran, "Optimal nonlinear estimation for localisation of wireless sensor networks," *Signal Processing, IEEE Transactions on*, vol. PP, no. 99, p. 1, 2011.

[34] Y. Cheng, X. Wang, T. Caelli, and B. Moran, "Tracking and localizing moving targets in the presence of phase measurement ambiguities," *Signal Processing, IEEE Transactions on*, vol. 59, no. 8, pp. 3514 –3525, aug. 2011.

[35] W. Li, X. Wang, and B. Moran, "Resolving rips measurement ambiguity in maximum likelihood estimation," in *Information Fusion (FUSION), 2011 Proceedings of the 14th International Conference on*, july 2011, pp. 1 –7.

[36] S. Szilvasi, J. Sallai, I. Amundson, P. Volgyesi, and A. Ledeczi, "Configurable

hardware-based radio interferometric node localization," in *Aerospace Conference, 2010 IEEE*, march 2010, pp. 1 –10.

# Appendix A

# Conference Contributions from this Dissertation

**A Study of Q-Range Ambiguity in the Radio Interferometric Positioning System**

Presented at: The 18th International Conference on Telecommunications, May 2011, Crecian Bay Hotel, Ayia Napa, Cyprus

# A Study of Q-Range Ambiguity in the Radio Interferometric Positioning System

David van der Merwe, Leenta Grobler and Melvin Ferreira

School of Electrical, Electronic and Computer Engineering

North-West University

Potchefstroom, South Africa

Email: {20276826, leenta.grobler, melvin.ferreira}@nwu.ac.za

*Abstract*—**The Radio Interferometric Positioning System (RIPS) was developed by Maroti *et al*. for the purpose of node localization in wireless sensor networks. They theorized that RIPS would produce ambiguous measurements when distances between nodes exceeded a carrier wavelength. This paper investigates this effect. In this investigation patterns in these invalid measurements are studied and then explained by looking at the mathematics behind RIPS. Findings made, provide a characterization of ambiguity in RIPS as well as new methods to extend the range of RIPS measurements beyond one carrier wavelength.**

## I. INTRODUCTION

The ability to determine the location of nodes in a wireless network opens the door to many useful applications in wireless ad-hoc networks, such a geographic routing, location based services and beamforming. In wireless sensor networks, determination of a nodes position is important in situations where sensors are placed in random positions that are not predetermined. The Radio Interferometric Positioning system (RIPS) was developed to solve this specific problem, although it may be a useful technique for for other applications too[1].

Many different methods of solving the problem of localization have been developed. Some systems rely solely on radio measurements and measure characteristics such as radio signal strength (RSS), time of flight (TOF) and angle of arrival (AOA)[2]. RIPS makes use of relative phase differences which is related to TOF. Others make use of ultrasonic sound such as the Cricket system[3]. Each method has its own strengths and weaknesses, therefore the choice of method depends on the requirements and limitations of the environment in which it is to be be used in. RIPS is promising because it possesses the accuracy associated with TOF measurement and can be implemented with relatively cheap hardware.

One limiting factor of RIPS, is that problems occur when making measurements between nodes that are separated by a distance greater than the wavelength of the carrier frequency used in the measurements. This places limitations on the use of higher frequencies, since the wavelength then becomes too short to allow for practical distances between nodes[4]. A solution for this problem that makes use of multiple measurements at different frequencies has been provided in [4]. This method has been practically implemented for frequencies as high as 2.4 GHz in [5], but to the best of our knowledge no study has

been made about where and why exactly this problem occurs. This might sound unnecessary as it is known that the problem occurs due to distances beyond one carrier wavelength, but our results show that this is not as straightforward as it would seem. This paper provides the following contributions:

- A characterization of ambiguity in RIPS.
- Possible applications for this characterization that extends the range of RIPS beyond a carrier wavelength.

The rest of this paper is divided into the following sections:

- RIPS Background
- Observed Patterns
- Mathematical Correlation
- Possible Applications
- Conclusions and Future Work

## II. RIPS BACKGROUND

In this section a background explaining how RIPS functions is given. This is done in order to give the reader of this paper the knowledge required to understand the findings presented. The following was first presented in [1]. Unlike conventional methods of localization that use pairwise measurements, RIPS makes use of sets of four nodes in its measurements as is shown in figure 1. This is done by having two of the four nodes acting as transmitters and the remaining two acting as receivers. Measurements are made by having each of the transmitter nodes transmit pure sine waves simultaneously at slightly different frequencies. This small difference in frequencies is key to how RIPS functions as it creates an interference signal that has a frequency as defined in (1).

$$f_e = f_A - f_B \tag{1}$$

Where $f_A$ and $f_B$ are the frequencies of the signals transmitted by the two transmitter nodes and $f_e$ is the envelope frequency. If the difference between the two transmitter frequencies is small enough it will be possible to measure this interference signal with low cost hardware. Each of the two receivers then each measure the phase of the interference signal that they receive. The phase measured at each node is equal to the phase difference between the two transmitter frequencies, as is shown in (2) and (3).

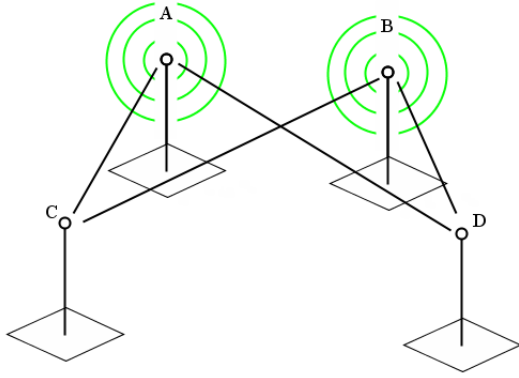$$\varphi_{AC} = -2\pi \left( \frac{d_{AC}}{\lambda_A} \right) \tag{2}$$

Fig. 1. Illustration of a RIPS measurement with nodes A and B transmitting and nodes C and D receiving.

$$\varphi_{BC} = -2\pi \left( \frac{d_{BC}}{\lambda_B} \right) \qquad (3)$$

$$\varphi_C = \varphi_{AC} - \varphi_{BC} \qquad (4)$$

Where $\varphi_{AC}$ and $\varphi_{BC}$ are the phases of the signals from transmitters A and B at receiver node C. $\lambda_A$ and $\lambda_B$ are the wavelengths of the the transmitted frequencies and $d_{AC}$ and $d_{BC}$ are the distances from nodes A and B to node C. The phase of the interference signal is given in (4) as $\varphi_C$. The equations for node D are similar.

A relative phase difference is then determined by subtracting the phase differences measured at the receiver nodes from each other in (5) .

$$\varphi_{ABCD} = \varphi_C - \varphi_D \qquad (5)$$

Once the relative phase difference has been determined a special value called the q-range can be determined.

$$d_{ABCD} = \varphi_{ABCD} \frac{\lambda_C}{2\pi} \qquad (6)$$

Where $\lambda_C$ is the wavelength of the carrier frequency $f_c$.

$$f_c = \frac{f_A + f_B}{2} \qquad (7)$$

The q-range is a linear combination of the distances between each transmitter and receiver.

$$d_{ABCD} = d_{AC} - d_{AD} - d_{BC} + d_{BD} \qquad (8)$$

In order to determine the values of the individual distances that make up a q-range, multiple measurements must be made using different combinations of nodes. Combinations of nodes must be chosen in such a way that they provide q-ranges that are linearly independent and therefore solvable. This aspect of RIPS falls outside the scope of this paper and is further discussed in [6]. These solvable sets of q-ranges can then be solved by different methods such as genetic algorithms, hyperbolic trilateration or by simply by using numerical methods.

This paper is concerned with what happens when measurements are made where at least one pair of the four nodes participating are separated by more that a carrier wavelength. In such a case the actual value for the q-range is no longer defined by (6) but by the following:

$$d_{ABCD} = \varphi_{ABCD} \frac{\lambda_C}{2\pi} + n\lambda_C \qquad n\epsilon Z \qquad (9)$$

This is a problem because the value provided by measurements would differ from the true q-range value. There is therefore a need to study where this occurs and why exactly it occurs.

### III. OBSERVED PATTERNS

In this section q-range ambiguity is studied through an empirical approach. This is done with the goal of identifying patterns that would aid in the characterization of q-range ambiguity. Intuitively one would think that q-range ambiguity would occur for any distance that exceeded $\lambda_C$, but initial tests revealed that this was not the case. Incorrect values occurred at distances just beyond $\lambda_C$, but when these distances were further increased correct values started occurring again. Thus it was decided to use a brute force approach to give a rough idea of were ambiguity occurred. This was done by using MATLAB to calculate q-ranges at fixed intervals on a fixed two dimensional grid. To simplify the situation the position of only one node was varied. This configuration of nodes is similar to that used by the hyperbolic trilateration method given in [7]. Hyperbolic trilateration analytically solves q-ranges in RIPS were three nodes are fixed anchor nodes with known positions and the fourth node's position is to be determined.
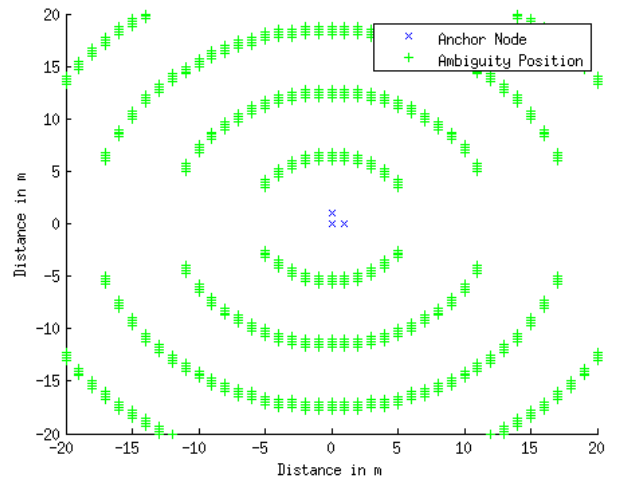


Fig. 2. A two dimensional map showing where ambiguity occurs. This was done by moving one of the four nodes all around the map using fixed intervals.

It should be noted that this MATLAB model is merely a direct implementation of the equations given in the previous section. No physical effects such as fading or multipath are

167

considered as the aim of this paper is to study q-range ambiguity as q-range ambiguity is caused by the basic mathematics behind RIPS.

For the scenario presented in figure 2 a carrier frequency of 50 MHz was used with a frequency separation of 1 KHz between the transmitter nodes, the distance between the stationary anchor nodes was 1 m and a resolution of 25 cm was used. The results from the scenario illustrated in figure 2 showed that ambiguity only occurred in intervals that centred around the transmitter nodes and then radiated outward. These intervals appeared to be spaced a distance of $\lambda_C$ apart, with the areas between them yielding correct q-range values. It should also be noted that since only one node is being moved in this case, the ambiguity occurring is due to the position of this node. The other three nodes all have stationary positions that are separated by less than $\lambda_C$ and therefore could not contribute to ambiguity.

## IV. MATHEMATICAL CORRELATION

The brute force test done in the previous section revealed that q-range ambiguity appears to occur in circles around transmitter nodes, leaving gaps where correct q-range values are obtained. In order to determine if this is actually the case, the mathematics behind RIPS must be investigated.

Incorrect q-range measurements occur when $n$ in (9) does not equal zero. Thus we have to isolate the variables that $n$ is dependent on in this case. The position of only one node is changing and is therefore the only thing having an effect on the q-range ambiguity in this case. We need to seek a stage in the mathematics were measurements related to the moving node are separate from the rest. Therefore we investigate the equations behind the phase offset measurements at the moving node. Equations (2) and (3) express the true value of the phase offsets measured at node D. The measured offsets will however differ from these when distances between nodes, are greater than a signal wavelength. Therefore a measured and true offset can be expressed in the following ways:

$$\varphi_{true} = -2\pi \left( n\lambda + \frac{Res}{\lambda} \right) \qquad (10)$$

$$\varphi_{measured} = -2\pi \left( \frac{Res}{\lambda} \right) \qquad (11)$$

Where $Res$ is a distance measured from the position of the last completed period to the position of the receiver and is illustrated in figure 3. The symbol $n$ represents the number of complete cycles the signal has completed before reaching the receiver. The number of completed cycles is omitted from the measured equation because only the phase of a signal is measured.

When (10) and (11) are each substituted into (5) it can be seen that the two $n$ values cancel each other out when reduced to the final form in (12). This holds if signals sent from the two transmitter nodes are in the same $n^{th}$ wavelength and the transmitter frequencies are close enough to have wavelengths of roughly the same values, as is usually the case in RIPS.

In the mathematical proof of the RIPS concept it is assumed that the difference between the two transmitter frequencies is smaller or equal to 1 KHz. It is therefore a valid assumption to make [1].

$$\varphi_C = -2\pi \left( \left( n_A\lambda_A + \frac{Res_A}{\lambda_A} \right) - \left( n_B\lambda_B + \frac{Res_B}{\lambda_B} \right) \right)$$

$$\varphi_C = -2\pi \left( \left( \frac{Res_A}{\lambda_A} - \frac{Res_B}{\lambda_B} \right) + \left( (n_A\lambda_A - n_B\lambda_B) \right) \right)$$

$$\varphi_{C_{measured}} \approx -2\pi \left( \frac{Res_A}{\lambda_A} - \frac{Res_B}{\lambda_B} \right) \qquad (12)$$

The small difference between the two transmitter errors means that the "correct" q-ranges observed do have a small error that is defined in (13) as

$$Error = n \left( \lambda_A - \lambda_B \right) \qquad (13)$$

The q-range values that where observed to be "correct" at distances past $\lambda_C$ are in fact incorrect, but the error is small relative to the q-range.

To summarize, the q-range ambiguity observed can be explained due to signals from the transmitter nodes being in different $n^{th}$ wavelengths at the receiver node. If the distance between the two transmitter nodes is under $\lambda_C$ it will mean that ambiguity only occurs when the signal from the transmitter node furthest from the receiver node is in the next wavelength and the other transmitter's signal is still in the previous wavelength as is illustrated in figure 3. If the transmitter nodes are close to each other, the other the areas where the $n$ values differ will be smaller, because this difference is caused by the difference in distance to the receiver from each transmitter.

Therefore the observed effect is dependent on the transmitter frequencies and physical positions being close to each other.
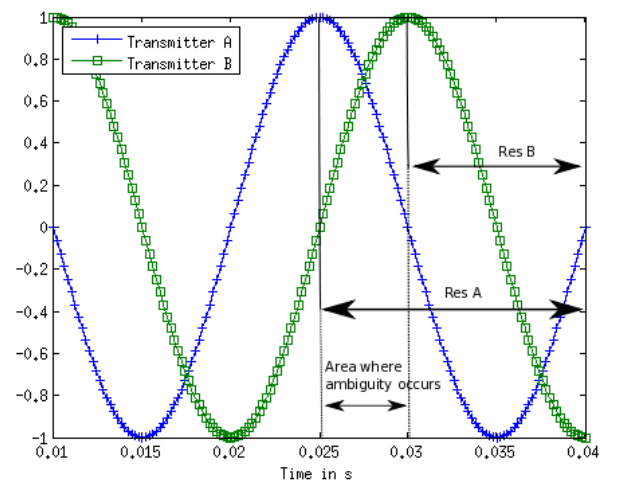


Fig. 3.   A graph showing the signals from transmitters showing the area where ambiguity occurs and Res A and B.

168

These findings can be used to describe a general case where all the nodes are scattered. The ambiguity caused by measurements at the second receiver will have the same shape, mostly overlapping the ambiguity areas of the first receiver.

## V. Possible Applications

The results obtained in this paper have shown that it is possible to make single q-range measurements over distances beyond $\lambda_C$ that produce results that are close to the true q-range using a single RIPS measurement. There is however still a problem in that there is no way to determine if a measurement delivered an incorrect q-range or not. This can be solved by making q-range measurements at different frequencies that do not have overlapping ambiguity areas. In such a case at least three different frequencies need to be used. This way when one frequency delivers an incorrect result the other two will produce correct results. Therefore it will be possible to distinguish correct results from incorrect ones. It should be noted that it is not possible to choose a set of frequencies that do not have overlapping ambiguity up until infinity, but it could be possible to choose frequencies in such a way that they do not overlap for a given range such as the maximum communication range of the devices that are being used.

Another possible use is to use single q-range measurements in tracking moving objects. In such a situation ambiguous results can be identified by comparing current measurements with previous ones. Once the object being tracked enters an ambiguity area, the measured q-range will differ greatly from the previous measurements and will thus be possible to identify.

Implementation on a device with an antenna array, as illustrated in figure 4, could make sense. This is due to the fact that the transmitter nodes need to be close to each other for the observed effect to be useful. In such an implementation each antenna on the device could act as an independent node. Such a configuration would also provide the advantage that the positions of the nodes (device antennas) would already be know to each other, meaning that there would be less distances to solve when determining positions from q-range measurements. One drawback of such an approach would be that it would not be ideal for a hyperbolic trilateration method of q-range solution as the nodes to be localized, would fall outside of the triangle formed by the three anchor nodes/antennas. This is a possible problem, because it is shown in [8], that hyperbolic trilateration is very sensitive to noise when localizing nodes in the area outside the triangle formed by the anchors.

## VI. Conclusions and Future Work

A study of q-range ambiguity in RIPS has been made, which resulted in a deeper understanding of where and exactly why q-range ambiguity occurs. Possible alternative solutions for q-range ambiguity have also been presented. Further work needs to be done to determine the effect of the slight difference between measured and true q-ranges at distances beyond
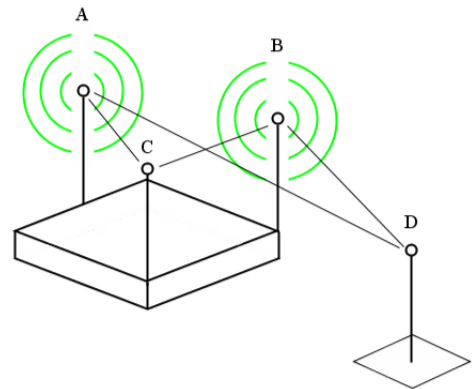


Fig. 4. An illustration of an antenna array device with antennas capable of acting independently making a RIPS measurement.

$\lambda_C$. There is also a need to research the exact details of implementing the possible uses described in the previous section.

## References

[1] M. Maroti, B. Kusy, G. Balogh, P. Volgyesi, A. Nadas, K. Molnar, S. Dora, and A. Ledeczi, "Radio interferometric geolocation," in *in Proc. ACM 3rd Conference on Embedded Networked Sensor Systems (SenSys'05)*, November 2005, paper link. [Online]. Available: http://www.truststc.org/pubs/148.html

[2] C. V. David Munoz, Frantz Bouchereau and R. Enriquez, *Position Location Techniques and Applications*. Academic Press, 2009.

[3] J. Hightower and G. Borriello, "Location systems for ubiquitous computing," *Computer*, vol. 34, no. 8, pp. 57 –66, aug 2001.

[4] B. Kusy, A. Ledeczi, M. Maroti, and L. Meertens, "Node-density independent localization," in *Information Processing in Sensor Networks, 2006. IPSN 2006. The Fifth International Conference on*, 0-0 2006, pp. 441 –448.

[5] B. Dil and P. Havinga, "A feasibility study of rip using 2.4 ghz 802.15.4 radios," in *Mobile Adhoc and Sensor Systems (MASS), 2010 IEEE 7th International Conference on*, 2010, pp. 690 –696.

[6] L. Lambert Meertens, "The dimension of the vector spanned by sets of radio-interferometric measurements," Kestrel Institute, Tech. Rep., 2005.

[7] B. Kusy and J. Sallai, "Analytical solution for radio-interferometric localization of mobile sensors," *Technical Report (ISIS-06-710)*, http://w3.isis.vanderbilt.edu, December, 2006 2006. [Online]. Available: http://w3.isis.vanderbilt.edu

[8] X. Wang, B. Moran, and M. Brazil, "Hyperbolic positioning using rips measurements for wireless sensor networks," in *Networks, 2007. ICON 2007. 15th IEEE International Conference on*, 2007, pp. 425 –430.